LUMINESCENCE AND ITS ELECTRICAL EXCITATION IN ZnSe AND ZnS

A thesis presented by

Neil Gordon

to the

University of St. Andrews

in application for the Degree

of Doctor of Philosophy

DECLARATION

I hereby certify that this thesis has been composed by me, and is a record of work done by me, and has not previously been presented for a higher degree.

The research was carried out in the Wolfson Institute of Luminescence, within the School of Physical Sciences in the University of St. Andrews, under the supervision of Professor J. W. Allen.

N. T. Gordon.

CERTIFICATE

I certify that Neil Gordon has spent nine terms at research work in the Wolfson Institute of Luminescence within the School of Physical Sciences in the University of St. Andrews under my direction, that he has fulfilled the conditions of the Resolution of the University Court, 1967, No.1, and that he is qualified to submit the accompanying thesis in application for the Degree of Doctor of Philosophy.

Research Supervisor.

CAREER

I first matriculated in the University of St. Andrews in October 1973. In 1977 I graduated with First Class Honours in Physics and obtained a Neil Arnott prize.

In October 1977, following the award of a S.R.C. scholarship, I enrolled as a research student under Resolution of the University Court, 1967, No.1, as a Candidate for the Degree of Doctor of Philosophy.

ABSTRACT

This thesis is concerned with the luminescent properties of ZnSe and ZnS:Mn. In particular, it is concerned with the possibility of exciting the luminescence in these compounds electrically.

The first part of the thesis discusses the properties of Schottky contacts on ZnSe. If these contacts are forward biased, holes can be injected into n-type ZnSe where they can excite luminescent centres. It is shown that the measured injection efficiency is much greater than would be predicted by a diffusion theory.

Manganese doped ZnS is considered in the second part of this thesis. It is possible that electroluminescent displays can be commercially produced using thin films or powder panels of ZnS:Mn. By using conducting, crystalline ZnS:Mn, however, it has been possible to study the mechanism by which the manganese centres are excited on the application of a large electric field. It was found that the band structure of ZnS plays an important part in this process.

Finally, a non-radiative Auger effect has been investigated in conducting ZnS:Mn. It is shown that the non-radiative transition rate is proportional to the concentration of free electrons in the material. Besides its theoretical interest, this effect could find some applications in material characterisation.

ACKNOWLEDGEMENTS

First of all, I would like to thank the S.R.C. for providing me with the funds necessary for producing this thesis.

I have been fortunate in receiving a great deal of practical help from other members of my research group. In particular, I would like to thank M. D. Ryall, Dr. H. R. Szawelska and Dr. J. M. Noras for their help and encouragement.

Dr. D. M. Finlayson very kindly lent me the magnet and cryostat which were used for the Hall effect measurements.

Finally, my supervisor Professor J. W. Allen deserves special thanks for his enthusiasm, help and encouragement throughout the last $3\frac{1}{2}$ years.

CONTENTS

Chapter 1

INTRODUCTION

Semiconductor physics has had an impact on people's everyday lives mainly because of the ease with which devices for amplification and, more recently, for performing logical calculations can be constructed from the elemental semiconductors silicon and germanium. In recent years, there has been a trend amongst researchers to study other semiconductors from the III-V and II-VI compounds. These compound semiconductors are not being investigated to try to compete with silicon and germanium in the areas in which they have traditionally been successful. Instead, they are being used to produce new devices for which the elemental semiconductors could not be used. For example, the small effective mass of electrons in GaAs makes this a suitable semiconductor for ultra-fast switching devices.

One application for which silicon and germanium can not be used is in the production of light emitting devices for displays. One reason for this is related to the fact that semiconductors strongly absorb radiation which has a photon energy greater than their band gap. The small band gaps of silicon and germanium make these semiconductors strong absorbers of visible radiation.

Solid state light emitting devices can be produced by making a p-n junction on a suitable semiconductor. When the junction is forward biased, holes are injected into the n-type region and electrons are injected into the p-type region. Light is emitted when the resulting excess of electrons and holes recombines either directly or via some

impurity centre. A limitation on this type of device is that it is only possible to produce radiation which has a photon energy less than or equal to the band gap. This means that silicon or germanium could only be used for producing infra red radiation. In addition, both of these semiconductors have an indirect band gap. Thus, the recombination of electrons and holes by a direct optical transition is forbidden by $\underline{k}$ conservation and any radiative recombination will require either phonon or impurity participation.

Efficient infra red sources can, however, be prepared using the III-V compound GaAs, which has a direct band gap. Most LEDs in commercial production today are made of solid solutions of GaAs and GaP. The semiconductor GaP has a larger band gap than GaAs but this is indirect. The solid solutions have an intermediate band gap. It is found that the predominant colour of LEDs of the form $GaAs_{1-x}P_x$ can be varied between red and green. For small x, the colour can be changed simply by changing x. For large x, however, the band gap becomes indirect and an impurity, such as nitrogen, has to be incorporated to increase the radiative efficiency.

The II-VI compounds ZnSe and ZnS are two semiconductors which could, in theory, be used to extend this range of colours. Both have direct band gaps which are large enough to encompass the entire visible region of the spectrum. Unfortunately, it is normally only possible to produce n-type material and hence p-n junctions are difficult. Robinson and Kun[1] (1975) have obtained some evidence for the formation of a p-type layer on a n-type ZnS_xSe_{1-x} substrate but this has not been repeated by other groups.

It is, however, possible to inject holes into n-type material using a Schottky contact. In this thesis, Schottky contacts were normally prepared by evaporating gold or aluminium onto an etched semiconductor surface. The fundamental properties of gold-ZnSe contacts prepared in this way are investigated in chapter 2. The use of these contacts to obtain injection electroluminescence is considered in chapter 3.

If the electrons and holes recombined directly, the light emitted from a ZnSe Schottky diode would be in the blue region of the spectrum. Unfortunately, most of the holes recombine via a deep centre to produce an orange luminescence. This centre is present in all the ZnSe grown in this laboratory and is possibly due to unintentional copper contamination.

The energy gap of solid solutions of ZnSe and ZnS can be varied between 2.72 eV and 3.65 eV by varying the composition. Assuming that the position of the recombination centre partially follows the valence band, it should be possible to produce blue LEDs by using a suitable mixed crystal of the form ZnS_xSe_{1-x}. A program of research was started in 1976 by Ryall and Allen[2] to use this semiconductor to produce blue LEDs. It was found that x had to be close to 1 to obtain blue luminescence and blue LEDs were eventually produced using a gold Schottky contact on n-type ZnS.

The hole injection efficiency which is obtained from a Schottky contact of this type is small but is much larger than would be expected for a metal-semiconductor contact. This is thought to be related to the presence of an oxide layer between the metal and the semiconductor. Part of the motivation for studying gold-ZnSe contacts was to

understand the mechanism by which holes are injected and hence help with the above research.

Chapters 4 and 5 are concerned with manganese doped ZnS. The manganese centres produce a characteristic yellow photoluminescence when this material is subjected to ultra violet excitation. If a crystal of ZnS:Mn is made conducting, it is found that the yellow luminescence disappears. It is thought that in the conducting material, an excited manganese atom can give its energy to a conduction band electron via an Auger process. This Auger effect is investigated quantitatively in chapter 4.

The electrical excitation of the manganese luminescence is studied in chapter 5. It is found that light is emitted from a thin layer of insulating ZnS:Mn on the application of a sufficiently large electric field. The initial pioneering work on high field electroluminescence was performed by Destriau[3] in 1936. This led to some commercial interest in the late 1950's with the aim of producing electroluminescent panels. Unfortunately, this research did not lead to a sufficient improvement in performance and the interest collapsed. The lack of progress was mainly because the mechanism responsible for the electroluminescence was not properly understood.

Recently, there has been renewed interest in high field electroluminescence because of a better understanding of the operating mechanism. In ZnS:Mn, electrons which are injected into the high field region are accelerated by the electric field until they attain sufficient energy to impact excite the manganese centres. At present, commercial interest is centred on two types of device, namely the d.c. powder panel[4] and the a.c. thin film device[5]. These are described in

more detail in chapter 5 and in figure 5.1.

In this thesis, however, high field electroluminescence has been investigated using a well-defined Schottky structure on conducting ZnS:Mn. This has made it possible to study the fundamental electroluminescent properties of ZnS:Mn rather than those of one particular device. A fundamental limitation on the performance of these devices has been found.

Finally, some conclusions of a general nature are contained in chapter 6.

Chapter 2

SOME PROPERTIES OF SCHOTTKY CONTACTS ON CONDUCTING ZnSe

2.a.i Introduction

Schottky contacts can be used to excite electroluminescence in ZnSe and ZnS as will be discussed in chapters 3 and 5. In chapter 3, a forward biased Schottky contact is used to inject holes into n-type ZnSe. In chapter 5, a reverse biased Schottky contact is used to produce a well-defined high field region in which the impact excitation of manganese centres in ZnS:Mn can be studied.

In this chapter, the fundamental properties of gold-ZnSe contacts will be investigated. Capacitance-voltage and photoemission measurements will be discussed in section 2.b and used to produce a crude model of the potential barrier. The nature of this barrier is important for injection electroluminescence as will be discussed in section 3.b. Various theoretical models will be considered.

2.a.ii Materials Used

The ZnSe used in these experiments was synthesised directly from the elements by heating them together in a sealed evacuated silica tube. Care was taken only to let a small amount of material react at one time as the reaction is exothermic and potentially explosive. After the excess zinc and selenium had been removed by vacuum distillation, the resulting high purity ZnSe was ready to be grown into a crystalline form. The crystal growth was performed by an iodine vapour transport technique[6] in which 5 mg/cc of iodine was loaded

together with about 20 g of ZnSe powder into a sealed silica tube. On heating the tube, an equilibrium is established between the iodine and the ZnSe, i.e.

$$ZnSe + I_{2(g)} \rightleftharpoons ZnI_{2(g)} + Se_{(g)} \quad (2.1)$$

The position of the equilibrium shifts to the right as the temperature is increased so that there is a net drift of ZnSe down a temperature gradient. By making one end of the tube hotter than the other, it is possible to control the rate of flow of the ZnSe. The flow rate was chosen as a compromise between crystal quality and crystal growth rate. Better quality crystals can be obtained with a slow flow rate although the growth time is longer. In practice, a growth temperature of 775°C and a temperature difference of 50°C was used. This transported 10 g of ZnSe in about 4 days. The resulting material was mainly polycrystalline although it was often possible to remove single crystals of up to 4 mm in length from the boule. There were no obvious differences between the characteristics of devices made on polycrystalline material and those made on single crystals.

The as-grown material was highly resistive and had to undergo a Zn/Al treatment to make it conducting. Slices were cut from the boule and heated in a mixture of zinc/10% aluminium at 930°C in a sealed, evacuated silica tube for about 36 hours. This produced n-type material which had a resistivity of a few ohm cm.

2.a.iii Device Construction

The structure of a typical device is shown in figure 2.1. The Zn/Al treated slices were cut into dice of dimensions 6 x 4 x 2 mm and the surfaces polished and etched in 1% bromine in methanol solution.

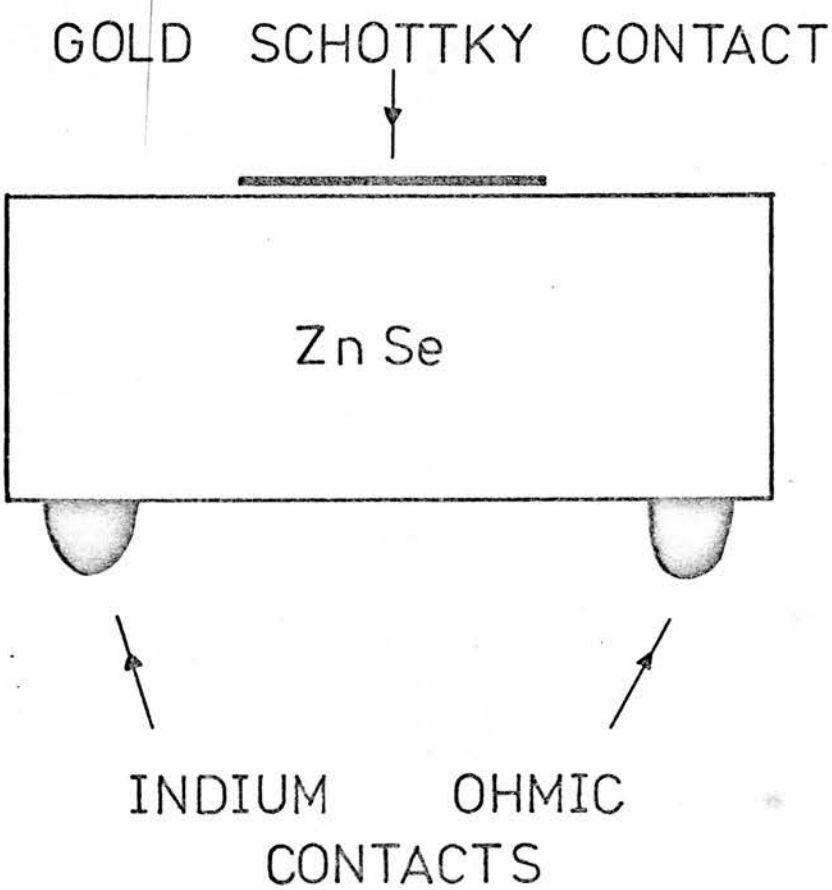

Figure 2.1 The structure of a typical device.

After the dice had been rinsed in methanol and carbon disulphide (which dissolves selenium), two indium contacts were pressed on to one face of the die. The contacts were formed by heating the chip to 320°C in a reducing atmosphere of N_2:10% H_2 followed by rapid cooling. This produced mechanically good contacts with a low electrical resistance.

After the device had been re-etched, the active Schottky contact was evaporated on to the opposite face of the die. Gold was normally used for the Schottky contact which was evaporated in a diffusion pumped, liquid nitrogen trapped system at a pressure of 10^{-6} Torr.

2.b.i.i The Metal-Semiconductor Barrier

The earliest theory for the barrier height of a metal-semiconductor contact was proposed independently by Mott[7] and Schottky[8]. This is shown schematically in figure 2.2. If the metal and semiconductor are well separated as in figure 2.2(a), then the metal work function ϕ_m is defined as the energy required to take an electron at the metal Fermi surface and leave it at rest outside the metal. Similarly, the electron affinity χ_s of the semiconductor is defined as the energy required to remove an electron from the semiconductor conduction band minimum and leave it at rest outside the semiconductor. On bringing the metal and semiconductor together, it can be seen from figure 2.2(b) that a barrier of height ϕ_{ms} will be formed at the interface where

$$\phi_{ms} = \phi_m - \chi_s \qquad (2.2)$$

The Fermi energy is related to the chemical potential and hence

Figure 2.2 The formation of a Schottky contact.

determines particle equilibrium between the two systems. In figure 2.2(b), the Fermi energy in the semiconductor is greater than that in the metal and hence electrons will flow from the surface of the semiconductor into the metal, leaving a depleted space-charge region at the semiconductor surface. Equilibrium is established when the potential drop across the depletion region equalises the Fermi energies as is shown in figure 2.2(c).

In practice, it is found that the barrier heights of Schottky contacts made on, for example, etched silicon surfaces[9] are fairly independent of the metal work function, in contradiction with equation (2.2). This discrepancy was resolved in 1942 by Bardeen[10] who proposed that the semiconductor surface had a continuum of surface states which was separated from the metal by a thin oxide layer. The surface charge could then effectively shield the semiconductor from the metal, making the barrier height less dependent on the metal work function.

When it became possible to produce intimate metal-semiconductor contacts by evaporating in ultra high vacuum conditions on to a freshly cleaved surface, it was still found that equation (2.2) was not obeyed.[11] This is because there is a redistribution of charge on forming a metal-semiconductor contact as is shown in figure 2.2(d).

It was pointed out by Heine[12] that the metal wavefunctions can not end abruptly at the interface and will, in general, penetrate a small distance into the semiconductor. This redistribution of charge creates an electric dipole at the interface and hence determines the barrier height. The effect of this dipole contribution to the barrier height has been discussed by Pelegrini[13] who approximates the band

structure by the effective mass theory and uses the effective mass approximation to calculate the tunnelling of electrons into the forbidden gap of the semiconductor. Recently, more exact calculations have been performed[14] by working out the actual band structure of a metal-semiconductor interface using the self-consistent pseudopotential method. This approach confirms the existence of metal induced gap states (MIGS) which penetrate into the semiconductor energy gap as was originally proposed by Heine. In ZnSe, the total charge density induced by the MIGS decays approximately exponentially with a decay depth of about 1.9 Å.

In practice, the situation is complicated by the fact that a freshly cleaved surface will reconstruct itself to minimise its surface energy. This reconstruction can be revealed by low energy electron diffraction (LEED) from the semiconductor surface. For the ZnSe (100) surface, a c (2 x 2) reconstruction is observed.[15] A further complication is that the heat of condensation which is released when a metal atom is adsorbed on to a semiconductor surface can be sufficient to eject an atom from the semiconductor surface leaving a vacancy, as has recently been proposed by Spicer.[16] These vacancies, which are formed close to the interface, can produce localised states of a different nature to the MIGS discussed earlier. Spicer et al.[16] believe that these vacancy states predominate in determining the barrier heights in the III-V compounds GaAs, InP and GaSb.

To summarise this review of the metal-semiconductor contact, the barrier height is given by equation (2.2) in the absence of charge redistribution at the interface. In practice, charge redistribution occurs into strongly localised states of the semiconductor surface,

forming a dipole. The exact nature of those states is controversial. The electric dipole bends the bands in the vicinity of the interface, hence altering the barrier height. If there is a strong peak in the density of these surface states, the barrier height will be determined (pinned) by the position of this peak.

2.b.i.ii Capacitance-Voltage Measurements

For an 'ideal' Schottky diode (i.e. no interfacial layer and no charge penetration into the semiconductor, cf. figure 2.2(c)) it is possible to determine the barrier height from the variation of the differential capacitance of the diode with applied voltage.[17] As was discussed in the last section, the formation of a metal-semiconductor contact causes electrons to flow from the semiconductor surface into the metal, hence forming a depletion layer. For a gold-ZnSe contact, the depletion approximation is sufficiently accurate. In this approximation, the depletion region which extends a distance W into the semiconductor is considered to be completely depleted of electrons. There is a sharp transition at the edge of the depletion region to the bulk semiconductor which has an electron concentration of n_o, as is shown in figure 2.3(a). The insulating layer has a capacitance given by

$$C = \varepsilon_o \varepsilon_s A / W \quad . \qquad (2.3)$$

The width W can be obtained by solving Laplace's equation

$$\frac{d^2V}{dx^2} = \frac{N_d^* e}{\varepsilon_o \varepsilon_s} \qquad (2.4)$$

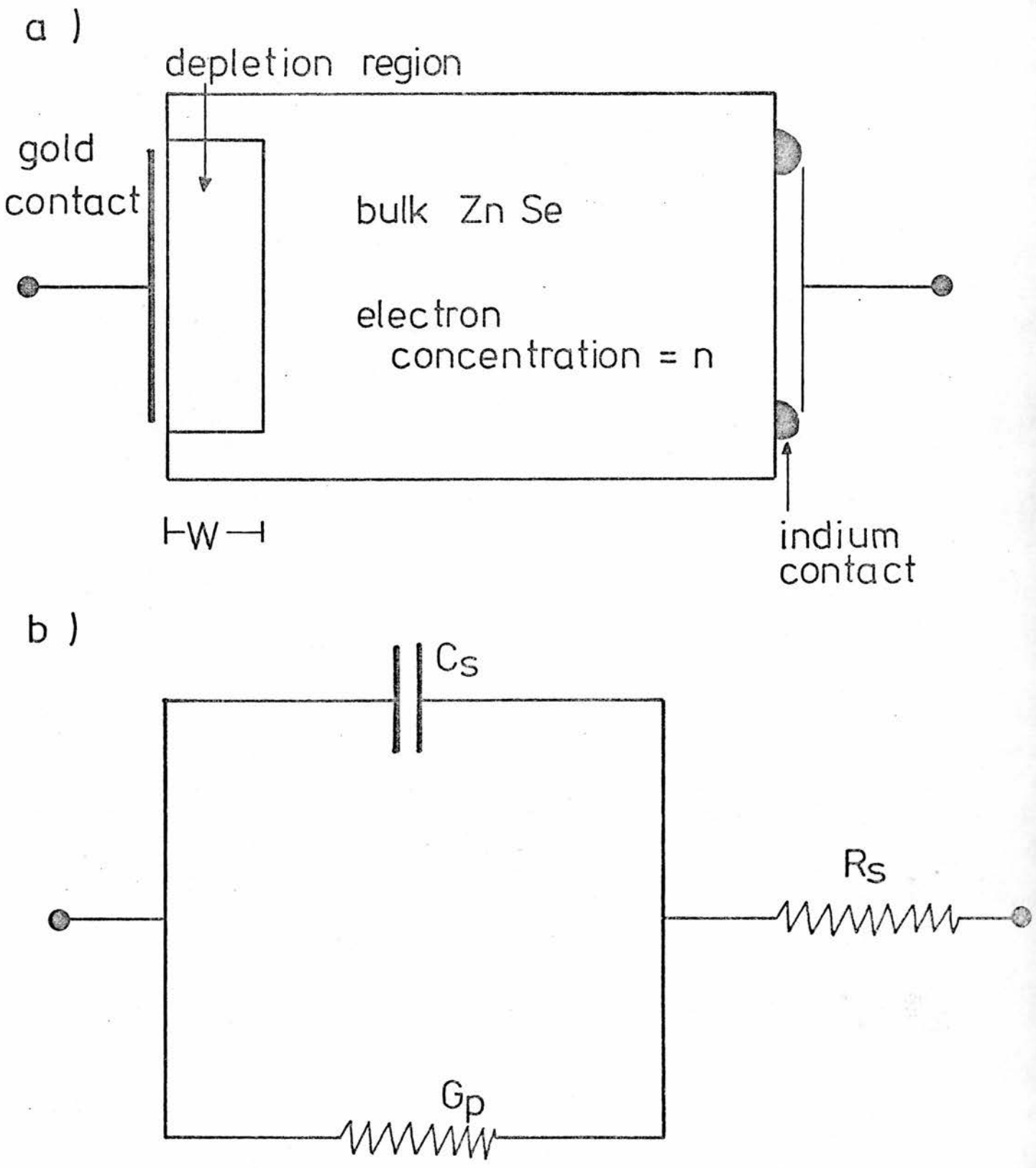

Figure 2.3 a) depletion approximation.
b) proposed equivalent circuit.

where N_d^* is the effective donor concentration, i.e. $N_d^* = N_d - N_a$. This has a general solution

$$V = \frac{1}{2}\left(\frac{N_d^* e}{\varepsilon_o \varepsilon_s}\right) x^2 + Ax + B \qquad (2.5)$$

The boundary conditions at the edge of the depletion region, x = 0, are that V = 0 and E = - dV/dx = 0 and hence

$$V = \frac{1}{2}\left(\frac{N_d^* e}{\varepsilon_o \varepsilon_s}\right) x^2$$

The total potential difference across the depletion region V_d is given by

$$V_d = V_{do} + V_r = \frac{1}{2}\left(\frac{N_d^* e}{\varepsilon_o \varepsilon_s}\right) W^2 \qquad (2.6)$$

where V_r is the applied reverse voltage and V_{do} is the built-in voltage in the absence of an externally applied voltage. From figure 2.2(c), it can be seen that

$$\phi_b = V_{do} + \phi_n \qquad (2.7)$$

where ϕ_n is the position of the Fermi energy below the conduction band edge in the bulk semiconductor. Substituting equation (2.3) into (2.6) gives

$$\frac{1}{C^2} = \left(\frac{2}{e N_d^* \varepsilon_o \varepsilon_s A^2}\right)\left(V_{do} + V_r\right) \qquad (2.8)$$

This equation enables both the effective donor concentration and the diffusion potential to be determined for an ideal diode.

In a real diode, the transition from the bulk semiconductor to the depletion region will not be completely sharp and there will be a transition region having a reduced concentration of electrons. The effect of this transition region has been discussed by Goodwin,[18] Atalla[19] and Dewald[20] who find that V_{do} in equation (2.8) should be replaced by $V_{do} - kT/e$. For a gold-ZnSe junction at room temperature, $kT/e \sim 0.026$ V which is much less than $V_{do} \sim 1.2$ V.

In practice, the small signal a.c. impedance of the diodes was measured as a function of voltage using a Wayne Kerr B601 Radio Frequency Bridge. This bridge worked by balancing the unknown impedance against a variable parallel R-C circuit. The a.c. test voltage had an amplitude of about 100 mV and a frequency of 1 MHz. It was found that although the parallel capacitance appeared to obey equation (2.8), the parallel resistance increased to a maximum and then dropped as the reverse bias was increased. The equivalent circuit shown in figure 2.3(b) is proposed to explain this behaviour. The series resistance R_s is the sum of the bulk resistance of the semiconductor and the two ohmic contacts. The parallel conductance was thought to be related to the d.c. current-voltage characteristics, i.e. $Gp \sim dI_{dc}/dV$. It was found experimentally that Gp decreased exponentially with voltage and hence could be neglected for small voltages. In figure 2.4, R_s and C_s^{-2} are plotted as a function of applied voltage, ignoring Gp. Certain features of figure 2.4 were common to all the diodes studied. Plots of C_s^{-2} against V were linear from about 0.6 V in the forward direction to above 5 V in reverse. There was no discontinuity at V = 0. The series resistance, which was

Figure 2.4 A typical capacitance-voltage plot.

typically a few ohms, remained constant over the same range. Outside this range, the series resistance increased, which is interpreted as being due to a conductance in parallel with the depletion region capacitance.

In the remainder of this thesis, it has been convenient to abbreviate the words 'capacitance-voltage' by C-V. Thus a graph of C_s^{-2} against V will be referred to as a C-V plot. Similarly, the point at which this graph intercepts the voltage axis will be referred to as the C-V intercept and given the symbol V_o.

The C-V plot illustrated in figure 2.4 has a voltage intercept V_o of 1.38 volts. This is one of the lowest values ever achieved and it will be shown in section 2.b.ii.i that this suggests a very thin oxide layer. The net donor density can be calculated from the gradient to be 5.35×10^{17} cm^{-3}. As the donor ionisation energy in ZnSe is sufficiently small for most of the donors to be ionised at room temperature, the electron density in the bulk material will be approximately equal to the net donor density. This enables us to estimate the position of the Fermi energy relative to the conduction band edge in the bulk semiconductor using

$$n \sim N_d^* = N_c \exp -\left(\frac{\phi_n}{kT}\right) \qquad (2.9)$$

Here, N_c is the effective density of states in the ZnSe conduction band which is 1.75×10^{18} cm^{-3} at room temperature. Substituting the appropriate value for n gives $\phi_n \sim 0.03$ eV which is negligible compared with the barrier height.

2.b.i.iii Photoemission

In 1931, Fowler produced a simple theory which described the variation with wavelength and temperature of the process in which a photon incident on a clean metal surface ejects an electron from the metal. The theory is based on the following hypothesis:

> '(the) number of electrons emitted per quantum of light absorbed is to a first approximation proportional to the number of electrons per unit volume of metal whose kinetic energy normal to the surface augmented by $h\nu$ is sufficient to overcome the potential step at the interface'.[21]

This number is called the number of 'available electrons'. The number of available electrons is therefore proportional to the volume of the section of the Fermi sphere which is shaded in figure 2.5. At T = 0 K, the Fermi surface is completely sharp and the required volume can easily be calculated to show that the normalised photocurrent R is given by.

$$R \propto (h\nu - \phi_b)^2 \qquad (2.10)$$

Thus, plotting the square root of the normalised photocurrent (i.e. the number of electrons emitted per incident photon) against the photon energy should give a straight line which intercepts the x-axis at $h\nu = \phi_b$. For photoemission into free space, this intercept will give the metal work function. For an ideal metal-semiconductor contact, it will give the metal-semiconductor barrier height ϕ_b as is shown in figure 2.2(c).

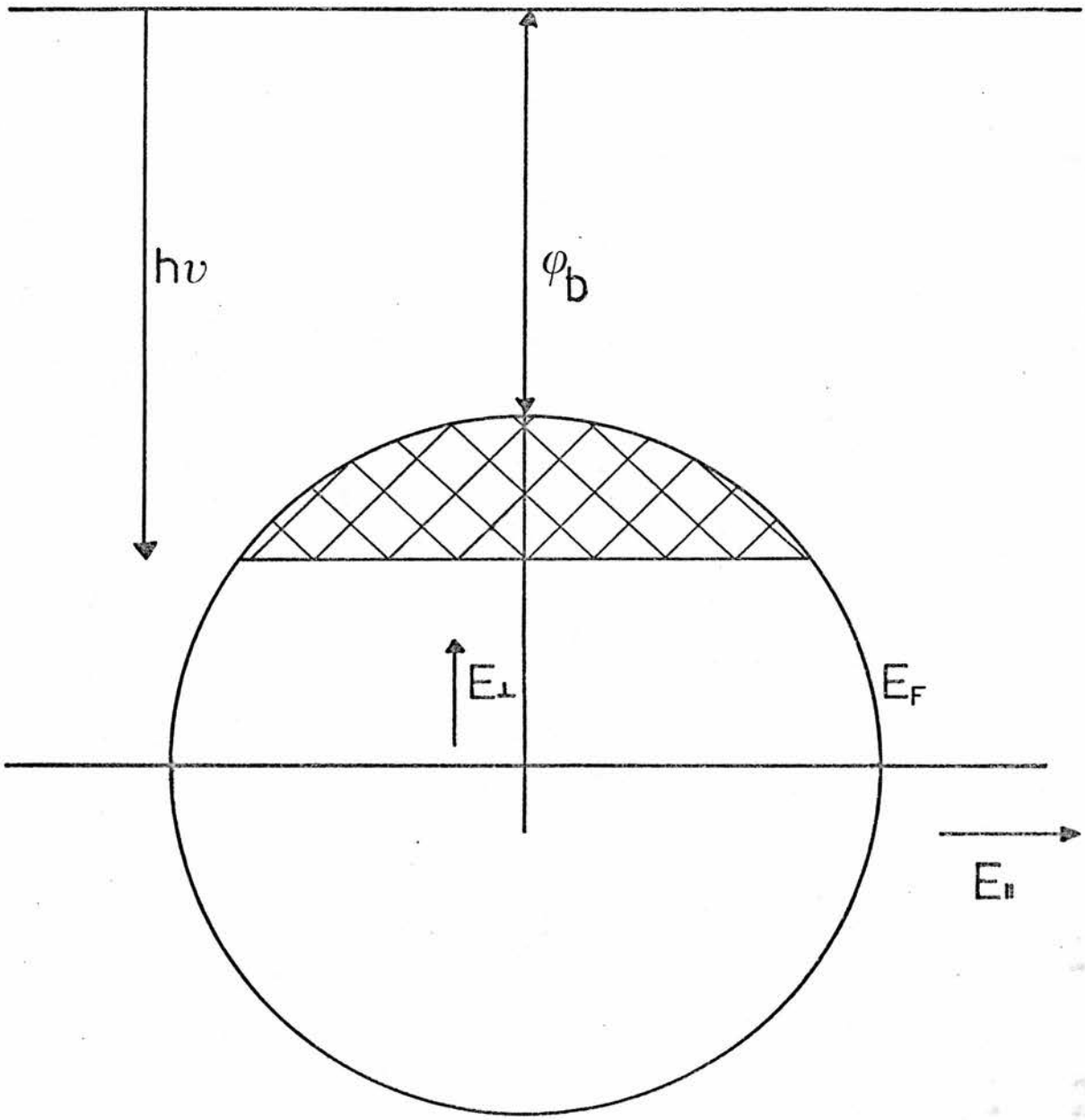

Figure 2.5 The electrons in the shaded part of the Fermi sphere can be photo-emitted over the barrier.

The experimental arrangement used for measuring the photocurrent is illustrated in figure 2.6(a). Chopped monochromatic light was directed on to the metal contact through the semiconductor as is shown on the figure. The biasing circuit of figure 2.6(a) was used to vary the barrier height, as will be discussed in the next section. For the present, this circuit can be ignored together with the voltmeter and the ammeter. Thus, the chopped light incident on the metal surface produced an a.c. photocurrent which was connected directly to a Brookdeal Bl002 current pre-amplifier. The impedance of the pre-amplifier, which was less than 100 ohm depending on the range, was much smaller than that of the diode (typically $\sim$ 1 mega ohm). This ensured that most of the photocurrent produced by diode flowed through the pre-amplifier (figure 2.6(b)). The function of the pre-amplifier was to amplify the a.c. component of the current flowing through it and produce a voltage at the output proportional to this a.c. component. Typically, an a.c. amplification of 10^7 V/A was used. Finally, the voltage was synchronously detected with a Brookdeal 401 lock-in amplifier and stored on a chart recorder. The monochromator wavelength could be continuously varied by a small motor which was also used to produce a 'blip' on the chart recorder paper at about 50 Å intervals.

Since it was desired to measure the number of photo-electrons ejected per incident photon, it was necessary to measure the relative photon intensity at the monochromator output as a function of wavelength. This was achieved using a Hilger Schwartz thermopile which had a voltage output proportional to the radiation power density incident on it.

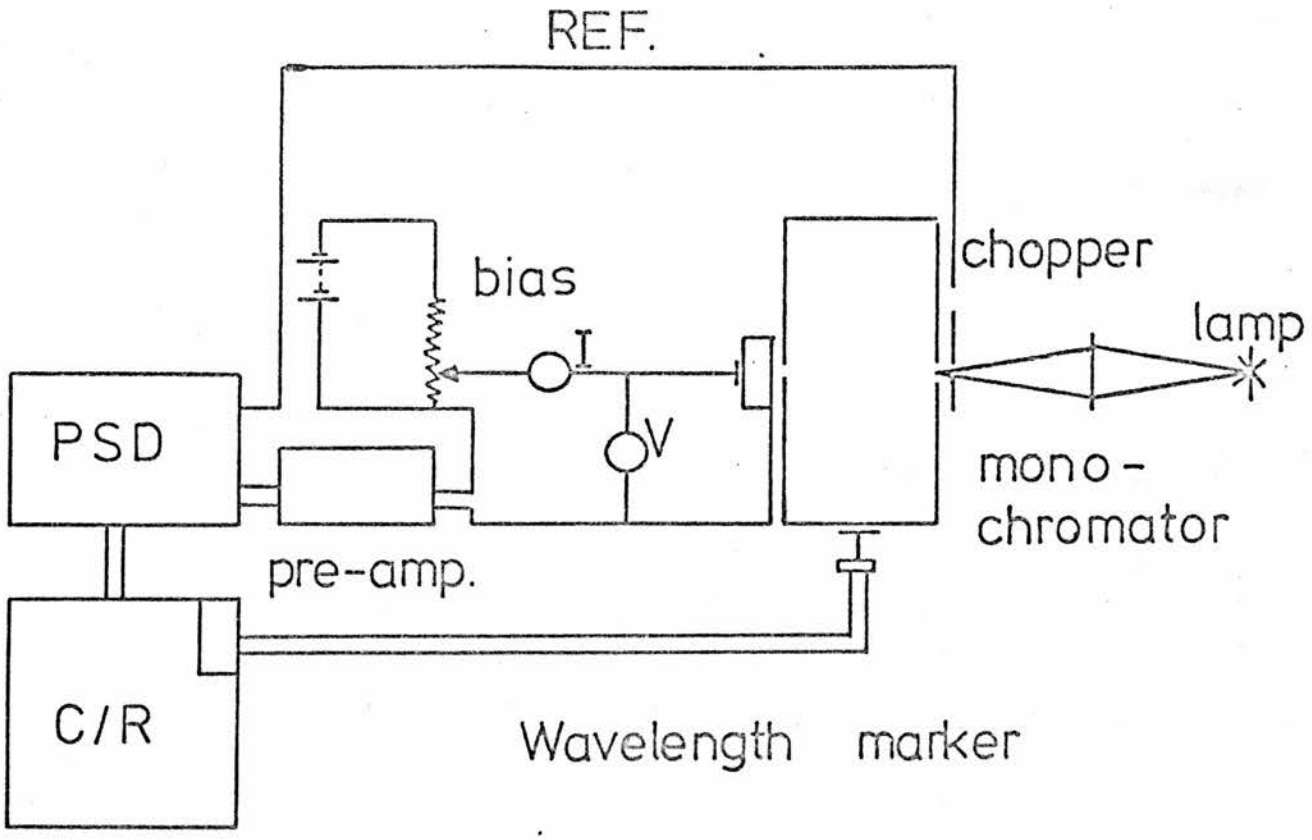

Figure 2.6(a) Experimental arrangement for measuring photo-emission.

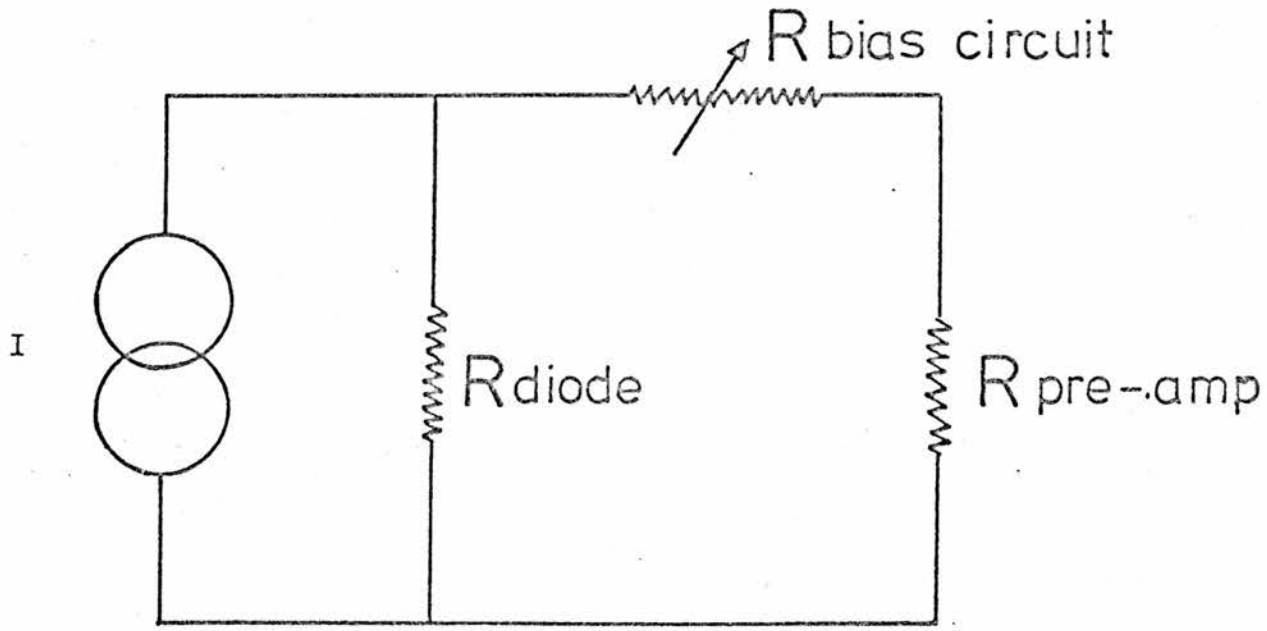

Figure 2.6(b) Equivalent circuit.

The variation of the square root of the normalised photocurrent with photon energy is plotted in figure 2.7(a) for one of the better diodes. Equation (2.10) is obeyed above 1.42 eV and the linear region could be extrapolated to give a barrier height of 1.325 eV. This does not compare very well with the barrier height of 1.20 eV which was determined from capacitance-voltage measurements. Figure 2.7(a) also shows that there is a measurable amount of photoemission down to about 0.2 eV below the threshold energy. This is partly due to the fact that the Fermi surface in the metal is spread out over a few kT and hence is not completely sharp. The theoretically expected effect of temperature on the shape of the Fowler plot is shown in figure 2.7(b) from which it can be seen that a 'thermal tail' is formed which extends for about 3kT below the threshold energy.

The photocurrent was often sufficiently large to be measured directly with a Keithley 602 Electrometer. In this case, the chopping wheel could be dispensed with and the d.c. response measured. It was always found that the d.c. response was the same as the a.c. response above the threshold. However, the 'low energy tail' of the d.c. response was often greater than that of the a.c. response. This effect could reduce the apparent d.c. photo-threshold by up to 0.025 eV.

2.b.i.iv Voltage Dependence of the Barrier Height

For an ideal metal-semiconductor contact, the potential energy of an electron in the semiconductor close to the top of the barrier will be the sum of the space-charge induced potential, as shown in figure 2.2(c), and an image force potential induced by the presence of the electron close to the metal surface.[22] Thus

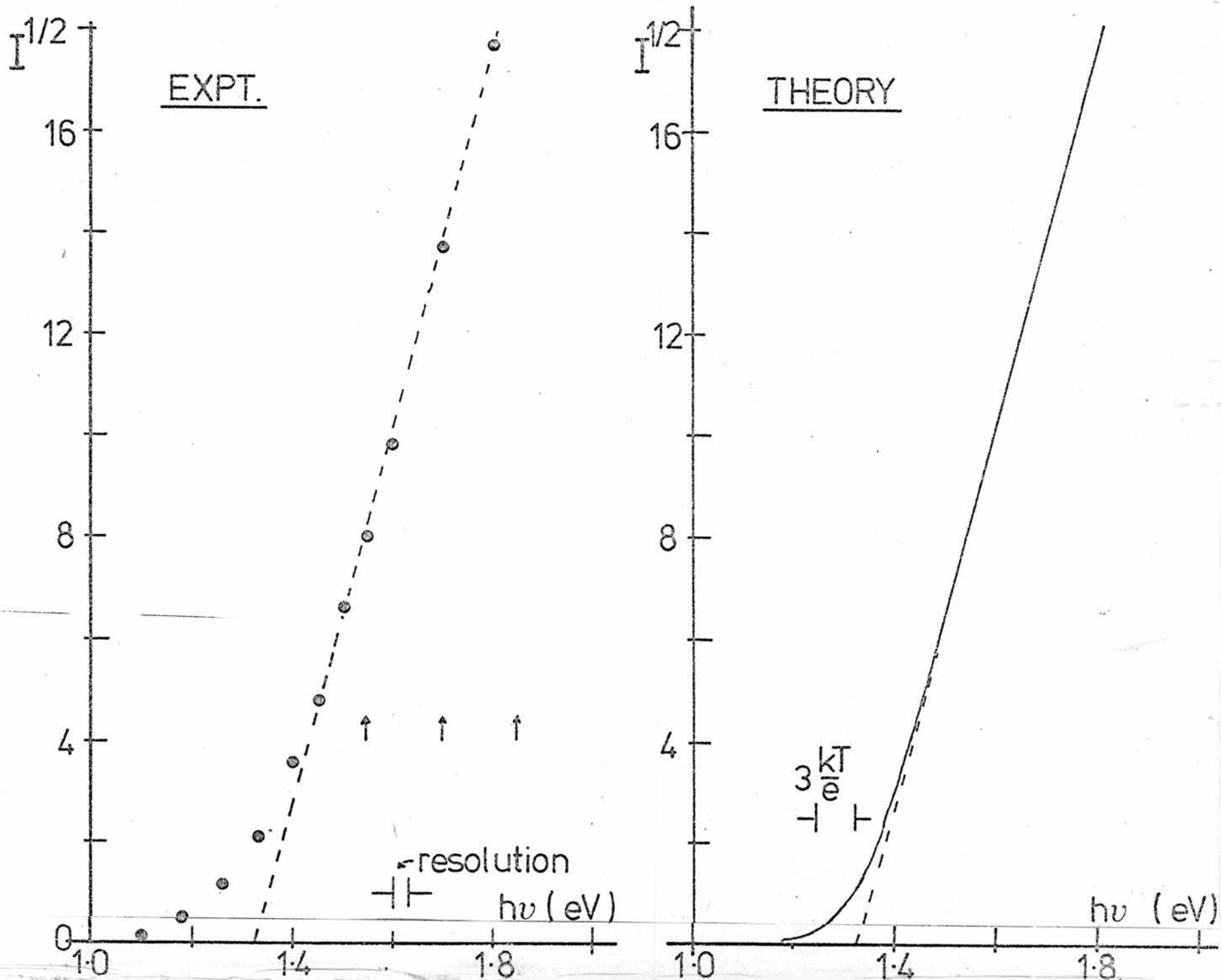

Figure 2.7 Experimental and theoretically expected Fowler plot.

$$V = V_b - e\mathcal{E}x - \left(\frac{e}{8\pi\varepsilon_0\varepsilon_d x}\right) \quad (2.11)$$

This shifts the position of the maximum in the potential energy to a position

$$x_m = \left(e/16\pi\varepsilon_0\varepsilon_d\mathcal{E}\right)^{1/2} \quad (2.12)$$

into the semiconductor and reduces the barrier height by an amount

$$\Delta\phi = \left(e\mathcal{E}/4\pi\varepsilon_0\varepsilon_d\right)^{1/2} \quad (2.13)$$

The parameter ε_d in equations (2.11)-(2.13) is known as the image force dielectric constant and is the mean dielectric constant which a photo-emitted electron experiences in crossing the potential maximum. Sze, Crowell and Kahng[23] have calculated the transit time for an electron to cross the potential maximum assuming a carrier velocity of 10^7 cm/s. They argue that the image force dielectric constant ε_d should be comparable to the dielectric constant which is experienced by electromagnetic radiation of approximately these periods (wavelength between 3.0 and 15 μm). By measuring the variation in the barrier height with electric field on gold-nSi contacts, they were able to deduce an image force dielectric constant of 12 which agrees with the optically measured dielectric constant of about 12 for silicon. It should, however, be noted that this result is not in agreement with what has been found by other authors. Studies of the field dependence of the reverse current by Kahng on silicon[24] and Benzer on germanium[25] were consistent with values of ε_d of the order of unity.

For ZnSe, the optical dielectric constant is 6.1[26] and this will be compared with the measured image force dielectric constant in this

section and also in section b.ii.iii. It was found, in practice, that the easiest experimental technique was to use a fixed wavelength and to measure the change in the photocurrent as the electric field was varied with the bias circuit (figure 2.6(a)). This was because the signal at zero bias could be offset accurately at the lock-in amplifier, hence enabling the small change in the signal produced by altering the applied voltage to be measured accurately. For a photon energy at which equation (2.10) applies, i.e.

$$R = a\,(h\nu - \phi)^2$$

then

$$(\phi - \phi_o) = (h\nu - \phi_o)\left[\left(\frac{R}{R_o}\right)^{\frac{1}{2}} - 1\right] \qquad (2.14)$$

Here, R_o and ϕ_o refer to the photocurrent and barrier height at zero applied bias. Since ϕ_o is known to be 1.325 eV (figure 2.7(a)), the drop in the barrier height can easily be calculated from equation (2.14) by measuring the change in the photocurrent. Note that provided equation (2.10) holds, equation (2.14) will be valid independently of the mechanism by which the barrier is lowered.

For image force lowering, the barrier height is expected to vary linearly with the square root of the electric field as in equation (2.13). The electric field can be calculated from the capacitance-voltage measurements as was shown in section 2.b.i.ii and is proportional to $(V + V_{do})^{\frac{1}{2}}$. Hence

$$\Delta\phi = (\phi - \phi_o) + \Delta\phi_o = \beta\,(V + V_{do})^{1/4} \qquad (2.15)$$

where

$$\beta = 9.58 \times 10^{-6} \left(\frac{N_d}{\varepsilon_d^2} \right)^{1/4}.$$

This is plotted in figure 2.8 for the diode of figure 2.7(a) using the three different photon energies which are indicated by arrows on figure 2.7(a). It should be noted that all three sets of points lie on the same straight line which corresponds to an image force dielectric constant of 5.69. It has been noted that the diffusion potential of 1.2 V which is obtained from C-V measurements is inconsistent with the photoemission threshold of 1.325 eV. Fortunately, the square root of the electric field only depends on this to the (1/4)th power and if a diffusion potential of 1.3 V had been assumed, the deduced image force dielectric constant would only have been changed to 5.43. The disagreement between the various methods for measuring the barrier height will be discussed in a later section.

Finally, it should be noted that the diode of figure 2.8 was not a typical diode. In fact, it will be shown in section 2.b.ii.iii that the characteristics of this diode most closely followed what would be expected of an ideal diode of all the diodes studied. Because of the general irreproducibility of the diode fabrication technique, a wide range of diode behaviour was observed which corresponded to a continuous departure from ideal behaviour. It is possible that this observation of a continuous departure from ideal behaviour sheds some light on the wide range of image force dielectric constants which has been reported by different research groups, each with a different, but well-defined, fabrication method (see section 2.b.ii).

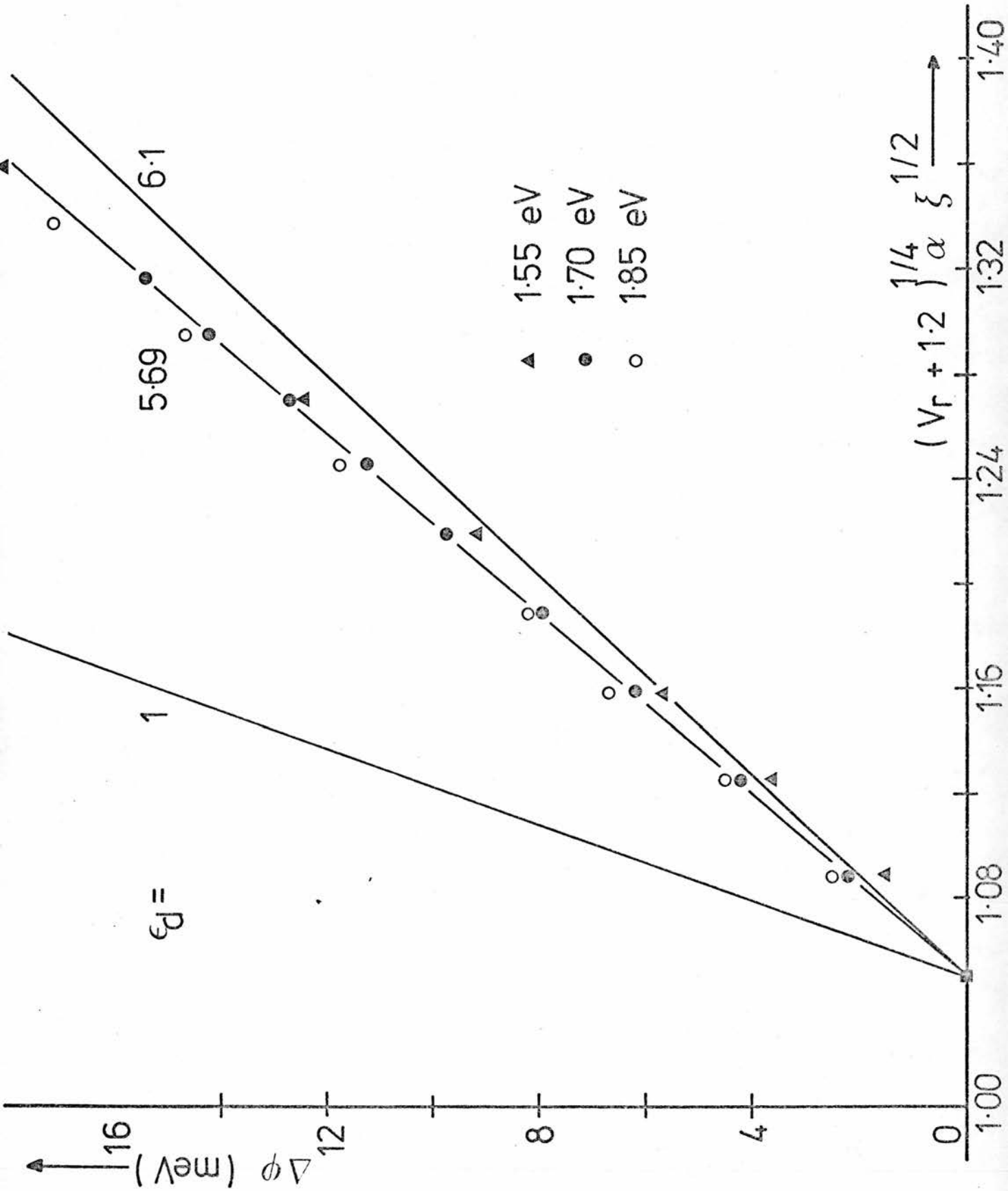

Figure 2.8 Measured variation of the barrier height with the square root of the electric field.

2.b.ii Effect of Oxide Layer

2.b.ii.i Capacitance-Voltage

The diode which was investigated in the previous section had a capacitance-voltage intercept (V_o) of 1.2 volts and it was observed that this was one of the lowest values ever achieved. In practice, it was found that V_o varied between 1.2 and 10 volts apparently independently of the sample preparation. The appearance of excessively large values of V_o has been explained by Goodman[27] and Cowley[28] in terms of an oxide layer between the semiconductor and the evaporated metal layer. It has been found from a previous investigation using Auger spectroscopy[29] that a layer containing zinc and oxygen is normally formed below the metal contact on diodes made in this laboratory. In preparing these diodes, the freshly etched sample was transferred under propanol to a high vacuum system which was pumped out to a pressure of 10^{-6} Torr. Unfortunately, the vacuum system took about one hour to reach this final pressure, allowing plenty of time for the surface to become oxidised.

Assuming a sticking coefficient of 1, the time taken for one mono-layer of oxide to be adsorbed is approximately equal to $10^{-3}/P$, where P is the pressure in Torr. Thus, even at a pressure of 10^{-3} Torr, a mono-layer of oxide could be adsorbed in as little as 1 second. Ludeke[15] has recently studied the oxidation properties of the ZnSe (100) surface by evaporation in ultra high vacuum followed by a controlled exposure to oxygen. The oxidation of the surface was continuously monitored using LEED, electron loss spectroscopy (ELS) and Auger spectroscopy. It was found that there was no measurable uptake of oxygen for exposures to pressures below 8×10^{-2} Torr. This was

independent of the exposure time. Above this pressure, there was a sudden irreversible uptake of oxygen which could be observed by the appearance of oxygen lines on the Auger spectrum of the surface. Simultaneously with this, there was a sudden drop in the selenium signal, indicating that oxygen was replacing selenium on the ZnSe surface. The chemical composition of the surface was not altered by additional exposure to oxygen. Ludeke suggests that the pressure dependence of the oxidation is due to pressure broadening of the O_2^- surface state. This enables the replacement reaction to commence by the transfer of an electron from the ZnSe valence band into the surface state. It is also interesting to note that the ELS spectrum of the oxidised surface was markedly different from that of ZnO. This result suggests the existence of a complex oxide in which Se, although largely depleted from the oxide, plays an important role.

Cowley[28] has analysed the expected capacitance-voltage characteristics for the model illustrated in figure 2.9(a) in which the semiconductor surface is separated from the metal by a thin oxide of width δ. The oxide-semiconductor interface contains a surface state density D_s (cm^{-2} eV^{-1}) and filling the surface states up to some energy, denoted by ϕ_o, results in a neutral surface. The oxide is assumed to have a well-defined band structure and the metal-oxide barrier ϕ_m' together with the oxide-semiconductor conduction band discontinuity χ_s' are assumed to be independent of the oxide thickness. It can be seen from figure 2.9(a) that if the oxide width is reduced to zero, the band bending V_b is equal to $(\phi_m' - \chi_s' - \phi_n)$. The quantity $\phi_m' - \chi_s'$ is denoted by ϕ_{ms} and from the discussion in section 2.b.i.ii, it can be seen that the capacitance-voltage intercept

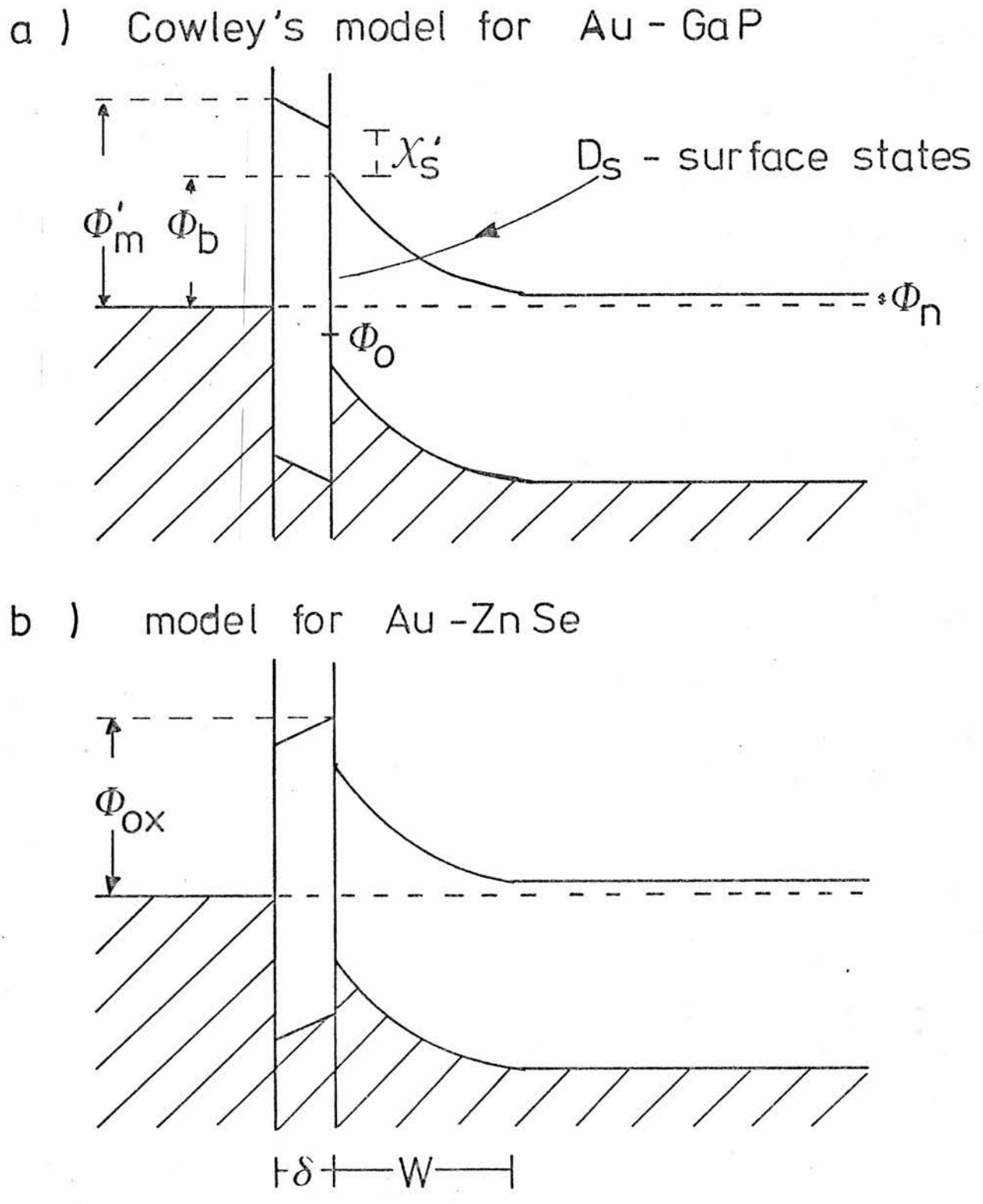

Figure 2.9 Models for the MOS structure.

$$V_o = \phi_{ms} - \phi_n$$

for no oxide.

The effect of the oxide can be understood qualitatively by considering it as a capacitor in series with the depletion capacitance C_d. The total capacitance is therefore given by

$$\frac{1}{C} = \frac{1}{C_{ox}} + \frac{1}{C_d} \quad . \tag{2.16}$$

It follows that at zero applied bias, 1/C and hence $(1/C)^2$ is increased by an amount depending on the oxide capacitance. A consequence of Cowley's theory is that the C-V gradient is independent of all oxide parameters and hence can be used to determine the donor density using equation (2.8). The C-V characteristics of a device with an oxide layer is therefore a straight line which intercepts the voltage axis at some value greater than ϕ_{ms} by an amount depending on the oxide parameters. For a device without surface states, it can be shown that

$$V_o = \phi_{ms} + \frac{V_1}{4} - \phi_n \tag{2.17}$$

where $$V_1 = \frac{2 \, e \, \varepsilon_o \varepsilon_s \, N_d \, \delta^2}{(\varepsilon_o \, \varepsilon_{ox})^2} \quad .$$

For a device with surface states, the situation is more complicated and depends on how much the applied bias fills or empties the surface states and also on whether or not the filling of the surface states can respond to the measurement frequency of typically 1 MHz. It is probable that the surface state quasi-Fermi level remains approximately pinned to the metal Fermi level for thin oxides. Making this assumption

together with the assumption that the surface states can respond to the measurement frequency, Cowley finds that

$$V_o = \phi_{ms} + \frac{\alpha}{1+\alpha}(E_g - \phi_o) + \frac{V_i}{4(1+\alpha)^2} \qquad (2.18)$$

where $\alpha = e D_s \delta / \varepsilon_o \varepsilon_{ox}$.

Although Cowley's theory successfully explains why an oxide layer produces a large C-V intercept, it is not of much practical use in determining oxide parameters from C-V measurements. In order to use equation (2.18) to estimate the oxide thickness δ , the following parameters have to be known:

(a) the metal-oxide barrier height ϕ_m'

(b) the semiconductor-oxide electron affinity χ_s'

(c) the 'mean' surface state density D_s

(d) the surface state neutral level ϕ_o

To illustrate the importance of knowing the surface state parameters, V_o has been plotted against oxide thickness in figure 2.10 for two different surface state densities of 0 and $10^{13}/cm^2/eV$. The latter value was deduced by Livingstone[29] from measurements of the a.c. conductance of a number of diodes. For figure 2.10, ϕ_{ms} was assumed to be 1.2 eV, N_d was taken as 5×10^{17} cm^{-3} and ϕ_o was estimated from [30] to be about 0.4 eV.

Cowley's theory does, however, make the useful prediction that the C-V gradient depends only on the donor density and is independent of any oxide layer. To test this, the capacitance-voltage characteristics of diodes made on four separate dice were measured. After

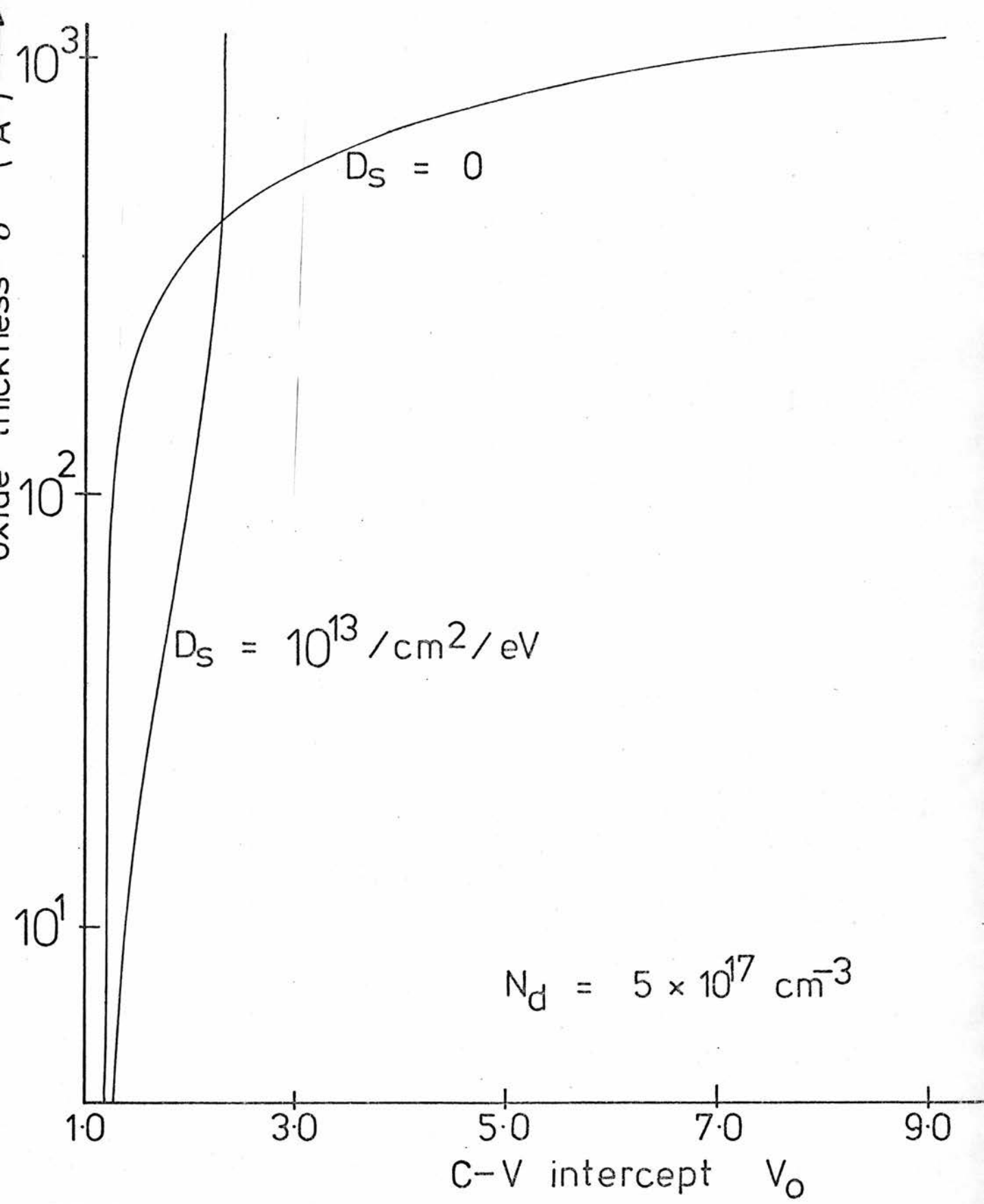

Figure 2.10 The oxide thickness which would be deduced from the measured C-V intercept using Cowley's theory.

measurement, the Schottky contacts were removed by polishing with diamond paste, the chips were re-etched and new Schottky contacts were evaporated. The process was repeated seven times. If the C-V gradient is independent of the oxide, then the donor density deduced from the gradient should not depend on the C-V intercept V_o. This is plotted in figure 2.11 in which each symbol represents a different chip. It can be seen from figure 2.11 that there is little or no correlation for the diodes with V_o less than 2.5. For larger values of V_o, it is perhaps possible to say that the measured value of N_d will be lower than the actual value although there are insufficient data to make any definite conclusion.

In order to illustrate his theory, Cowley made some measurements on Au-GaP contacts. He was able to correlate the C-V intercept V_o with his preparation conditions in that diodes which were prepared in a poor vacuum tended to have a large V_o. This was investigated here by always etching all four dice simultaneously in the same beaker and evaporating gold contacts on to all the dice at the same time. The voltage intercept V_o is plotted against the device preparation number in figure 2.12. In general, there was little or no correlation between the preparation conditions and the measured V_o.

If it is assumed that the C-V gradient gives a reasonable estimate of the donor concentration, then the variation of N_d with preparation number should give a rough depth profile of the donor density. This is plotted in graph 2.13 for seven preparations in which gold was evaporated and an eighth in which an aluminium contact was evaporated.

Figure 2.13 also sheds some light on the mechanism by which a Zn/Al treatment produces n-type conducting ZnSe. Bjerkland and

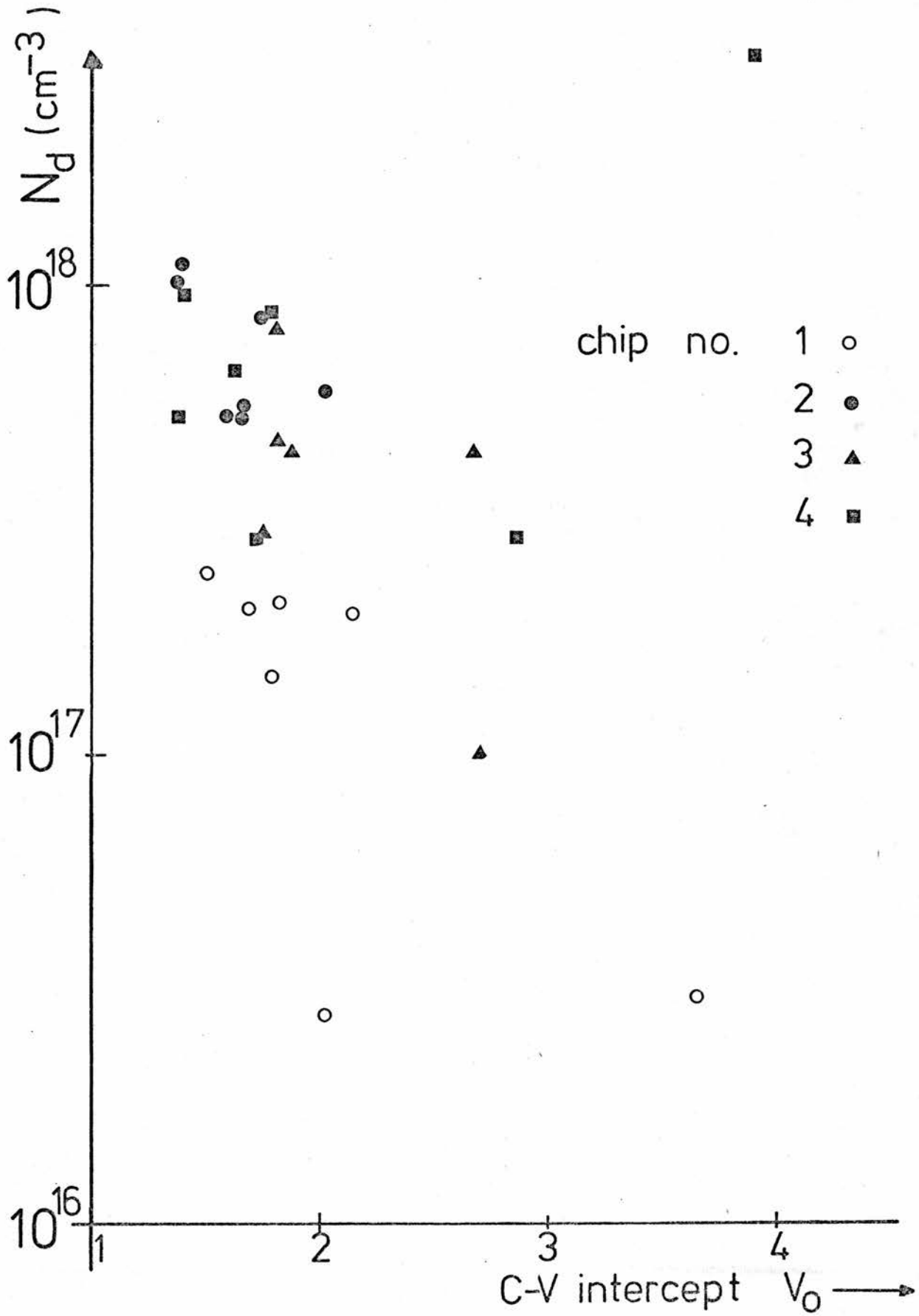

Figure 2.11 Dependence of the measured donor concentration on the capacitance - voltage intercept.

Figure 2.12 Dependence of the C-V intercept on the preparation conditions.

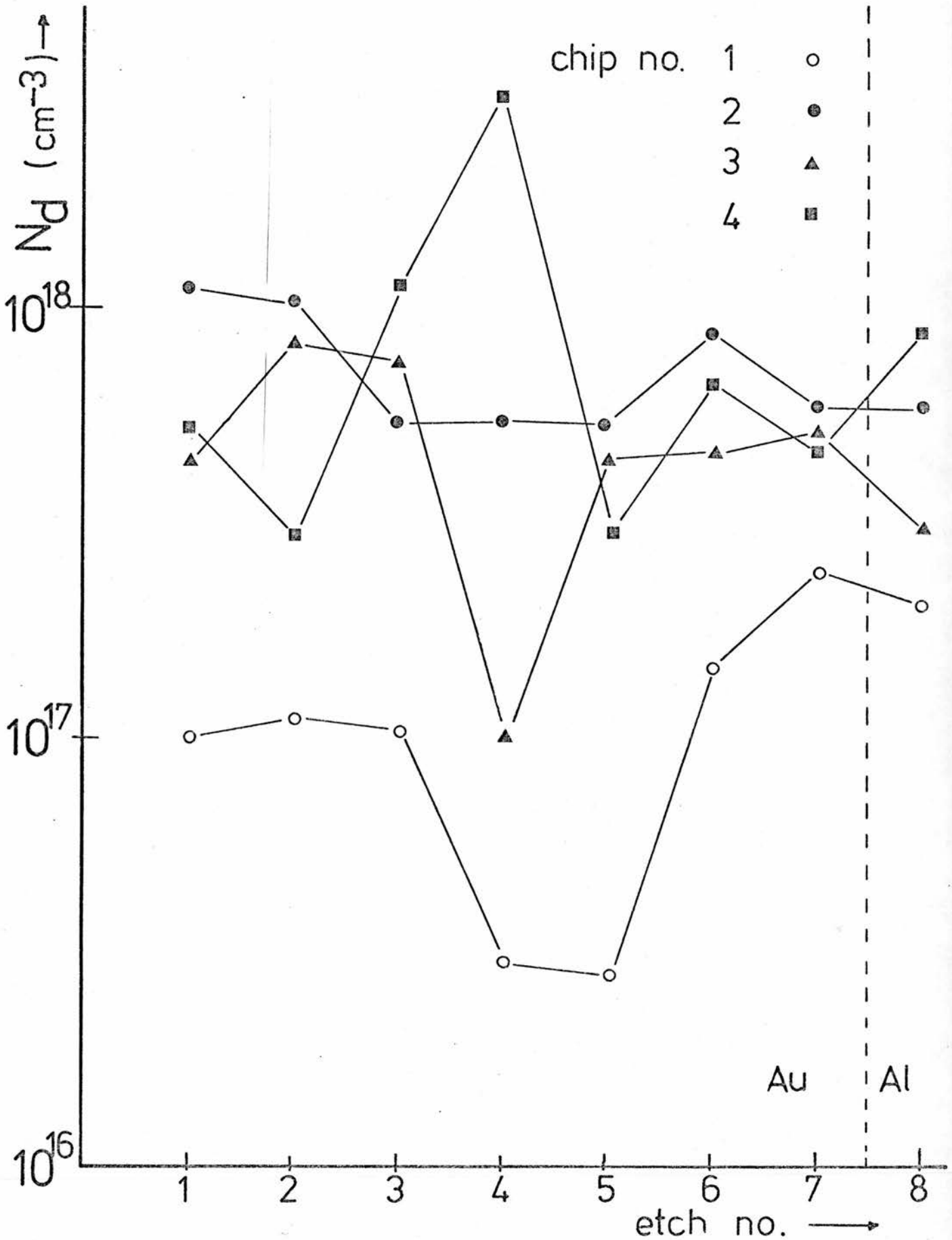

Figure 2.13 Approximate depth profile of the donor density in the chips.

Holwech[31] have measured the diffusion of aluminium into ZnSe using an optical technique. They find that the diffusion profile approximately obeys Fick's law and has a penetration depth of about 40 μm for the diffusion time of 36 hours used here. The samples were polished with carborundum and 6μ diamond paste between etches and it is estimated that the total polishing throughout the 8 preparations corresponded to a depth of about 0.3 mm. As there was no measurable decrease in N_d over this distance, it appears that whatever lowers the conductivity in a Zn/Al treatment diffuses at a faster rate than the aluminium. It is possible that a Zn/Al treatment results in a flow of compensating zinc vacancies out of the sample, leaving an excess of donors.

2.b.ii.ii Photoemission

There is a problem concerned with photoemission experiments as to whether ϕ_m' or ϕ_b is being measured, see figure 2.9(a). Cowley[28] assumes that the interfacial layer is transparent to electrons and hence the photoemission threshold gives the barrier height ϕ_b. Some information on this problem can be obtained by plotting the C-V intercept V_o against the photoemission threshold ϕ_o. This is shown in figure 2.14 for all the diodes in which both parameters were measured. It can be seen from this figure that 7 out of the 10 diodes have V_o smaller than ϕ_o. It should also be noted that ϕ_o was found to vary by over 400 meV between 1.28 and 1.70 eV. This contrasts with Cowley's results on GaP in which ϕ_o remained constant to within a few tens of millivolts and was independent of the interfacial thickness δ. The model which is illustrated in figure 2.9(b) is proposed to explain these results. Here, there is a negative voltage drop across the oxide

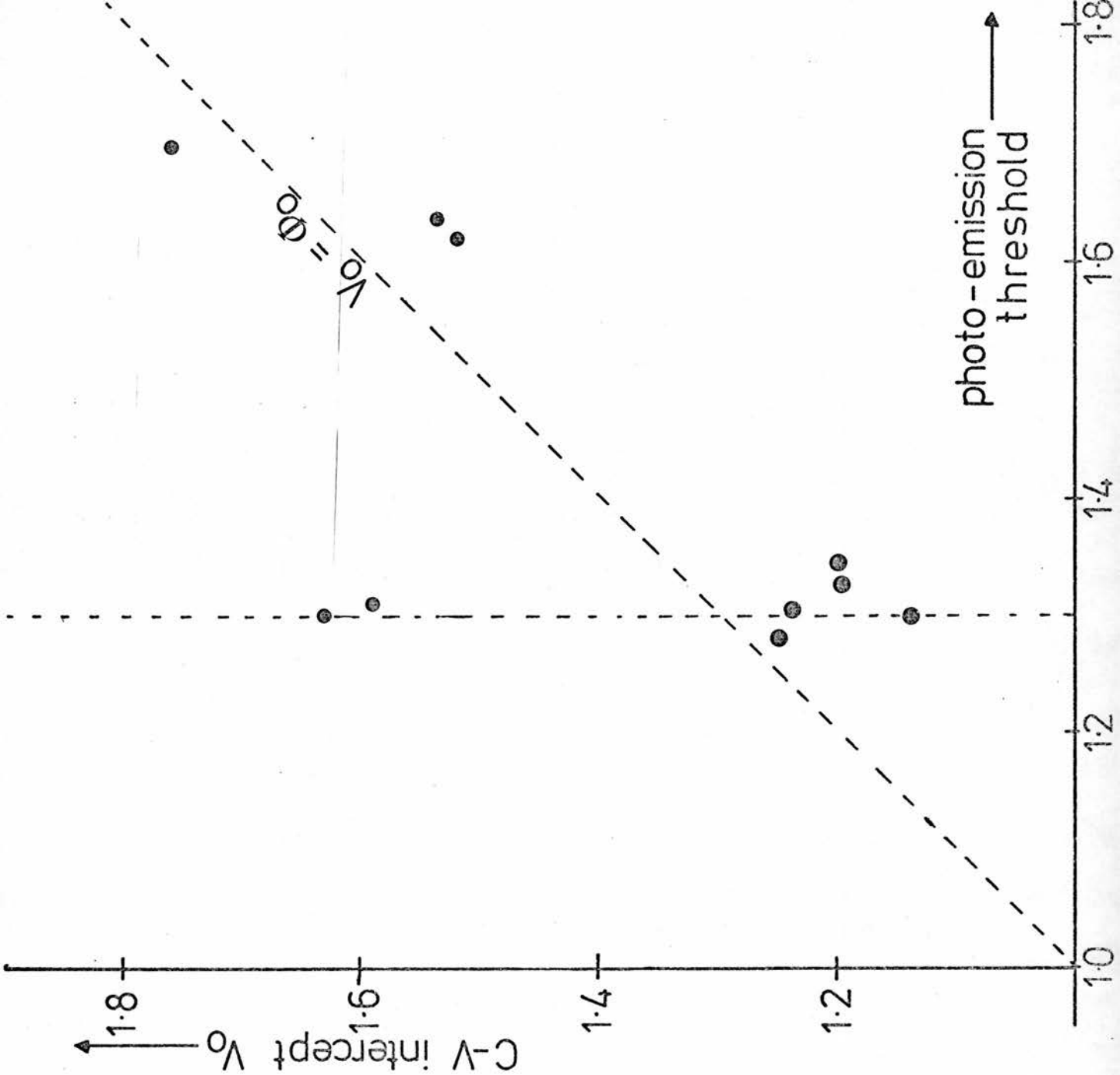

Figure 2.14 Connection between the C-V intercept and the photo-emission threshold.

and the measured barrier height is as illustrated. The arguments for this model are summarised below.

(a) If ϕ_m' of figure 2.9(a) was being measured, then the photoemission threshold would not be expected to vary much from diode to diode.

(b) If ϕ_b of figure 2.9(a) was being measured, V_o would always be greater than ϕ_o.

(c) It will be shown in the next section that, in general, the photoemission threshold varies more rapidly with voltage than would be expected by image force lowering. This is consistent with the model of figure 2.9(b) but not of figure 2.9(a).

(d) A net surface state density of less than $10^{13}/cm^2/eV$ is normally all that would be required to produce the reverse field in the oxide.

For example, it is shown in appendix A that the density of surface states required to reverse the oxide electric field is approximately

$$D_s \sim 3.14 \times 10^3 N_d^{\frac{1}{2}} .$$

Thus, even for a donor density of $10^{18}\ cm^{-3}$ a surface state density of only $3.14 \times 10^{12}/cm^2/eV$ would be required. This is similar to the actual density deduced by Livingstone[29] and others from conductance measurements.

(e) A reverse field could explain the high hole injection efficiency which is discussed in chapter 3.

Finally, a theoretical calculation has been performed to estimate the transparency of a thin oxide layer to photo-electrons. This has been reproduced in appendix B and uses the WKB approximation to estimate the tunnelling probabilities. It was found that a barrier as thin as 20 Å was largely opaque to photo-electrons. It would therefore be expected, on theoretical grounds, that a photoemission experiment would measure the oxide barrier rather than the semiconductor barrier ϕ_b for an oxide layer greater than 20 Å.

2.b.ii.iii Voltage Dependence of ϕ

In section 2.b.i.iv, the voltage dependence of the photoemission threshold was described for one particular diode. It was found that these results could be explained by image force lowering with an image force dielectric constant ε_d close to the theoretically expected value of 6.1.

The maximum in the image force potential can be estimated from equation (2.12) to be at about 10 Å from the metal surface. It is therefore evident that the field dependence of the barrier height will be very sensitive to the presence of an oxide layer. It is also clear that the field dependence of the barrier height can not be due to image force lowering for diodes with an oxide thickness greater than 10 Å. For thicker oxides, it is thought that ϕ_{ox} is being measured as was noted in the last section. However, the barrier lowering was found to be proportional to the square root of the electric field for all the diodes tested and hence a value for ε_d could be deduced. This parameter varied between 0.2 and 5.69, i.e. ε_d was always less than the theoretically expected value. Hence, the barrier height tended to change

more rapidly with field than would be expected from image force lowering (equation (2.13)). Using the model which was developed in the last section, it is shown in appendix A that

$$\Delta\phi = -\delta\left[\frac{\varepsilon_s}{\varepsilon_{ox} + e D_s \delta}\right]\mathcal{E} \qquad (2.19)$$

The data for figure 2.8 have been re-plotted according to equation (2.19) in figure 2.15. The reason why $\Delta\phi$ appears to be proportional to both $\mathcal{E}$ and $\mathcal{E}^{\frac{1}{2}}$ is because of the small range of electric field over which it was possible to make measurements. There was a considerable amount of low frequency noise when a voltage was applied to the diode and this became too great for the P.S.D. to handle when greater than about 2.5 volts was applied.

Equation (2.19) shows that the measured barrier height will vary rapidly with field in diodes which have a thick oxide. This implies that the image force dielectric constant which would be deduced by fitting the variation to equation (2.13) will be small for diodes with a thick oxide. The deduced dielectric constant is plotted against the C-V intercept in figure 2.16 and shows the expected trend.

Thus the measured value of ε_d has been shown to depend on the presence and properties of the interfacial layer. It is possible that this can account for the wide range of ε_d which has been reported for other systems.[23-25]

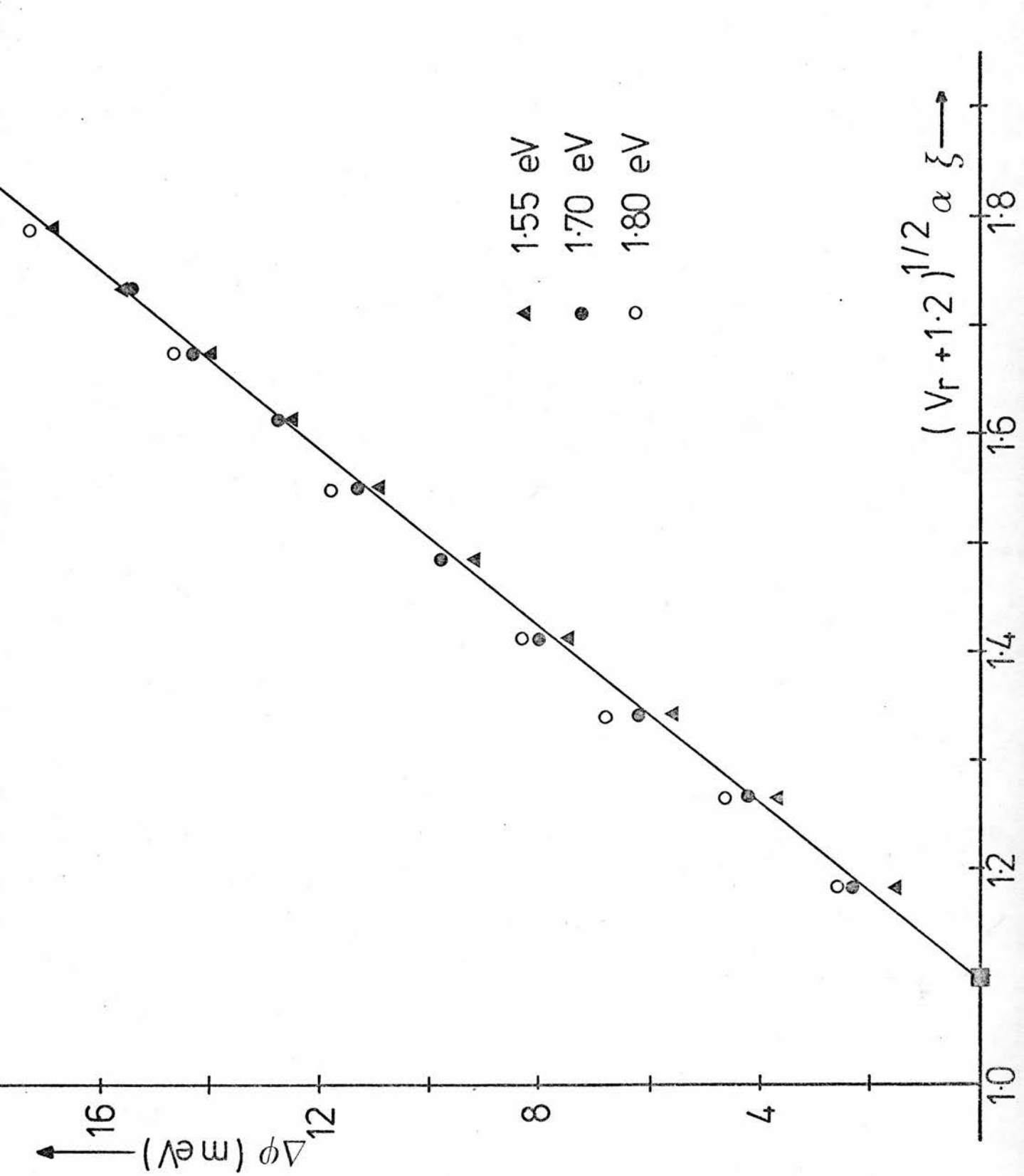

Figure 2.15 The variation of the barrier height with the electric field.

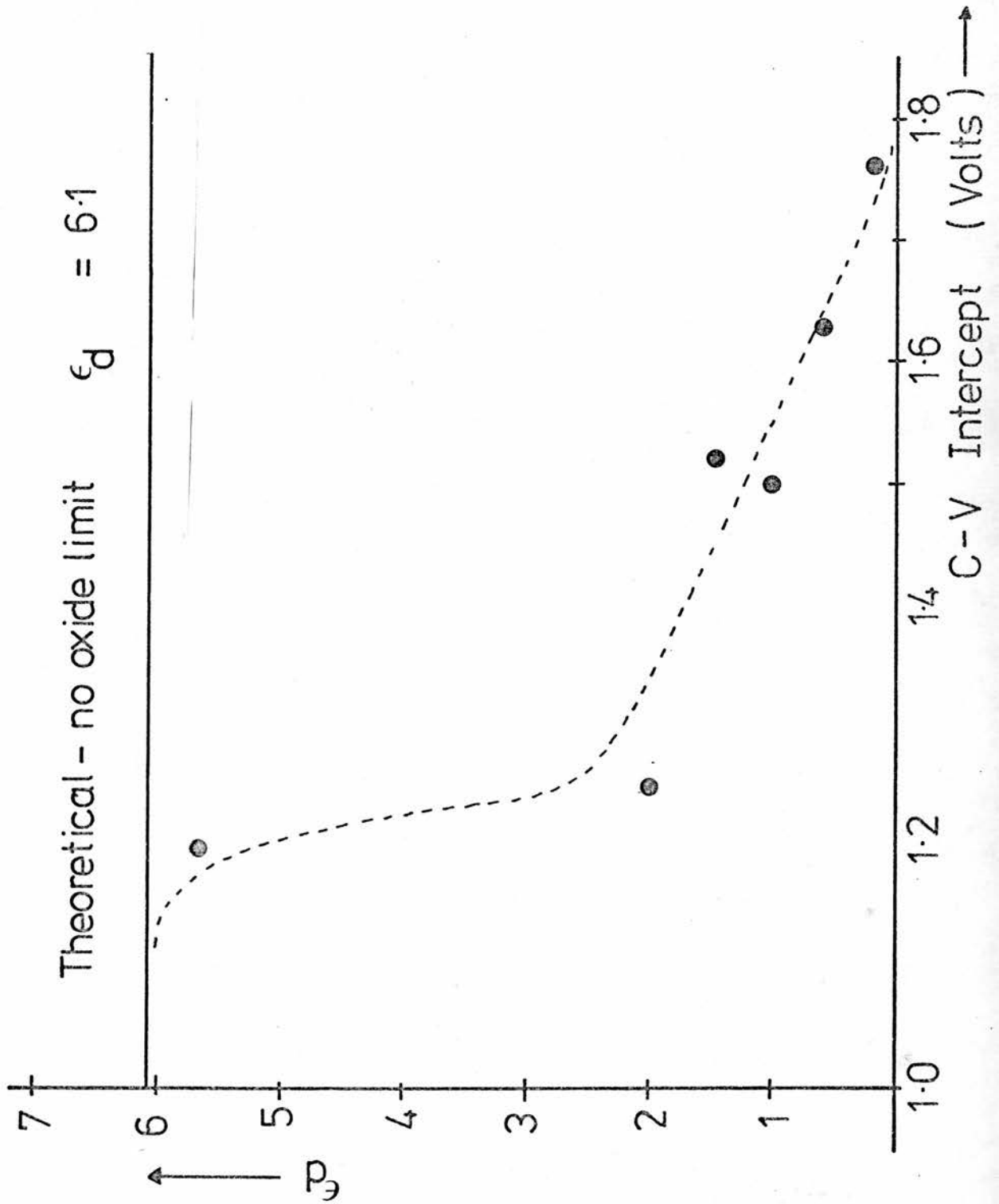

Figure 2.16 The variation of the measured image force dielectric constant with the C-V intercept (oxide thickness)

2.c Current-Voltage Characteristics

2.c.i Introduction

There are a number of reports in the literature[30, 32] that Schottky contacts with nearly ideal characteristics can be produced by evaporating a metal contact on to an etched ZnSe surface. The diodes investigated here have characteristics which are far from ideal, although their preparation is similar to that reported by the other groups.

Capacitance-voltage measurements provide evidence for the existence of an oxide layer in some, but not all, of the diodes investigated. It is thought that the presence of an oxide contributes to the non-ideal behaviour. In practice, the non-ideality of the devices studied here is useful for the following reasons:

(1) For an ideal Schottky diode, the maximum obtainable current in reverse bias is small. Thus, the electroluminescence from a reverse-biased device would be expected to be very small. This is not the case here and the reverse bias electroluminescence from non-ideal ZnS:Mn Schottky diodes is investigated in chapter 5.

(2) It turns out that the current in the forward direction is greater than would be expected for an ideal Schottky diode. This surprising result will be investigated in this section.

(3) There is strong evidence that the enhanced hole injection which is observed in forward biased electroluminescence is related to the presence of an oxide layer between the metal and the semiconductor.

It should be noted that there were considerable experimental problems associated with the ageing and irreproducibility of the devices. Ageing was a problem whenever large biases were applied in either direction and hence was a particular problem for measurements under reverse bias. It was sometimes found that on applying a reverse bias to a diode, the current would half in the time taken to take the reading. In spite of this, some diodes were produced which exhibited stable characteristics in both directions and all the diodes were comparatively stable in the forward direction, especially at low voltages. Only the forward characteristics will be considered in this section.

2.c.ii The Thermionic Emission and Diffusion Theories

The first attempts to explain the rectification and current-voltage characteristics of a metal-semiconductor interface were the diffusion theories of Mott[7] and Wagner.[33] They assumed that the current in the depletion region could be described by the equation

$$j = n e \mu \xi - D e \frac{dn}{dx} \qquad (2.20)$$

This equation was subject to the boundary conditions:

$$n = N_c \exp -\left(\frac{E_c - E_{Fs}}{kT}\right) \quad \text{at } x = 0$$

$$\text{and} \quad n = N_c \exp -\left(\frac{E_c - E_{Fm}}{kT}\right) \quad \text{at } x = l \qquad (2.21)$$

where x = 0, l refer to the depletion region edge and the metal-semiconductor interface respectively (see figure 2.17(a)). The Fermi

a) thermionic emission

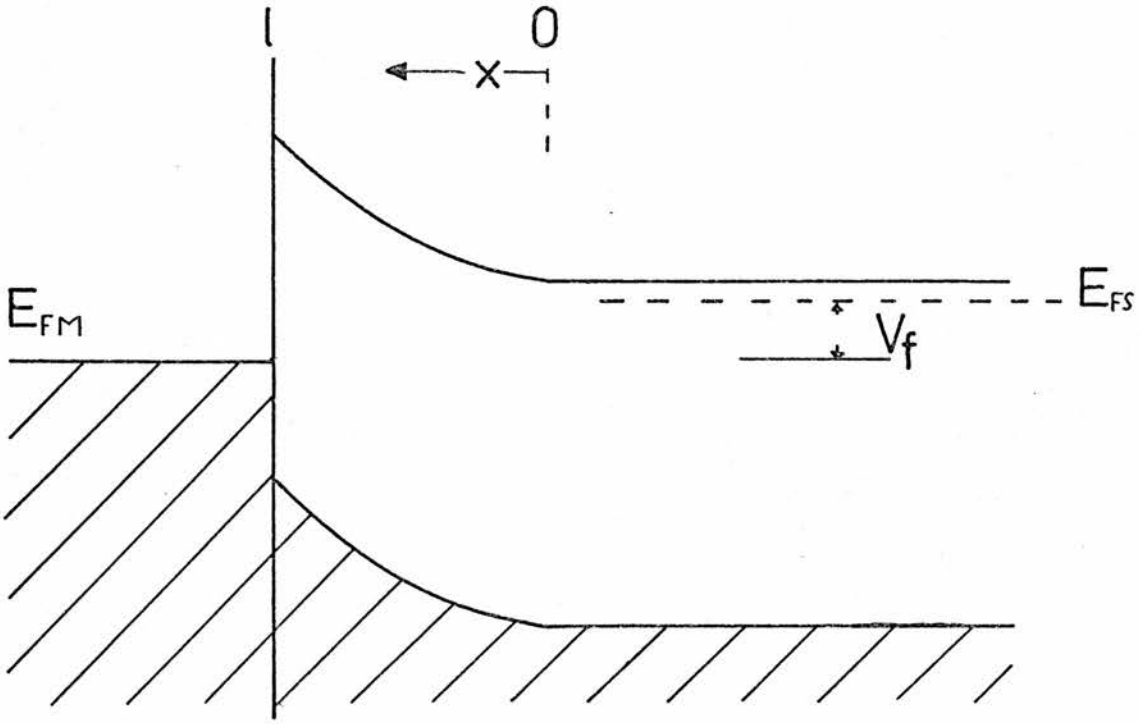

b) thermionic-field emission

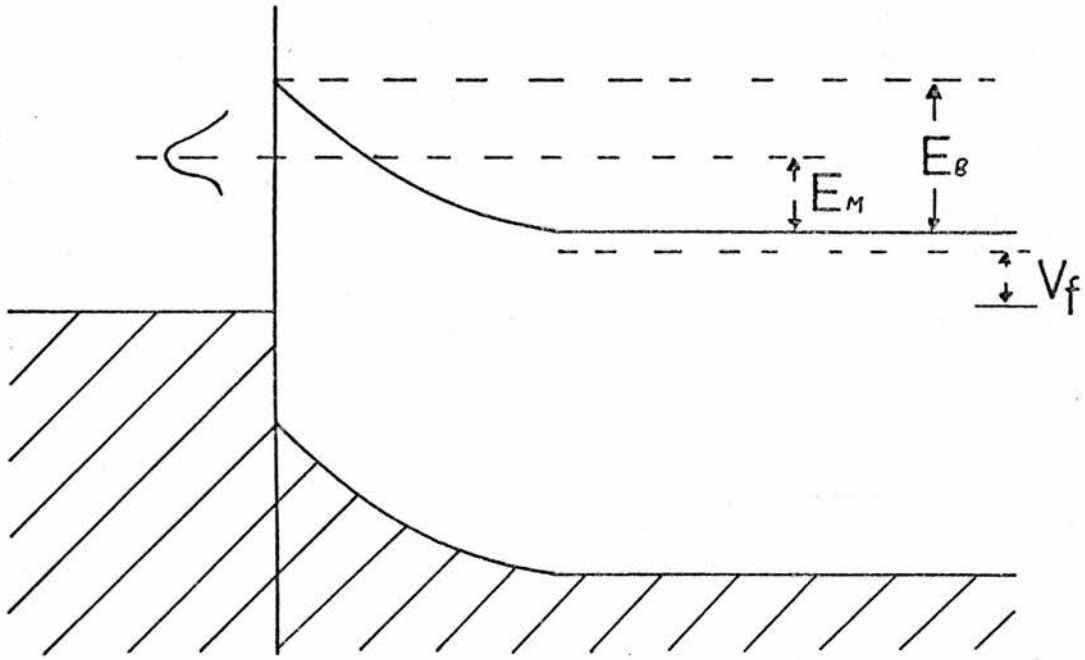

Figure 2.17 Two models for current transport in forward biased Schottky diodes.

energies E_{FM} and E_{FS} refer to the metal and semiconductor Fermi energies respectively.

Under zero applied bias, the two terms in equation (2.20) are equal and opposite resulting in no net current. Under a forward bias, the diffusion term dominates resulting in the electrons having a net drift velocity, defined by $v_d = j/ne$, against the built-in electric field. Simple kinetic theory arguments show that the maximum drift velocity which is possible under these circumstances is equal to $v_{th}/4$, where v_{th} is the thermal velocity of the electrons. In fact, equation (2.20) will not be valid unless its solution has the property that

$$v_d < v_{th}/4 \qquad (2.22)$$

throughout the entire depletion region. It turns out that this condition is not satisfied for most diodes which are encountered in practice. It will only be satisfied if the mobility is particularly low.

In the thermionic emission theory, it is assumed that the drift velocity at $x = l$ is the theoretical maximum of $v_{th}/4$. This will be the case provided that no electrons are reflected back from the metal. Then, the current density will be given by

$$j = n_l e v_{th}/4 \qquad (2.23)$$

where n_l is the concentration of electrons at $x = l$. If it is also assumed that the small current out of the semiconductor is insufficient to disturb thermal equilibrium, then the semiconductor Fermi level E_{FS} can be considered to extend up to the interface. Hence

$$n_1 = N_c \exp - \left(\frac{E_c(x=\ell) - E_{FS}}{kT} \right)$$

$$= N_c \exp - \frac{e}{kT} (\phi - V) \qquad (2.24)$$

Substituting (2.23) into (2.24) gives

$$j = \left(A^* T^2 \exp - \frac{e\phi}{kT} \right) \exp \frac{eV}{kT} \qquad (2.25)$$

where

$$A^* = \frac{m^*}{m} A = \left(\frac{4\pi m^* e k^2}{h^3} \right).$$

This equation gives the current flowing from the semiconductor to the metal. At zero applied bias, there will be an equal and opposite current from the metal to the semiconductor which implies that

$$j = A^* T^2 \exp - \frac{e\phi}{kT} \left(\exp \frac{eV}{kT} - 1 \right). \qquad (2.26)$$

This is the thermionic emission theory which was originally produced by Bethe.[34] Note that this theory contains two assumptions which will over-estimate the current produced by a given voltage. In obtaining equation (2.23), it was assumed that no electrons were reflected back from the metal. In addition, the concentration of electrons at the semiconductor surface n_1, was obtained by assuming that the electron quasi Fermi level remained constant across the depletion region. In general, this will tend to drop towards the metal Fermi level (as is assumed in the diffusion theory) making n_1 smaller.

Rhoderick[35] has recently analysed the conditions under which the thermionic emission theory is expected to hold. It has already been noted that the thermionic emission theory will only hold if the flow of electrons is too small to affect the thermal equilibrium. Rhoderick considers whether or not the electrons will be in thermal equilibrium at a distance of one mean free path (λ) from the interface. He argues that they will be in equilibrium, to a good approximation, provided that the barrier height is still greater than kT above the conduction band edge at that point. Thus, the thermionic emission theory is expected to hold provided

$$\Delta\phi = e\mathcal{E}_{max}\lambda > kT \qquad (2.27)$$

or equivalently

$$\mu\mathcal{E}_{max} > \bar{v}/3$$
$$\sim 9 \times 10^{16}\ cm^{-3} \qquad (2.28)$$

The electric fields considered here were normally greater than 10^5 V/cm (this assumes $N_d > 10^{16}\ cm^{-3}$) and hence

$$\mathcal{E}_{max} > 6 \times 10^7\ cm/s$$
$$> \bar{v}/3$$

It follows that this condition was satisfied for all the diodes considered here. Rhoderick goes on to show that the emission theory still holds, in practice, even for diodes which do not satisfy equation (2.28) and hence that this condition is too severe. In fact, Rhoderick was unable to find experimental evidence for any diode for which the diffusion theory was the better approximation to the I-V characteristics.

From the above discussion, diodes which have no interfacial layer would be expected to follow equation (2.26) whereas those with an intervening insulating layer would be expected to have a smaller current than would be predicted by this equation. Equation (2.26) approximates to equation (2.25) for $V > kT/e$, in which case $\ln I$ should vary linearly with V with a gradient of e/kT. This is plotted in figure 2.18 for a number of temperatures between 100 and 300 K for a ZnSe diode. It was found that although the current did vary exponentially with voltage, the reciprocal of the gradient E_o was not equal to kT/e. The variation of E_o with kT/e is plotted in figure 2.19 from which it can be seen that E_o was relatively insensitive to temperature. In fact, the diode of figures 2.18 and 2.19 showed the greatest variation of E_o with temperature of all the diodes studied. This diode had a C-V intercept of 1.2 volts which indicated that it had a thin oxide. The photoemission threshold was 1.345 eV.

Also plotted in figure 2.18 are the current-voltage characteristics which would be expected from equation (2.26) assuming the measured barrier height of 1.345 eV. At 300 K, the experimental characteristic is reasonably close to the theoretical one in that the gradients are similar, although the measured current is about a factor of 10^5 times too large. The theory is, however, particularly bad at describing the characteristics at 100 K. Here, the gradient is $2\frac{1}{2}$ times too small and the measured current about 10^{30} times too large (note that this is off the bottom of the scale in figure 2.18). The observation from figure 2.18 that the current-voltage characteristics are fairly insensitive to temperature suggests that the transport of electrons through the barrier may involve some form of tunnelling. This is considered in the next section.

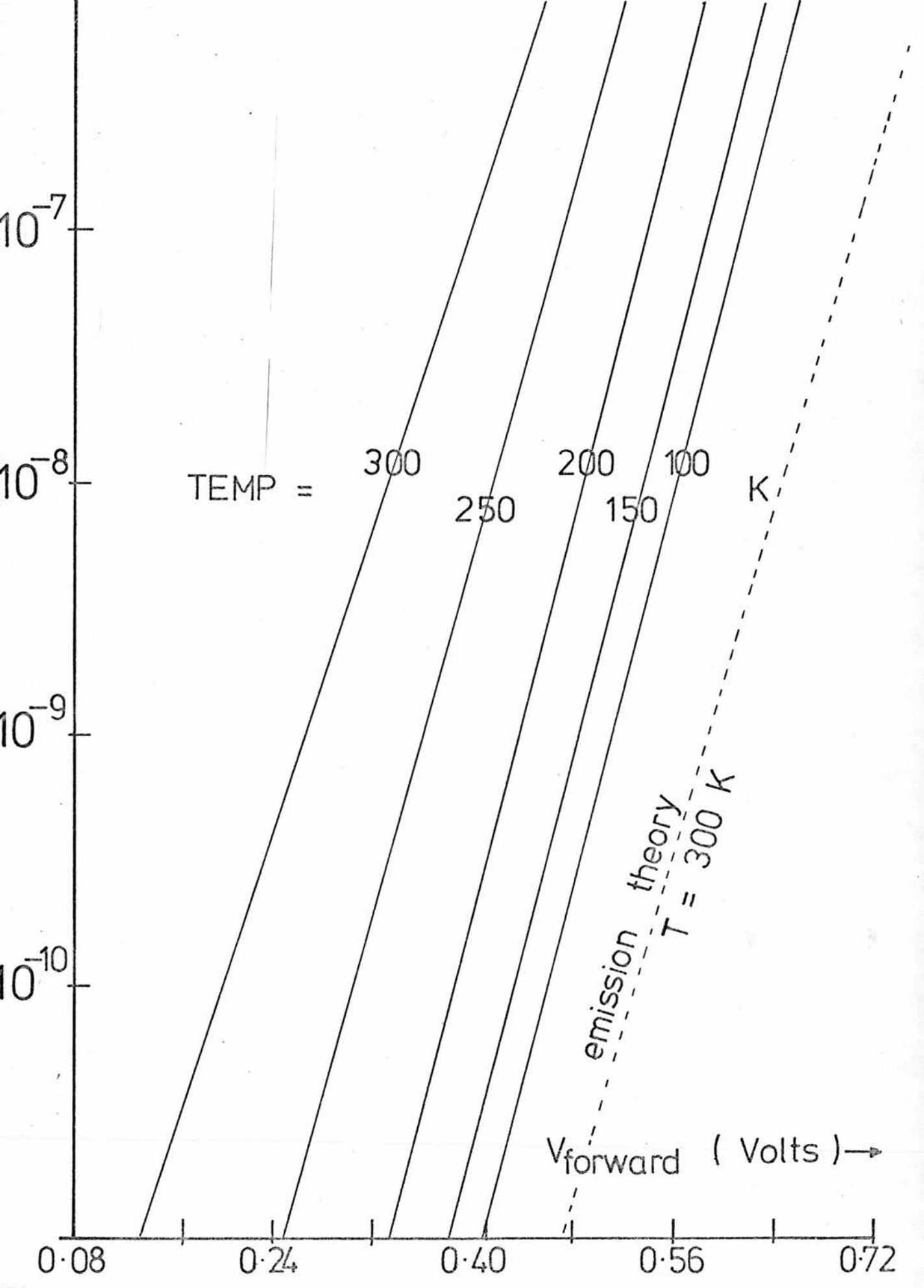

Figure 2.18 Current - voltage characteristics of an Au-ZnSe contact.

2.c.iii Thermionic Field Emission

The diode whose characteristics are plotted in figures 2.18 and 2.19 has a potential barrier to electrons of about 1.345 eV, as has been measured by photoemission. In the last section, it was estimated that at 100 K, the measured current flux through this diode was over 10^{29} times greater than the maximum that could be thermally emitted over a barrier of this height. It is therefore possible that this excess current is tunnelling through the barrier.

For a rectangular barrier of height ϕ and width W, the WKB approximation gives the tunnelling probability as

$$P = \exp - (\alpha \phi^{1/2} W) \qquad (2.29)$$

where

$$\alpha = 2 (2 m^*)^{1/2} / \hbar .$$

For a Schottky barrier, both the width and the average height of the barrier decrease with the energy of the electron above the semiconductor Fermi energy. Thus the tunnelling probability will increase very rapidly with $(E - E_{FS})$. On the other hand, the number of electrons will decrease very rapidly with $(E - E_{FS})$ since

$$n(E)\,dE \propto (E - E_c)^{1/2} \exp\left(\frac{E - E_{FS}}{kT}\right). \qquad (2.30)$$

Padovani and Stratton[36] have argued that the electron flux through the barrier, which is the product of these two quantities, should go through a sharp maximum at some particular energy E_m above the bulk semiconductor conduction band edge (see figure 2.17(b)) given by

$$E_m = E_B \cosh^{-2}\left(\frac{E_{00}}{kT}\right). \qquad (2.31)$$

where $$E_B = e\,(V_{do} - V)$$

and $$E_{oo} = \frac{e\hbar}{2}\left(\frac{N_d}{\varepsilon_o \varepsilon_s m^*}\right).$$

For the diode whose characteristics are plotted in figures 2.18 and 2.19, $N_d = 1.91 \times 10^{17}$ cm^{-3} and hence

$$\left(\frac{E_m}{E_B}\right) = 0.93 \text{ at } 300 \text{ K}$$
$$\left(\frac{E_m}{E_B}\right) = 0.57 \text{ at } 100 \text{ K}$$

Thus tunnelling through the barrier would certainly be expected to predominate at 100 K. By expanding the transparency of the barrier about E_m to first order, Padovani and Stratton were able to deduce that to this approximation, the current-voltage characteristics should be

$$J = J_s \exp\left(e V / E_o\right) \qquad (2.32)$$

where

$$E_o = E_{oo} \coth\left(E_{oo} / kT\right) \qquad (2.33)$$

and

$$J_s \sim \left(\frac{A^* \pi^{\frac{1}{2}} T E_{oo}^{\frac{1}{2}} e^{\frac{1}{2}} (V_{do} - V)^{\frac{1}{2}}}{k \cosh\left(E_{oo} / kT\right)}\right) \exp -e V_{do} / E_o \qquad (2.34)$$

The variation of E_o with temperature is predicted by equation (2.33) and this is compared with the experimental results in figure 2.19. The variation with temperature is found to be much less than is predicted by equation (2.31) (line No.3 in the figure). Also plotted in figure 2.19 is the variation which would be predicted by assuming a donor density of 15.3×10^{17} cm^{-3} (line No.1) and 12.3×10^{17} cm^{-3} (line No.2) instead of the measured density of 1.91×10^{17} cm^{-3}. The

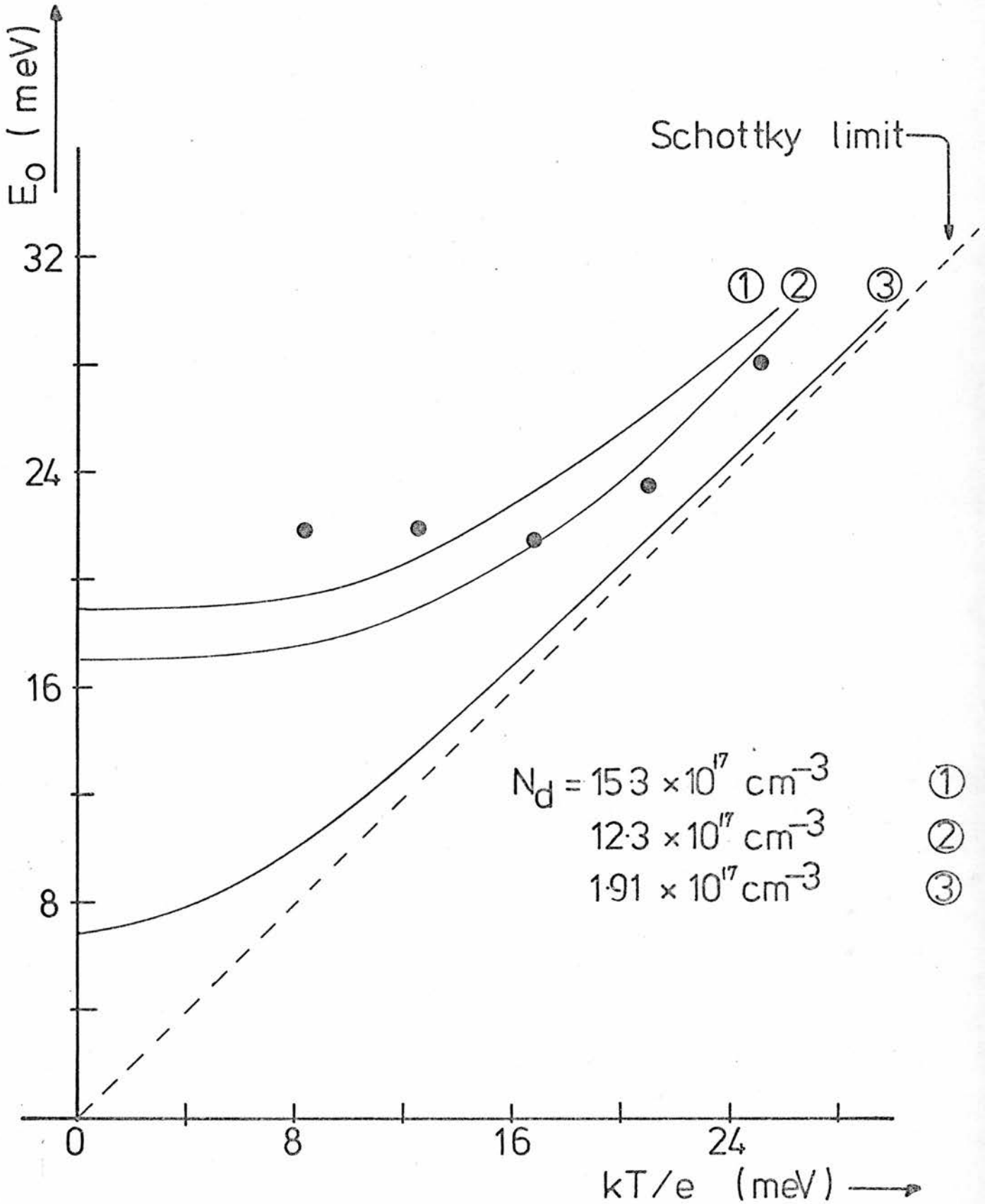

Figure 2.19 The variation of the forward I-V activation energy E_o with temperature. The solid lines give the theoretically expected variation for thermionic - field emission.

fit is not convincing for any of these lines and it is also unlikely that the measured donor density could be wrong by a factor of 10 (random errors usually amounted to less than 2%).

Examination of equation (2.32) suggests that plotting $\ln\left(J_s \cosh (E_{oo}/kT)/T\right)$ against E_o^{-1} should produce a straight line with a gradient V_{do}. This is plotted in figure 2.20 and gives a gradient of 1.0 ± 0.2 volts.

To summarise this section, the experimental current-voltage characteristics would appear to indicate that the electron transport was mainly by tunnelling. The results have been compared with what would be expected for an ideal Schottky diode with a barrier height equal to the measured height. The agreement is poor in that the theory predicts a larger variation with temperature than is observed. The agreement can be improved if it is arbitrarily assumed that the donor density is about ten times larger than is deduced from C-V measurements. Possible explanations will be postponed until after the current-voltage characteristics of diodes which have an interfacial layer have been discussed in the next section.

2.c.iv Effect of Oxide

The diode which was used to illustrate the various theories for the electron transport in the last two sections had a very low C-V intercept. It is thought that this indicates a thin oxide. It would be expected that for a given voltage, the current obtained for a diode with an oxide would be less than that from a diode with no oxide, i.e. some correlation between V_o and the current-voltage characteristics would be expected. However, it was found that, in general, the excess

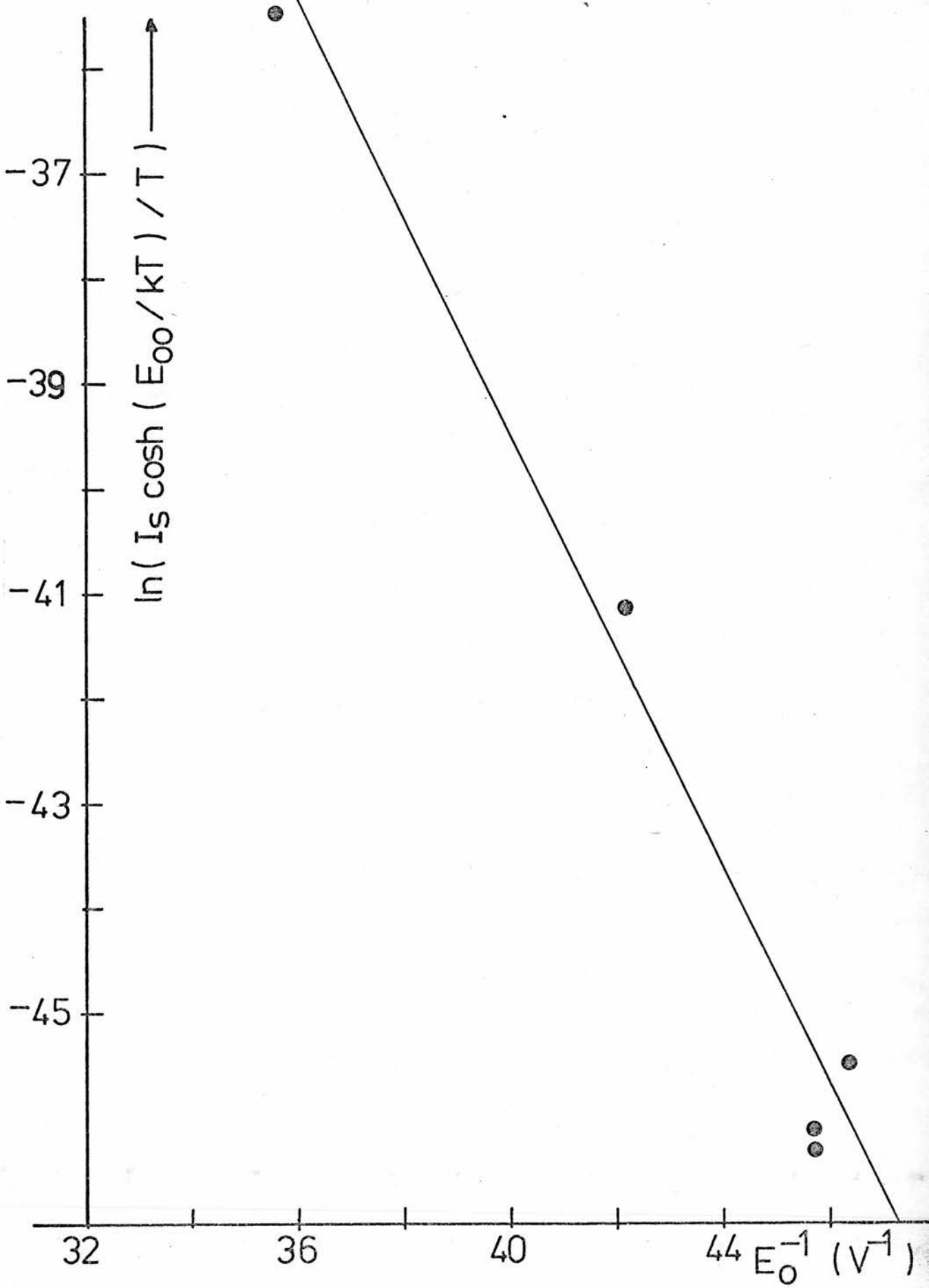

Figure 2.20 Temperature dependence of the saturation current plotted according to equation (2.33).

current was as large for diodes with as without an oxide. This lack of correlation can be seen from figure 2.21 where the room temperature current-voltage ideality factor n is plotted against the C-V intercept. The ideality factor is obtained by fitting the current-voltage measurements to a form

$$I = I_o \exp \frac{eV}{nkT} . \qquad (2.35)$$

It will be used here only as a convenient dimensionless parameter which describes the lnI against V gradient. Its use should not be taken as indicating any particular model for the departure from 'ideal' behaviour.

Figure 2.22 shows that n values between 1.25 and 6.5 were frequently observed and there is no strong correlation between n and V_o. In fact, it was always found that n was greater than 1, the lowest ever value being n = 1.12 which was deduced for the diode of figure 2.18 at room temperature.

It was initially thought that the excess current might be leaking through the surface rather than flowing through the contact. This was investigated by preparing a number of devices in which the Schottky contact was surrounded by a guard ring, as is shown in figure 2.22. The circuit ensures that the guard ring is kept at the same potential as the Schottky contact, but that only current flowing through the central Schottky contact is measured. The current-voltage characteristics plotted in figure 2.23 show that this diode was even more 'leaky' than the diode without the guard ring in figure 2.18.

Figure 2.21 Lack of correlation between the n-value and the C-V intercept.

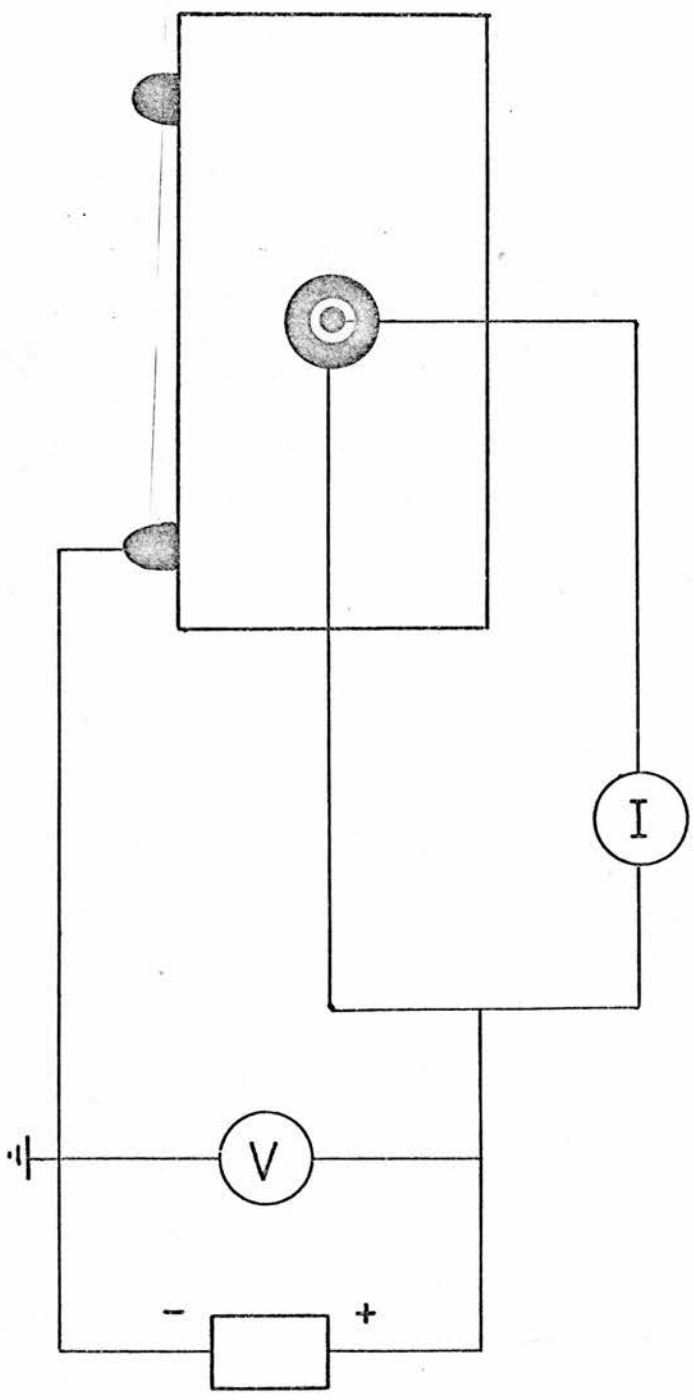

Figure 2.22 Use of guard ring to eliminate any surface current.

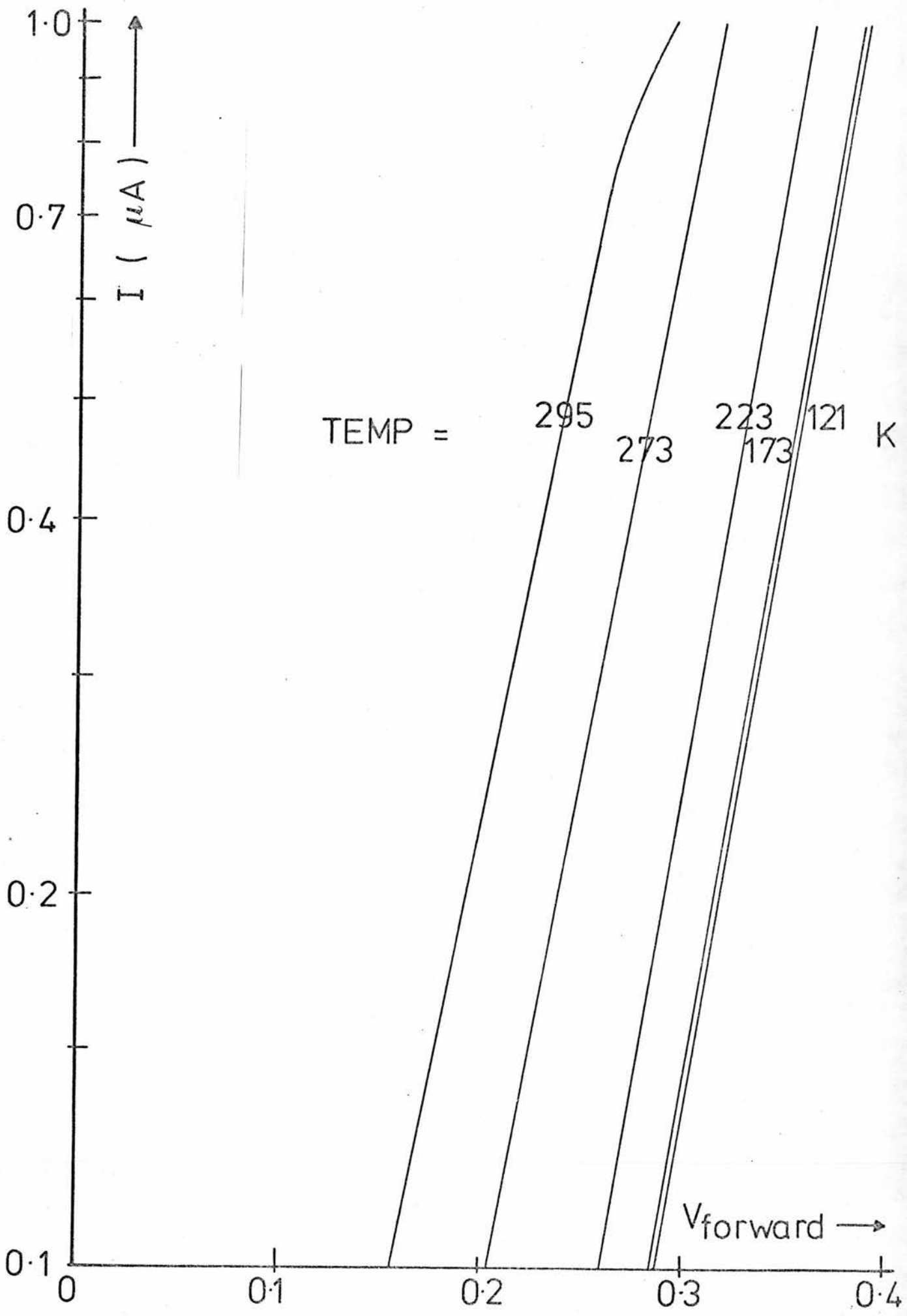

Figure 2.23 The I-V characteristics of diode with guard ring.

As a further check, the potential of the guard ring was varied between zero and that of the Schottky contact while the current was monitored. There was no detectable change in the current induced by changing the guard ring potential over this range. The chip used for these experiments was a single crystal of ZnSe. It was found that this diode lit up under large forward currents. The crystal was carefully polished to give two parallel, optically smooth surfaces and was remade to enable the distribution of light across the contacts to be observed. It was noted that most of the light was emitted at localised spots on the contact but that these spots were uniformly distributed rather than localised at the edge of the contact. It would therefore appear that the excess forward current was a 'bulk' rather than a surface leakage.

Finally, figure 2.24 gives some idea of the enormous range of I-V characteristics which could be produced. The I-V characteristics of all the diodes on this graph were fitted to a form (2.35) and $\ln I_o$ was plotted against 1/n. There is some evidence that a compensation law is operating in which $\ln I_o$ varies linearly with 1/n. This is equivalent to saying that all the I-V curves go through a common point at approximately I = 18 μA, V = 0.7 volts. The significance of this, if any, is not known.

2.c.v Possible Explanations

From the arguments given in the preceeding sections, it can be seen that the current density was too large to be explained by:

(a) thermionic emission over a barrier of the same height as is measured by photoemission experiments;

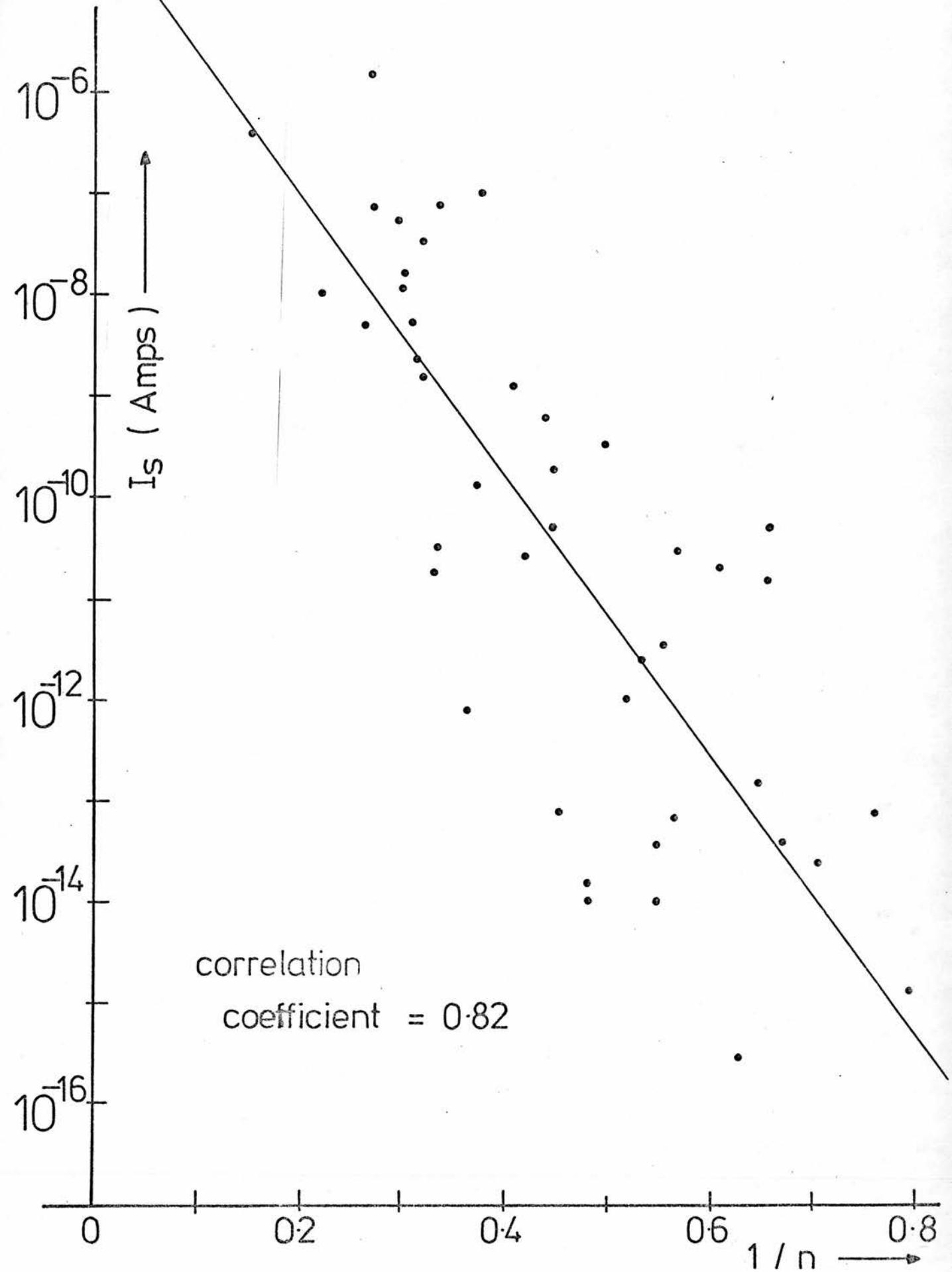

Figure 2.24 A compensation law for the forward I-V characteristics.

(b) tunnelling through a Schottky barrier, the width of which was the same as is measured by its capacitance.

It should be noted that both C-V measurements and photoemission measurements only give the averaged properties of the barrier. For example, if the diode is composed of two regions, 1 and 2, which have different donor densities, then the capacitance of region 1 will obey the equation

$$\frac{1}{C_1^2} = a_1^2 \left(V + V_0 \right)$$

whereas region 2 will obey

$$\frac{1}{C_2^2} = a_2^2 \left(V + V_0 \right)$$

Thus, the total capacitance of the diode will vary with voltage according to

$$\left(\frac{1}{C} \right)^2 = \left(\frac{1}{C_1} + \frac{1}{C_2} \right)^2$$

$$= \left(a_1 + a_2 \right)^2 \left(V + V_0 \right)$$

It follows that the donor density which would be deduced from the C-V gradient will be a weighted average of the densities in the two regions.

These ideas immediately lead to the following explanations:

(a) The crystals which were used in these experiments were non-uniformly doped, resulting in some regions having a much greater donor

density than the average which is deduced from C-V measurements. On the application of a forward voltage, the electrons will pour through these high density regions.

There are two main problems with this explanation. First of all, it is necessary to have a mechanism to explain the non-uniform donor density (see also section 4.e.ii). It is perhaps possible for donors to migrate to dislocations or grain boundaries in polycrystalline samples. In polycrystalline samples, it is also possible for different grains to have different donor densities. The second problem is that electrons which can tunnel through the depletion region will still have to get through the oxide. It is therefore unlikely that non-uniform doping can explain the observation of excess current in diodes with an oxide.

(b) The barrier height or oxide thickness was non-uniform. It has already been noted that the 'averaged' barrier height which was obtained from the photoemission threshold varied by over 400 meV from diode to diode. It is possible that the actual barrier height varied by much more than this over the contact area. After emission over the barrier, the electrons will still have to cross the oxide which will be considered to be a resistance in series with the diode. Thus, the equivalent circuit for the device would be a number of ideal Schottky diodes, each in series with a resistor as is shown in figure 2.25. The current-voltage characteristics of such a device will automatically have $n \geq 1$ and will be less sensitive to temperature.

As a crude illustration of these ideas, the current-voltage characteristics of an actual device were modelled using the circuit of figure 2.25. Figure 2.26 shows the current-voltage characteristics which were calculated from this circuit using the values given in table 2.1. An interesting feature of figure 2.26 is that although the current-voltage

equivalent circuit of MOS contact

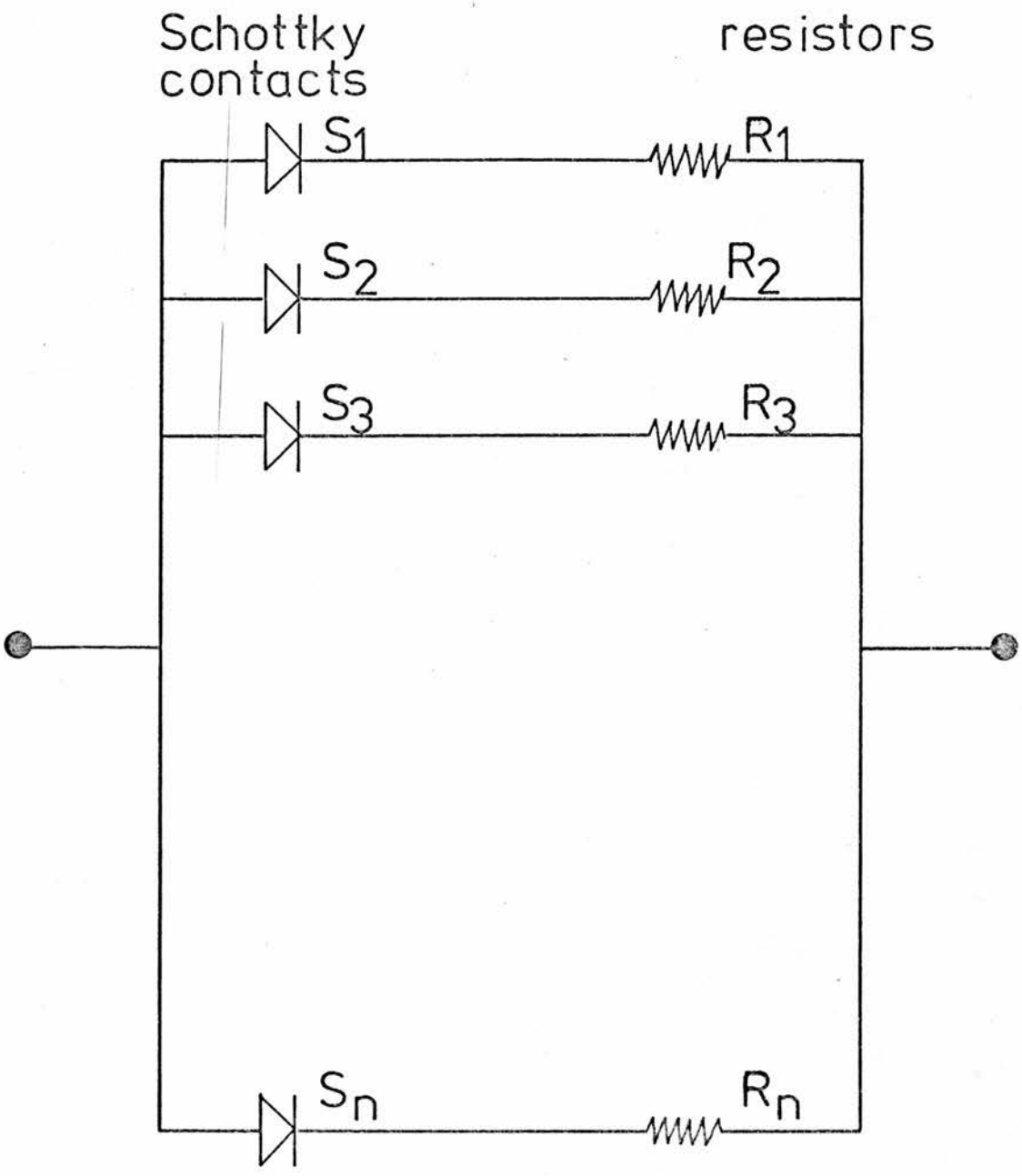

Figure 2.25 Proposed equivalent circuit for real MOS contact.

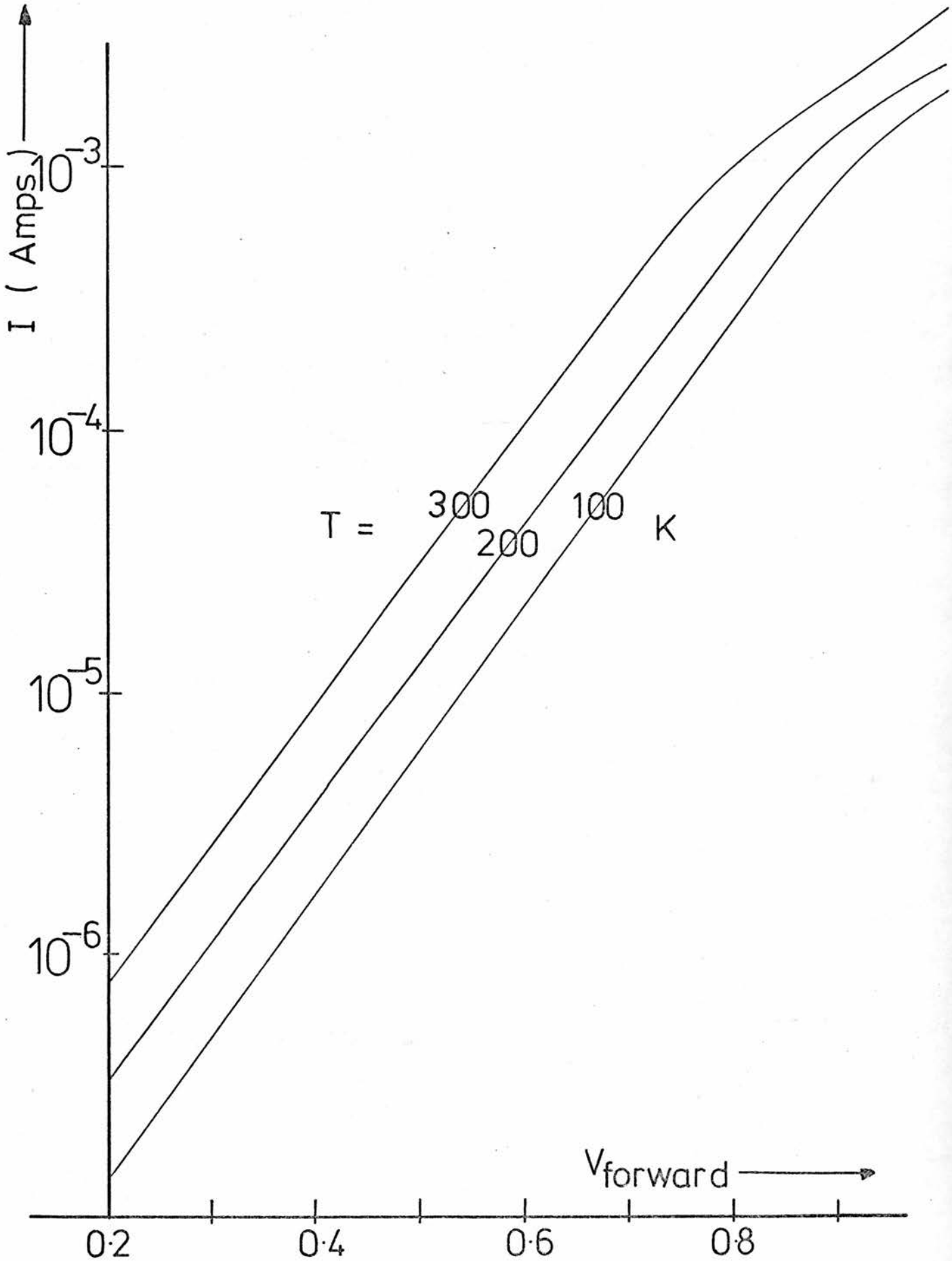

Figure 2.26 Theoretical I-V characteristics produced by the equivalent circuit of figure 2.25.

characteristics of the individual diodes are highly thermally activated the characteristics of the diodes in parallel are fairly insensitive to temperature. The reason for this is given below.

Consider a single diode of barrier height ϕ in series with a resistance R. For high applied voltages, the current-voltage characteristics will tend to

$$I = \frac{V - \phi}{R}$$

which is independent of temperature. The equivalent circuit contains a number of resistors R_1, R_2, R_3, etc. If the resistance decreases exponentially with ϕ an exponential current-voltage characteristic will result which is relatively insensitive to temperature. The correct variation of R with ϕ can be obtained by assuming that $R \propto 1/f$ (the fraction of the diode area) and that this fraction varies exponentially with the barrier height.

In conclusion, it should be noted that the observation of light spots in forward biased electroluminescence is consistent with a non-uniform contact. However, the nature of this non-uniformity is not known with any certainty.

2.d Summary

Au-ZnSe Schottky contacts display a lot of interesting physics which is still not properly understood. It has been shown that a wide range of behaviour can be produced by incorporating an oxide layer between the metal and the semiconductor. In section 2.b.ii.ii, a model of the barrier was proposed to explain the capacitance-voltage and photoemission experiments. This model will be used in chapter 3 in an attempt to understand the high hole injection efficiency which is observed in these devices.

TABLE 2.1

Computer Simulation of Current-Voltage Characteristics

Diode Number	Fraction of Diode Area	ϕ_o (V)	R (ohms)
1	3.4×10^{-8}	0.285	1.1×10^{5}
2	2.2×10^{-7}	0.495	7.0×10^{3}
3	1.7×10^{-6}	0.695	6.2×10^{2}
4	3.0×10^{-5}	0.895	1.0×10^{2}
5	1.7×10^{-4}	1.195	9.5×10^{0}
6	1.0×10^{0}	1.450	3.0×10^{0}

APPENDIX 2A

2A.i Variation of the Barrier Height with Applied Field

From the discussion in section 2.b, it can be seen that the barrier height which is measured in a photoemission experiment is equal to

$$\phi_{ox} = \phi_m' + V_{ox} \qquad (2A.1)$$

where V_{ox} is the voltage dropped across the oxide and the other symbols are as illustrated on figure 2.9.

The variation of this quantity with the depletion region field follows directly from the boundary condition at the semiconductor-oxide interface. Thus

$$\varepsilon_o \varepsilon_s E_s = \varepsilon_o \varepsilon_{ox} E_{ox} + \sigma_s \qquad (2A.2)$$

where E_s and E_{ox} are the electric fields in the semiconductor and oxide respectively and σ_s is the charge on the surface states. Assuming that the surface state quasi Fermi level is pinned to the metal Fermi level, then the surface charge is given by

$$\sigma_s = -q D_s \left(\phi_m' - V_{ox} - \chi_s' - E_g - \phi_o \right) \qquad (2A.3)$$

This equation can be obtained by adding the various energies in figure 2.9. Substituting this into equation (2A.2) and putting $E_{ox} = -V_{ox}/\delta$ gives

$$\varepsilon_s E_s = \frac{\varepsilon_{ox} V_{ox}}{\delta} - q D_s \left(\phi_{ms} + V_{ox} - (E_g - \phi_o) \right) \qquad (2A.4)$$

where

$$\phi_{ms} = \phi_{m}' - \chi_{s}' \quad .$$

Solving equation (2A.4) for V_{ox} and substituting this into equation (2A.1) gives

$$\phi_{ox} = \phi_{m} + \frac{\alpha}{1+\alpha}\left(E_g - \phi_o - \phi_{ms}\right) - \left[\frac{\varepsilon_s}{\varepsilon_{ox}}\frac{\delta}{(1+\alpha)}\right] E \qquad (2A.5)$$

where

$$\alpha = \ell D_s \delta / \varepsilon_o \varepsilon_{ox} \quad .$$

This shows that the variation of the barrier height with electric field is

$$\Delta\phi = \frac{\varepsilon_s}{\varepsilon_{ox}}\frac{\delta}{(1+\alpha)} E_s \qquad (2A.6)$$

$$= -\left[\frac{\varepsilon_s \varepsilon_o}{\varepsilon_o \varepsilon_{ox} + \ell D_s \delta}\right] .$$

2A.ii Density of Surface States Required to Reverse the Oxide Electric Field

If the oxide field and the voltage drop across the oxide are zero, the boundary condition (2A.2) becomes

$$\varepsilon_o \varepsilon_s E_s = \sigma_s \qquad (2A.7)$$

where

$$\sigma_s = -\ell D_s \left(\phi_{ms} - (E_g - \phi_o)\right) \qquad (2A.8)$$

The semiconductor electric field E_s is related to the built-in voltage V_{do} by

$$E_s = \left(\frac{2 N_d \varrho}{\varepsilon_o \varepsilon_s} \right)^{\frac{1}{2}} V_{do}^{\frac{1}{2}} \quad (2A.9)$$

Combining equations (2A.7), (2A.8) and (2A.9) and re-arranging gives

$$D_s = \left(\frac{2 \varepsilon_o \varepsilon_s V_{do}}{\varrho} \right)^{\frac{1}{2}} \frac{N_d^{\frac{1}{2}}}{((E_g - \phi_o) - \phi_{ms})} \quad (2A.10)$$

Putting

$$\phi_o = 0.4 \text{ eV}$$
$$\phi_{ms} = 1.2 \text{ eV}$$
$$V_{do} = 1.4 \text{ eV}$$

gives

$$D_s \sim \left(3.14 \times 10^3 \times N_d^{\frac{1}{2}} \right) \text{ cm}^{-2} \text{ eV}^{-1} \quad (2A.11)$$

APPENDIX 2B

Photoemission Across a Thin Potential Barrier

The purpose of this section is to consider whether or not a thin oxide layer on a metal surface will be transparent to photo-electrons. Consider figure 2B.1. On illuminating the metal surface with monochromatic radiation, some photons will be absorbed, transferring their energy to an electron in the metal. If the oxide layer is very thick, then only electrons which have an energy greater than the barrier height can escape. If, however, the oxide layer is thin, there is a possibility that electrons which have less energy than the barrier height can escape by tunnelling through the oxide.

In the following, the total flux of photo-emitted electrons both through and over the barrier will be calculated for a barrier thickness of 20 Å and illustrated in a Fowler plot. This will be compared with what would be expected if the tunnelling flux had been neglected. Hence, it will be shown that an oxide of 20 Å behaves very much like a 'thick' oxide as far as photoemission is concerned.

It was stated in section 2.b.i.iii that the total flux over a barrier of height ϕ_o is given by

$$R \propto (h\upsilon - \phi_o)^2 \qquad (2B.1)$$

The energies of the emitted electrons will vary between 0 and $(h\upsilon - \phi_o)$. Let n(E)dE be the number of electrons emitted with energies between E and E + dE. The total flux is therefore given by

$$R = \int_0^{(h\upsilon - \phi_o)} n(E)\, dE \qquad (2B.2)$$

Equating this to equation (2B.1) and differentiating with respect to $(h\nu - \phi_o)$ gives

$$n(\varepsilon)\, d\varepsilon \propto \varepsilon\, d\varepsilon \qquad (2B.3)$$

where $\varepsilon = (h\nu - \phi_o)$. This function also gives the distribution of excited electrons as is shown in figure 2B.1. Let P be the probability that an electron with x directed energy ε can tunnel through the barrier. Then within the WKB approximation

$$\ln P = - \propto (\phi_o - (h\nu - \varepsilon))^{1/2} W$$

$$\text{for } h\nu > \phi_o + \varepsilon . \qquad (2B.5)$$

$$P = 1 \quad \text{for } h\nu < \phi_o + \varepsilon .$$

The total electron flux is therefore

$$R = \int_o^{h\nu} P(\varepsilon)\, n(\varepsilon)\, d\varepsilon . \qquad (2B.6)$$

Inserting the expressions for $P(\varepsilon)$ and $n(\varepsilon)$ into this equation gives

$$R \propto \int_o^{(h\nu - \phi_o)} \varepsilon\, d\varepsilon + \int_{(h\nu - \phi_o)}^{h\nu} \varepsilon \exp - \propto W (\phi_o - (h\nu - \varepsilon))^{1/2} d\varepsilon \qquad (2B.7)$$

above barrier tunnelling

$$= \tfrac{1}{2} (h\nu - \phi_o)^2 + \int_o^{\infty} \left[\frac{2}{(\propto W)^4} t^3 + \frac{(h\nu - \phi_o) 2t}{(\propto W)^2} \right] e^{-t}\, dt$$

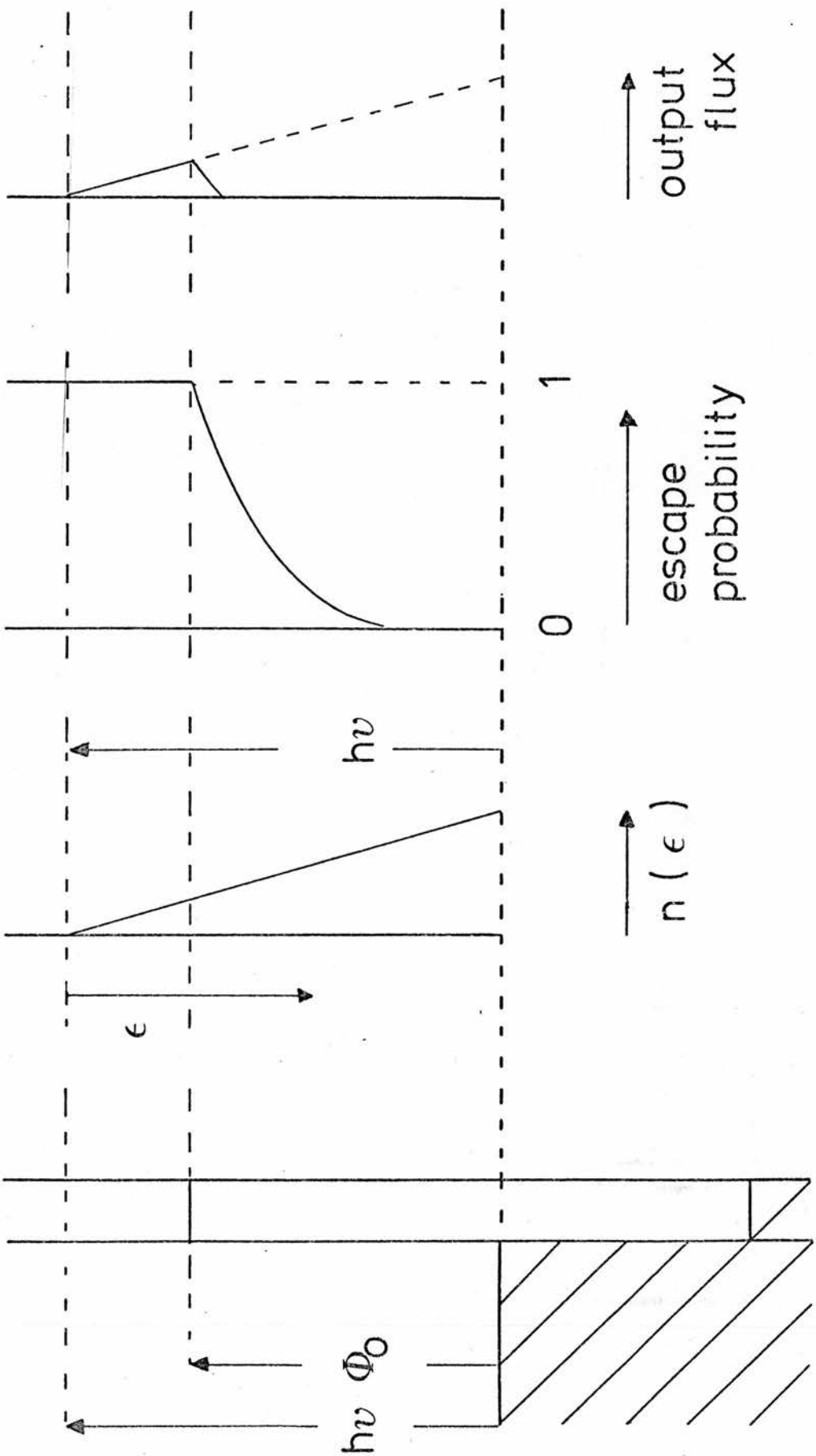

Figure 2B.1 Effect of a semi-transparent barrier on the flux of photo - emitted electrons.

by putting $t = \alpha W(\phi_o - (h\upsilon - \varepsilon))^{\frac{1}{2}}$ in the second integral and setting the upper limit to infinity. Thus

$$R = \tfrac{1}{2}(h\upsilon - \phi_o)^2 + \left[\frac{2}{(\alpha W)^4} 3! + \frac{2(h\upsilon - \phi_o)1!}{(\alpha W)^2}\right] \quad (2B.8)$$

Taking $m^*/m = 0.25$, $W = 20$ Å and writing $x = h\upsilon - \phi_o$ gives

$$R = \underbrace{\tfrac{1}{2}x^2}_{\text{above barrier}} + \underbrace{(0.02)x + (1.2 \times 10^{-3})}_{\text{tunnelling}} \quad (2B.9)$$

This is plotted in figure 2B.2 together with what would be expected in the absence of tunnelling. It can be seen that a 20 Å thick oxide behaves very much like a thick barrier. The photoemission intercept with tunnelling is about 0.03 eV below the actual barrier height and there is a low energy tail.

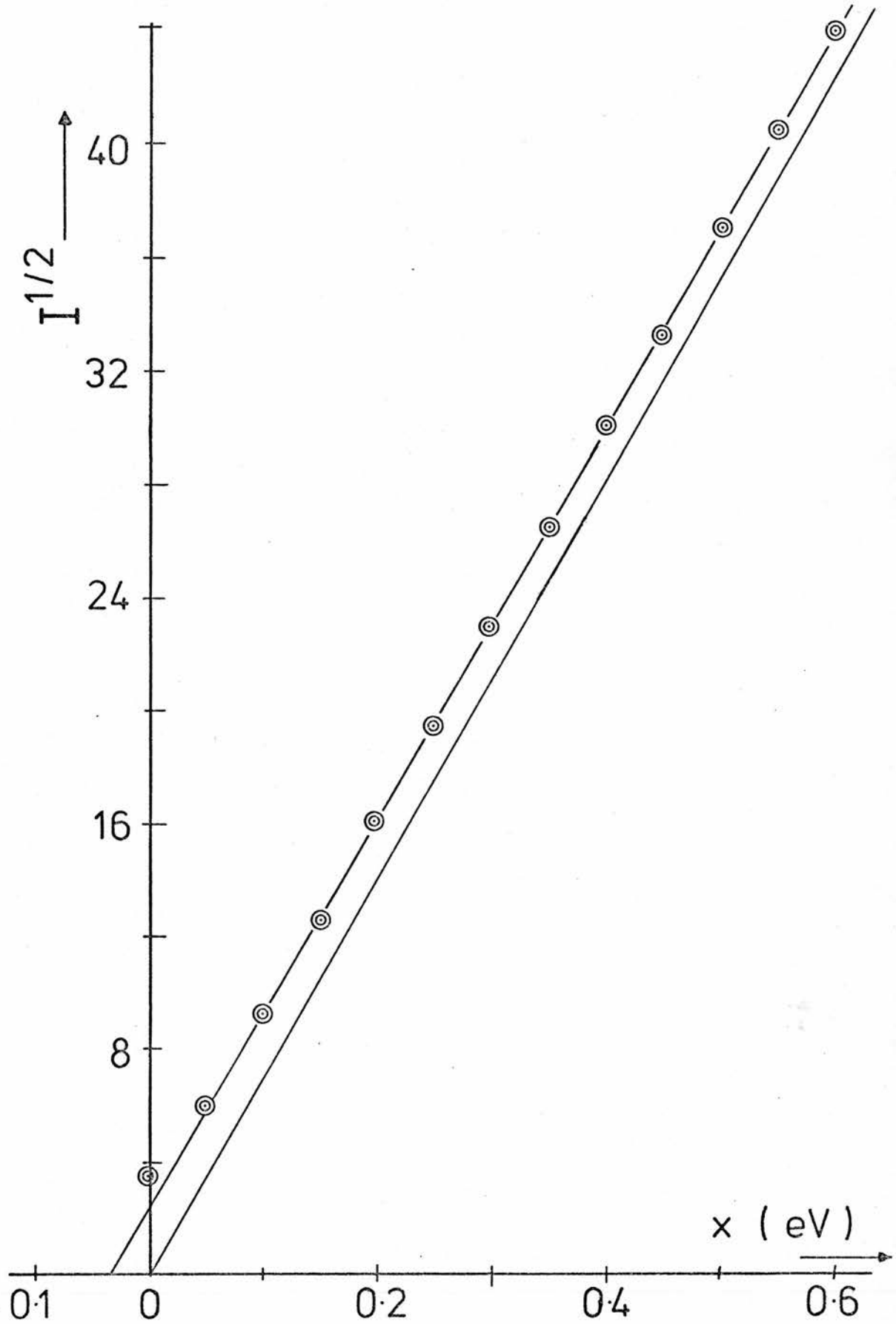

Figure 2B.2 Effect of tunnelling on the deduced Fowler plot. In the absence of tunnelling , the plot goes through the origin as shown.

CHAPTER 3

INJECTION LUMINESCENCE FROM Au-ZnSe CONTACTS

3.a Introduction

In chapter 2, the current-voltage characteristics of forward biased Au-ZnSe Schottky contacts were investigated. In n-type material, a forward bias induces an electron current from the semiconductor to the metal and a hole current from the metal to the semiconductor. Thus, a forward biased Schottky contact can be used to inject holes into n-type ZnSe. Light will be emitted from the junction provided that some of these holes recombine radiatively.

The electroluminescence from a forward biased contact on ZnSe has been investigated by Livingstone,[37] Woods,[38] Ryall[39] and Mach.[32] All the authors observe a substantially greater efficiency than would be expected from a direct metal-semiconductor contact. This is thought to be due to the presence of an interfacial layer between the metal and the semiconductor.

The most direct evidence for the luminescence being due to the recombination of electrons and holes in n-type material has been obtained by Ryall and Allen.[39] The spectra of a number of diodes were measured at temperatures between 100 K and 300 K and were found to contain a peak in the blue region of the spectrum which was due to the recombination of free excitons. It was, however, found that the electroluminescence of the diodes was predominantly yellow due to the injected holes recombining via some level in the band gap. This level appears in all the ZnSe produced in this laboratory and is possibly

either self-activated or due to unintentional copper contamination. A detailed investigation of this centre has been carried out by Grimmeiss, Ovren, and Allen[40] and also by Grimmeiss, Ovren, Ludwig and Mach.[41]

Livingstone, Turvey and Allen[37] have investigated the mechanism by which the holes are injected into the semiconductor. They find that electroluminescence is only observed from diodes which have an intermediate oxide layer. The maximum external quantum efficiency was about 10^{-6} and was independent of oxide thickness up to about 2,000 Å. The quantum efficiency at constant current was measured and found to be temperature independent between 100 K and 200 K. It follows that the hole injection efficiency is not expected to be strongly temperature dependent over this range. The electroluminescent efficiency drops rapidly above this temperature and Livingstone et al. believe that this is because the radiative efficiency is dropping. Thus, the hole injection efficiency is thought to be temperature independent over the range 100 K - 300 K.

To investigate the role of the oxide layer, a series of 24 diodes were made and forward biased to give a current of 100 mA. A note was taken of those diodes which lit up visibly under these conditions and the results are plotted in figure 3.1. It was found that with one exception, diodes would light up only if they had a C-V intercept which was greater than 1.64 volts. It can be seen from figure 2.10 that this corresponds to an oxide thickness of either 300 or 30 Å, depending on the surface state density.

Figure 3.2 shows the experimental variation of the quantum efficiency with voltage for a typical diode at 100 K and 300 K. The

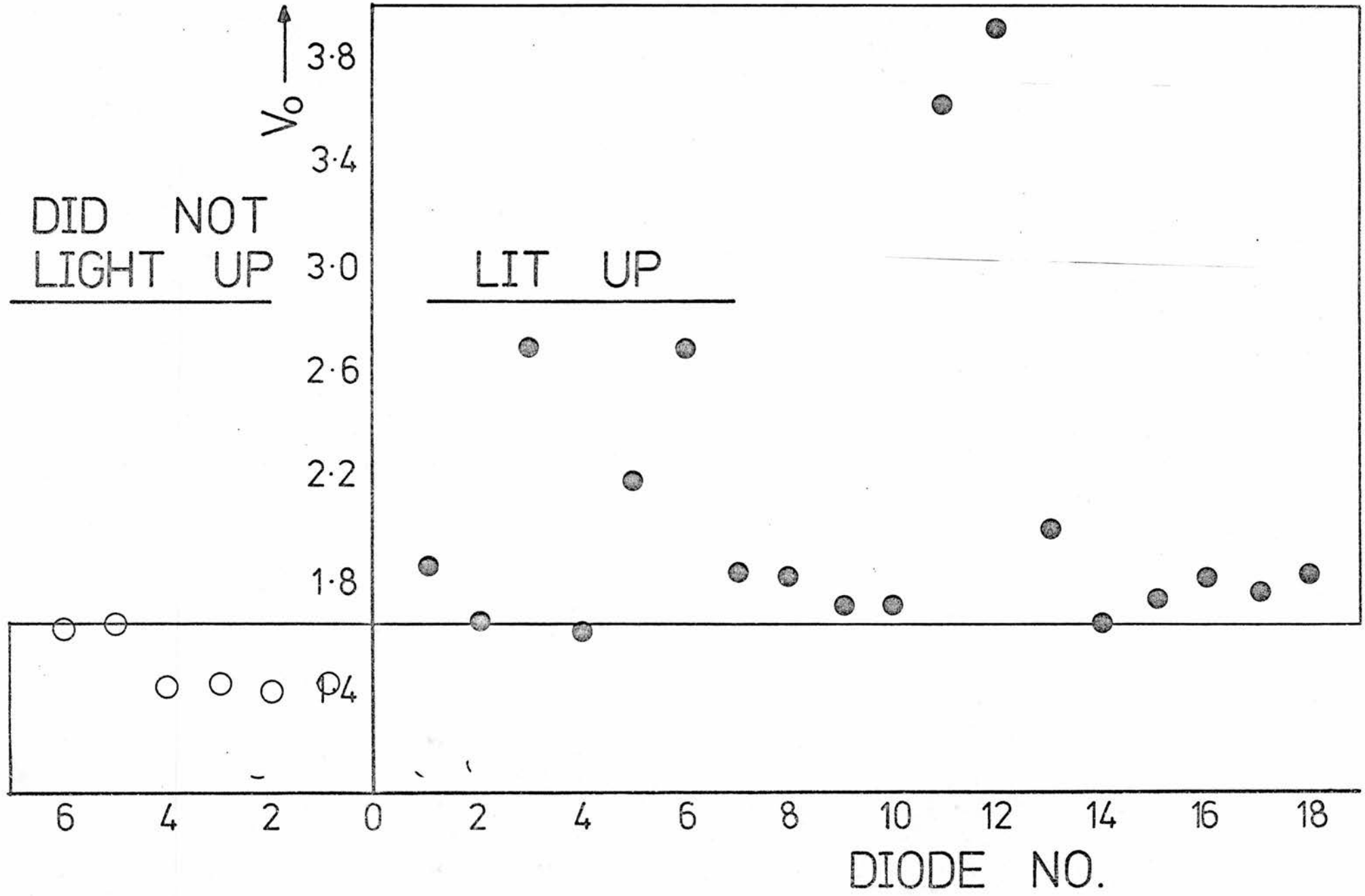

Figure 3.1 Importance of large V_o (i.e. large oxide) for good LEDs.

Figure 3.2 Experimental variation of the quantum efficiency with forward voltage.

shape of these curves was fairly similar for all the diodes tested. In general, the quantum efficiency began to increase rapidly at between 1.3 and 1.5 volts and then saturated. It was often found that the quantum efficiency dropped slightly at higher voltages. This was possibly due to thermal quenching of the radiative transitions because of sample heating.

3.b Mechanism of Hole Injection

3.b.i Diffusion Model

The simplest model for hole injection is that the holes diffuse in from the metal by a similar process to what occurs in a p-n junction. The basic model is illustrated in figure 3.3(a). If it is assumed that the hole concentration can be described by a hole quasi Fermi level (IMREF), then this will lie somewhere between the metal and the bulk semiconductor Fermi levels, as is shown in the figure.

Clearly, the maximum hole current which is consistent with this theory corresponds to the case when the hole Fermi level crosses both the oxide and the depletion region without change. In general, transport through the oxide would be expected to move the hole IMREF towards the bulk semiconductor, hence reducing the hole current.

The maximum possible hole concentration at the depletion region edge is given by

$$p_o = N_v \exp\left(\frac{E_v - E_{FM}}{kT}\right) = N_v \exp -\left(\frac{E_g - e V_f}{kT}\right) \qquad (3.1)$$

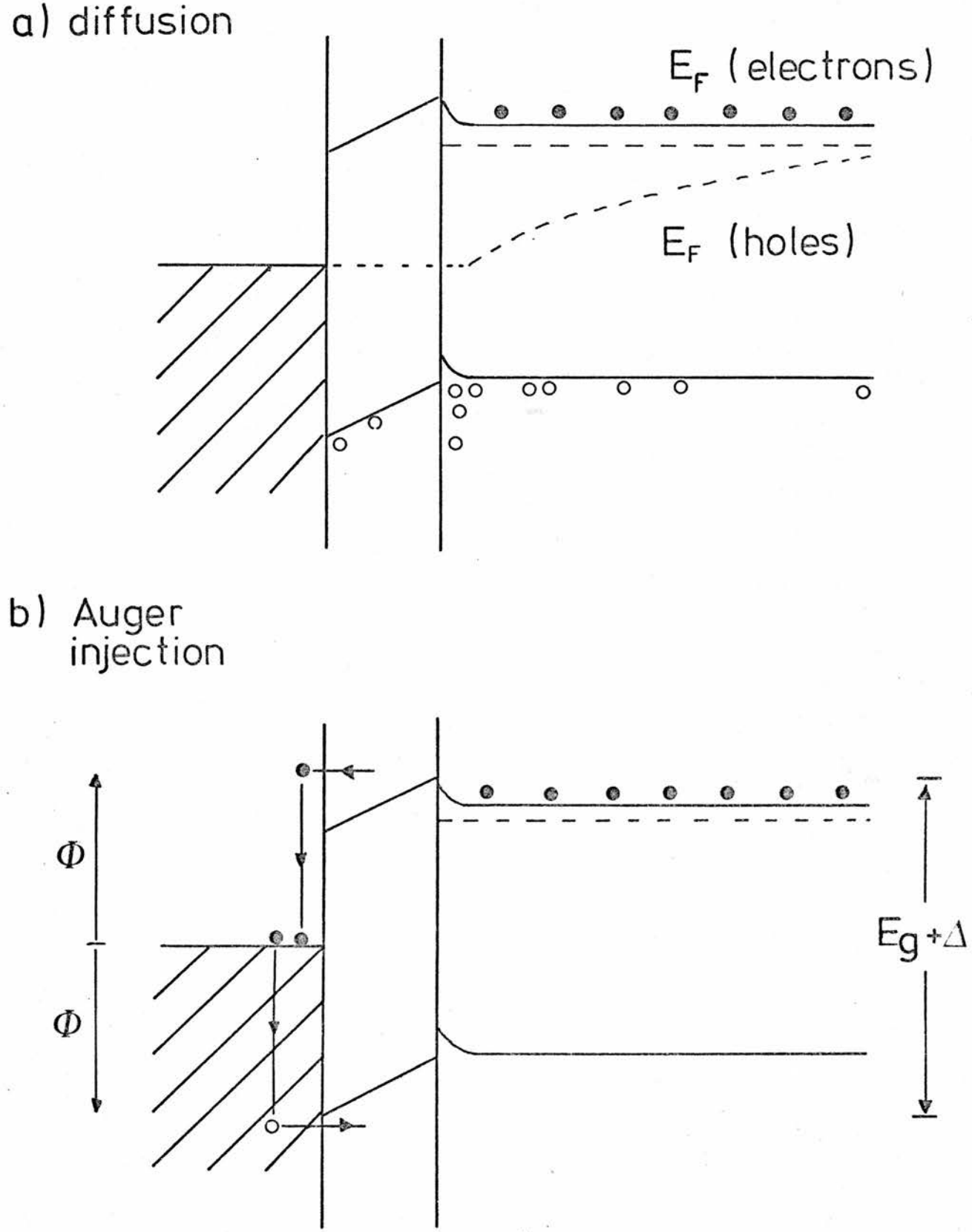

Figure 3.3 Models for hole injection via a MOS contact.

As a result of recombination, the hole density will decay into the semiconductor

$$p = p_o \exp - x/L_p \qquad (3.2)$$

resulting in a hole current of

$$J_p = -e D \frac{dp}{dx} = e \frac{D}{L_p} p_o = e \left(\frac{D}{\tau_p}\right)^{\frac{1}{2}} p_o . \qquad (3.3)$$

Combining equations (3.1) and (3.3) gives

$$J_p = \left(e \left(\frac{D}{\tau_p}\right)^{\frac{1}{2}} N_v \exp - \frac{E_g}{kT} \right) \exp \frac{e V_f}{kT} . \qquad (3.4)$$

This gives $I_p = 1.52 \times 10^{-13}$ A for a forward bias of 1.8 V assuming

$$D = 1 \text{ cm}^2/\text{s}^{26}$$
$$N_v = 1.16 \times 10^{19} \text{ cm}^{-3}$$
$$E_g = 2.72 \text{ eV}$$
$$\tau_p = 10^{-10} \text{ s}$$
$$V_f = 1.8 \text{ V}$$

This hole current would correspond to an injection efficiency of about 10^{-10} which is much less than the measured efficiency of 10^{-5}.[37] The model also has the problem that it predicts that the injected hole current should be strongly temperature dependent. For example, the injection efficiency at 100 K would be predicted to be about 10^{-43}. It

was found experimentally, that the hole injection efficiency was very insensitive to temperature, as has already been noted.

The above argument is based on the assumption that the holes do not recombine in the depletion region. The observation of exciton lines in the emission spectrum[39] shows that some of the holes must recombine in the bulk semiconductor. This is because excitons can not exist in the depletion region on account of the large electric field. However, as the exciton emission accounts for only a small fraction of the total emission, it could be argued that most of the electron-hole recombination is taking place within the depletion region.

There are two reasons why this is thought not to be the case.

1. The voltages which are necessary for forward biased electroluminescence will significantly reduce the depletion region width and possibly eliminate it altogether. It is shown in [42] that the voltage required to remove the depletion region is given by

$$V_E = \frac{1}{1+\alpha}\,\phi_{ms} + \frac{\alpha}{1+\alpha}\,(E_g - \phi_o) \qquad (3.5)$$

where

$$\alpha = e\,D_s\,\delta\,/\varepsilon_{ox}$$

D_s = density of surface states

and δ = oxide thickness

Clearly, there are two limiting cases. If there are no surface states, then $V_E = \phi_{ms}$. If there are a very large number, the semiconductor neutral level will tend to line up with the metal Fermi level, and hence $V_E = E_g - \phi_o$, as can be seen by letting α tend to infinity

in equation (3.5). If ϕ_o is estimated to be about 0.4 V[30] then

$$1.2 < V_E < 2.36 \quad . \tag{3.6}$$

Normally, α was estimated to be less than 1 which implies

$$1.2 < V_E < 1.78 \quad . \tag{3.7}$$

Thus, a forward bias of 1.8 V is expected to be sufficient to remove the depletion region from most of the diodes tested.

2. A simple calculation is given below which overestimates the hole current due to recombination in the depletion region. The predicted hole current is less than the diffusion current calculated previously.

The recombination rate is proportional to the product of the electron and hole concentrations, i.e.

$$\frac{d\,p(x)}{dx} = -k\, n(x)\, p(x) \quad . \tag{3.8}$$

In the following, the concentrations of electrons and holes at x will be overestimated in order to overestimate the recombination rate. Let the electron concentration at the depletion region edge be n_o. If the electron quasi Fermi level remains constant across the depletion region then

$$n(x) = n_o \exp - \frac{e\,V(x)}{k\,T} \quad . \tag{3.9}$$

In general, the electron quasi Fermi level will be expected to drop towards the metal quasi Fermi level. Thus, the electron concentration

at x will be less than or equal to the concentration predicted by equation (3.9) for all x .

Similarly, the hole concentration can be overestimated by assuming that the hole quasi Fermi level remains constant at the metal Fermi level across the depletion region. Hence

$$p(x) < p_o \exp\left(\frac{e V(x)}{kT}\right) . \qquad (3.10)$$

where p_o is the hole concentration which would be present at the depletion region edge if the hole quasi Fermi level remained constant across the depletion region. Clearly, equation (3.10) vastly overestimates the hole concentration as recombination will force the hole quasi Fermi level towards the bulk semiconductor level.

Substituting equations (3.9) and (3.10) into (3.8) gives

$$\frac{d}{dx} p(x) = -(k n_o) p_o = -\frac{p_o}{\tau_p} .$$

where τ_p is the hole lifetime in the bulk semiconductor. The hole current due to recombination in the depletion region is therefore given by

$$J_p = -e \frac{d}{dt} p \; W$$

$$= \left(e \frac{W}{\tau_p} N_v \exp -\frac{E_s}{kT}\right) \exp \frac{e V_f}{kT} \qquad (3.11)$$

Inserting the values used for equation (3.4) into equation (3.11) shows that $I_p = 1.52 \times 10^{-14}$ A at room temperature for each 100 Å of depletion region width. The temperature dependence of this

recombination current is, of course, similar to that of the diffusion current calculated previously. Thus, the large injection efficiency which is observed in practice can not be explained by a diffusion theory in which the recombination of the injected holes is mainly in the depletion region.

There is another problem with the diffusion models in that they predict that an oxide layer would tend to impede rather than assist hole transport. Card and Rhoderick[43] have recently explained how an oxide layer can increase the hole injection efficiency in Au-nSi contacts. In these MIS structures, the SiO_2 produces a large barrier through which both the electrons and holes have to tunnel. The basic model is that the electron current is reduced by having to tunnel through the oxide. The hole current remains almost the same as it is already diffusion limited. It follows that the ratio of the hole to the electron current will increase. If the oxide is made too thick, however, the holes will no longer be able to tunnel fast enough to maintain the diffusion current and hence the hole current will drop. Card and Rhoderick found that the maximum injection efficiency could be obtained with an oxide of about 30 Å thickness. The efficiency dropped rapidly for oxides thicker than 50 Å.

It is clear that this mechanism can not explain the large hole currents observed here since the process does not increase the hole current but only limits the electron current. In addition, the fact that little injection was observed for oxides thicker than 50 Å is inconsistent with the results quoted earlier.

3.b.ii Avalanche Breakdown

Mach[32] has proposed that the hole injection in ZnSe-Au contacts could be some form of avalanche breakdown in the oxide. This is an attractive idea which would involve electrons attaining sufficient energy to create electron-hole pairs in the oxide. There would be no barrier to the holes created in this manner from entering the bulk semiconductor. The threshold energy to produce electron-hole pairs in the oxide is expected to lie between 3.25 and 4.87 eV. (The energy gap of ZnO is about 3.25 eV at room temperature.) For the diodes considered here, electroluminescence is possible with an external voltage of less than 1.8 V. Capacitance-voltage measurements indicate that most of the applied voltage is dropped across the depletion region, rather than the oxide. It is therefore unlikely that avalanche breakdown can occur under the small voltages necessary for forward biased luminescence.

In addition, this model predicts that the breakdown voltage will depend strongly on the oxide thickness. This is not observed in practice.

3.b.iii Auger Injection

Another mechanism has been proposed by Watanabe, Chikamura and Wada[44] and has been considered by Lawther and Woods.[38] They suggest that some of the hot electrons entering the metal can impact excite deep electrons to leave holes close to the metal-oxide interface. This excess of holes will diffuse into the semiconductor, hence producing the injection luminescence.

Kanter[45] has investigated the mean free paths of 'slow electrons' in gold. He finds that for electrons with energy 2 eV above the Fermi energy, the electron-phonon mean free path is about 250 Å whereas the electron-electron mean free path is 400 Å. There is therefore a good chance that the incident hot electron will collide with a metal conduction band electron to produce a hot hole. Hole injection will occur if some of these holes have sufficient energy to cross the hole barrier, as is illustrated in figure 3.3(b). It is clear that the maximum hole energy which can be produced is equal to the energy of the incident electron, i.e. the electron barrier height ϕ .

Thus, efficient injection will occur if (figure 3.3(b))

$$2\phi > E_g + \Delta \qquad (3.12)$$

where Δ is the voltage dropped across the oxide.

The band gap of ZnO is 3.25 eV and ϕ was typically 1.5 eV. It follows that equation (3.12) is not satisfied for ZnO. However, it was noted in chapter 2 that the interfacial layer is probably a complex oxide containing selenium[15] and hence could have a smaller band gap than ZnO.

This model has the advantage that the hole injection efficiency would be expected to be temperature independent provided equation (3.12) was satisfied. The process is expected to be more efficient than the diffusion process. The oxide layer will have the following two effects. Firstly, it will produce a larger barrier height, making it easier to satisfy (3.12). The second effect will be to produce an electric field in the right direction to sweep the holes into the bulk semiconductor. If there is no oxide, the field will be in the opposite direction.

3.c Summary

A forward biased Au-ZnSe contact can be used to produce injection luminescence. The efficiency of these devices is considerably greater than would be predicted by a diffusion theory. It is not clear how the holes are injected although an Auger mechanism, as in section 3.b.iii, could account for most of the observed phenomena.

CHAPTER 4

AUGER QUENCHING IN ZnS:Mn

4.a Introduction

This chapter reports an investigation into the quenching of the yellow photoluminescence in ZnS:Mn which occurs when the material is made n-type conducting. The quenching is attributed to an Auger process in which an excited manganese atom can decay by transferring its energy to a conduction band electron instead of emitting a photon.

This process was first proposed by Allen, Ryall and Wray[46] who found that the manganese luminescence in ZnSe:Mn disappeared after the material had been Zn/Al treated to make it conducting. The absorption spectrum of the ZnSe:Mn was measured at helium temperatures at 1.5 cm^{-1} resolution before and after the Zn/Al treatment. It was found that the zero phonon line of the $^4T_1 - {}^6A_1$ transition which is characteristic of manganese in the d^5 configuration, was present in exactly the same position (2.23 eV) in both cases. No extra splitting of the absorption line was found. In addition, the intensity was unchanged. This shows that the absence of the manganese luminescence is not due to the manganese having been removed by the Zn/Al treatment and that the manganese is still present in the divalent state in the conducting material. Thus, the Auger process was proposed to explain the absence of the manganese luminescence.

The experimental results presented here support this explanation and enable the coupling constant γ between the manganese and the conduction band electrons to be estimated. In addition, the work

reported here is the first attempt to provide a quantitative description of this type of Auger effect.

4.b The Auger Process

At temperatures low enough for thermal quenching to be negligible, an excited manganese atom can decay either by emitting a photon or by an Auger process (see figure 4.1). The transition rate for the Auger process is expected to vary linearly with the electron concentration. It follows that the total transition rate is given by

$$\tau^{-1} = \tau_R^{-1} + \gamma n \qquad (4.1)$$

where

τ_R is the radiative lifetime

n is the concentration of conduction band electrons

γ is the coupling constant

The radiative efficiency η_R is equal to the ratio of the radiative rate to the total rate, and hence

$$\eta_R = \frac{\tau_R^{-1}}{\tau^{-1}} = \frac{1}{1 + \gamma n \tau_R} \qquad (4.2)$$

It should be possible to test this relationship by measuring η_R for a large number of samples with different concentrations of free electrons. Unfortunately, the technology of doping ZnS is not sufficiently advanced to enable this experiment to be carried out. Instead, it was possible to vary the electron concentration in each sample over 4 orders of magnitude by the thermal ionisation of shallow donors.

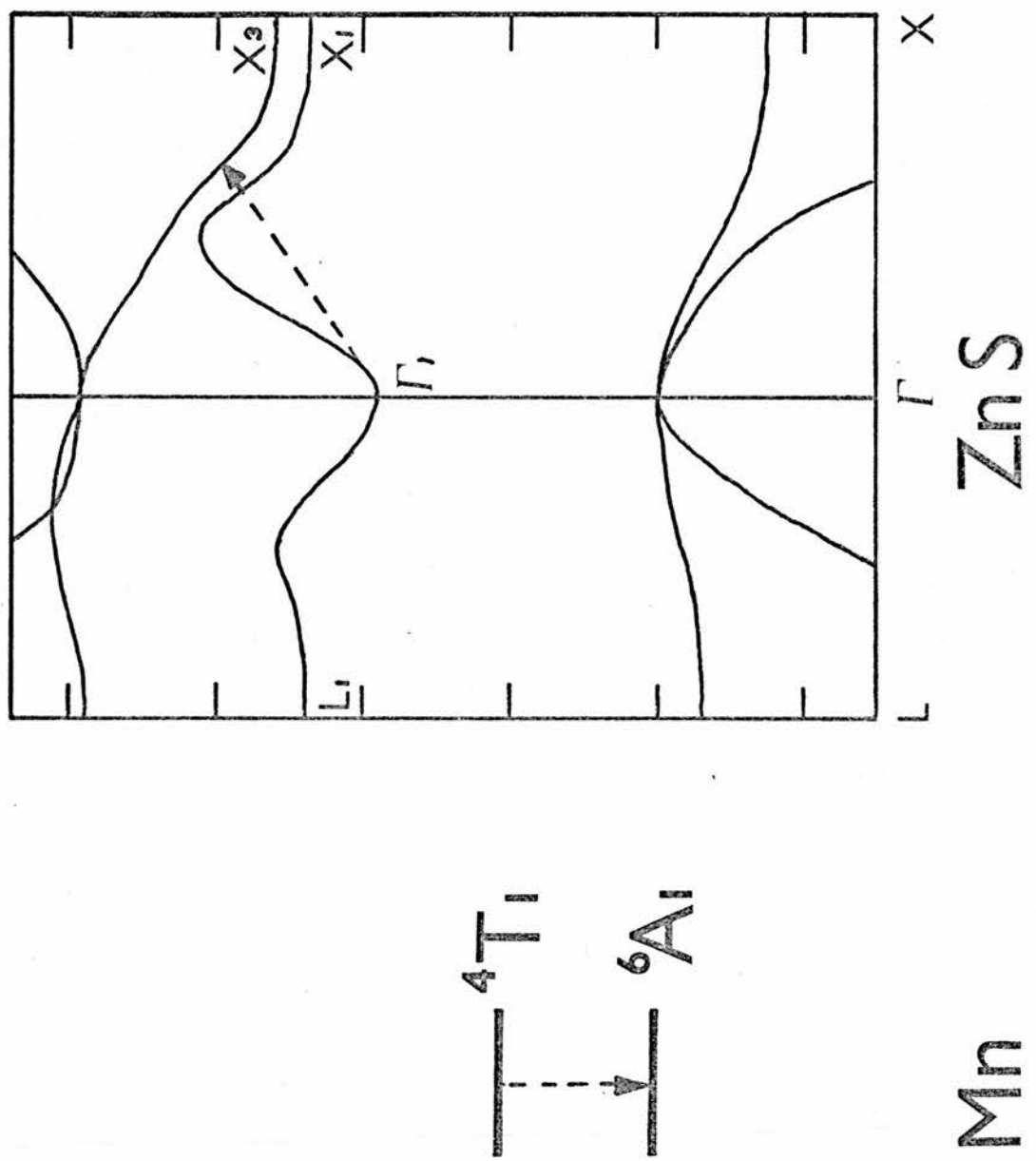

Figure 4.1 The Auger process in which an excited manganese centre gives its energy to a conduction band electron.

4.c Some Experimental Details

4.c.i Photoluminescence

The absorption spectrum of ZnS:Mn[47] is reproduced in figure 4.2, together with the assignment of the various peaks. In the photoluminescence experiments, the manganese was normally excited at 5 000 Å, which is at the peak of the $^6A_1 \rightarrow {}^4T_2$ absorption. The $^4T_2$ state decays non-radiatively and very rapidly to the $^4T_1$ first excited state which is responsible for the characteristic yellow luminescence. An Oriel interference filter with a band width of 50 Å was used in conjunction with a 50 W tungsten bulb to produce the 5 000 Å radiation. The 3 650 Å line from a mercury lamp was also used to excite the luminescence and gave similar results. The emitted radiation was normally chopped and synchronously detected using a S4 photomultiplier after dispersion in a Rank Hilger monochromator. Often, it was more convenient to use a second intereference filter centred at the peak of the manganese luminescence (5 800 Å) instead of the monochromator. Note that all the spectra in this thesis have been corrected for system response.

4.c.ii Materials Used

Auger quenching was investigated using ZnS from three different sources. Good quality crystals were grown from Optran grade B.D.H. ZnS powder by M. D. Ryall of this laboratory. After reacting the ZnS with about 0.5% MnS, the resulting ingot was grown using the iodine vapour transport method of Nitsche.[48] The same procedure was carried out on some crystalline ZnS from AWRE. In addition, some melt grown

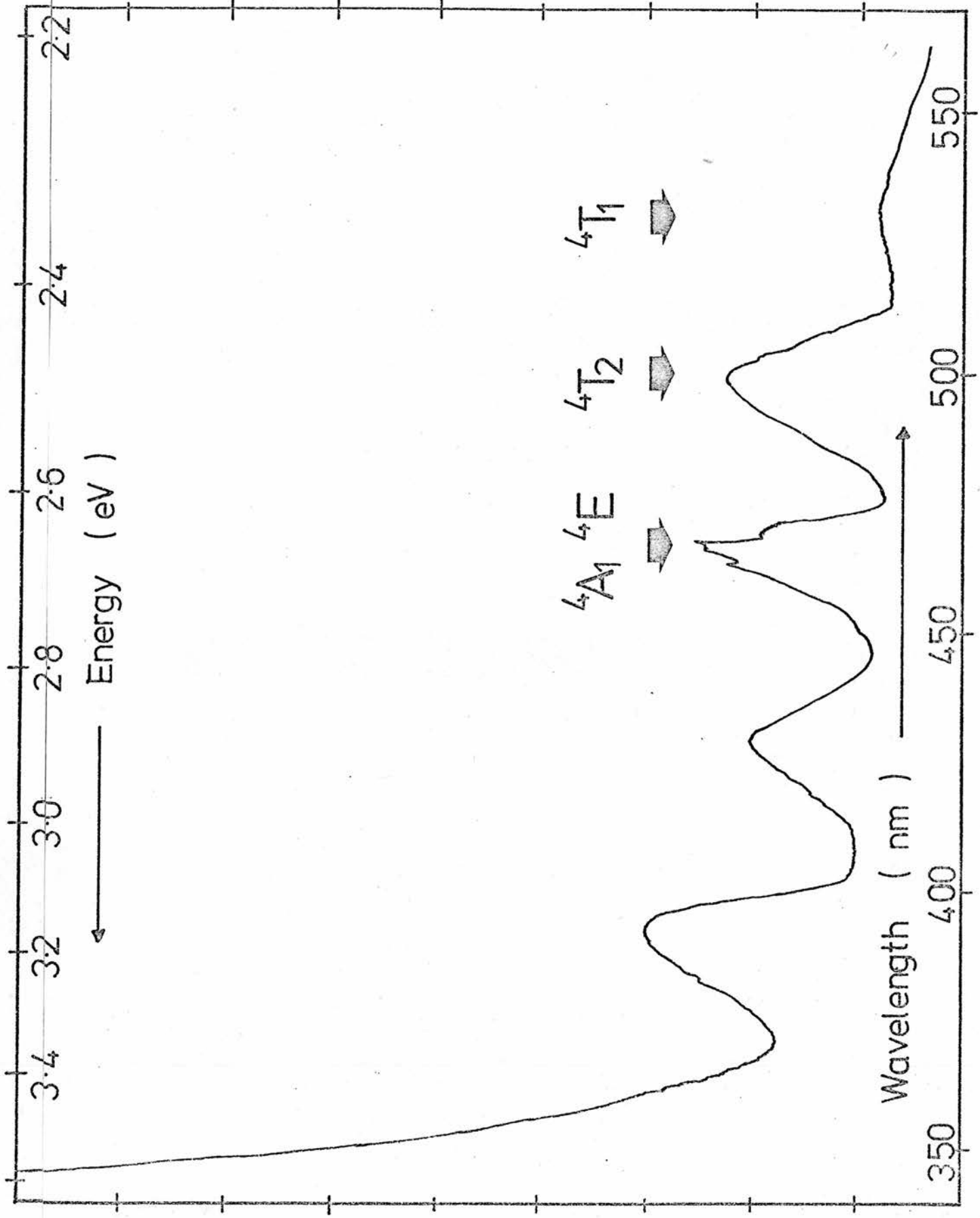

Figure 4.2 The absorbtion spectrum of ZnS:Mn.

ZnS:Mn containing 0.5% MnS was obtained from the Eagle Picher Company Limited.

Conducting ZnS was prepared using the zinc/aluminium treatment described by Kukimoto[49] in which a graphite boat was used to prevent the molten aluminium from reacting with the quartz furnace tube. The actual design of the boat, shown in figure 4.3, ensured that the ZnS remained submerged in the zinc/aluminium bath. About 2-4% aluminium was normally used and the tube was left at a temperature of 980°C in a vertical furnace for between 10 and 110 hours. After this time, the red hot tube was inverted (to separate the crystal from the molten zinc) and rapidly quenched in cold water.

Ryall and Allen[2] have found that a long treatment time or a high aluminium concentration leads to the ZnS being reduced to grey Al_2S_3 via the reaction

$$3\ ZnS + 2\ Al \rightleftharpoons 3\ Zn + Al_2S_3$$

Longer treatment times were obtained by adding a small amount of ZnS powder to try to prevent the crystal from being attacked. The successfulness of the method varied, although the most uniformly doped samples so far produced have used treatment times in excess of 100 hours.

It is not known exactly how a Zn/Al treatment produces conducting material. One possible process is that aluminium diffuses into the ZnS to fill up the zinc vacancies. The diffusion rate of aluminium in ZnSe has been measured by Bjerkland and Holwech.[31] Assuming that the diffusion rate in ZnS is roughly similar, it is very unlikely that substantial aluminium diffusion would be obtained with treatment times

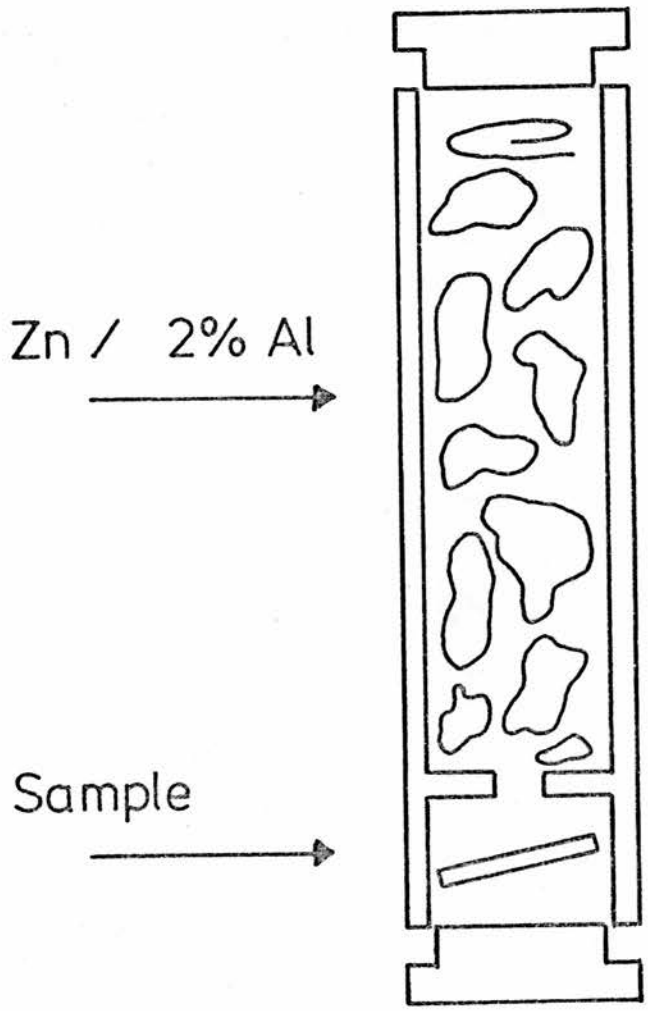

Figure 4.3 Graphite boat used for Zn/Al treatment.

as short as 10 hours. (It was pointed out in chapter 2 that the depth profile of the shallow donor concentration in ZnSe is inconsistent with aluminium diffusion.)

A more likely mechanism is that compensating zinc vacancies diffuse out of the material to leave an excess of donors. If this is the case, the saturation density of donors will depend on the concentration of impurities which have been unintentionally incorporated into the starting material. It is therefore possible that ZnS with a higher and more uniform donor density could be obtained by introducing aluminium at the growth stage, as is often done with ZnSe.

4.d Experimental Results

4.d.i Properties of the Insulating Material

Suitable starting material for investigating the Auger affect which was described in the introduction should have the following properties.

(A) The luminescence band due to the manganese $^4T_1 \rightarrow {}^6A_1$ transition should be strong and well separated from the other luminescence bands.

(B) The luminescence in the starting material should not be quenched over the temperature range of interest.

Unfortunately, the photoluminescence spectra of both the B.D.H. and the AWRE material had a strong band in the blue which overlapped the manganese band, especially at high temperatures. It was, however, sometimes possible to subtract off the contribution of this band.

The photoluminescence spectrum for the as-grown Eagle Picher material excited at 3 650 Å at 120 K is shown in figure 4.4(a). There is only one emission band between 4 000 and 8 000 Å. This should be compared with figure 4.4(b) which shows the corresponding spectrum for the same sample after going through a conductivity treatment. At the high energy end of the spectrum, there is a broad peak with a number of dips in it. These dips correspond well with the positions of the absorbtion peaks in figure 4.2 and are therefore due to self-absorption by the manganese. The manganese emission band in figure 4.4(b) appears broadened and shifted downwards in energy. This suggests that this band is the sum of two bands, the second of which has been introduced by the Zn/Al treatment. Fortunately, the second band does not appear to be excited with 5 000 Å radiation. In this case, the position of the emission peak is not affected by the Zn/Al treatment. However, the width of the luminescence band is about 2.5% greater in the conducting material.

The variation of the width of the manganese band with temperature can be fitted to the formula

$$W = W_0 \left(\coth \left(\frac{\hbar \omega_s}{2kT} \right) \right)^{1/2} \qquad (4.3)$$

For the insulating material, a good fit can be obtained over the whole range with $\hbar\omega_s$ = 38 meV (see figure 4.5). This can be compared with $\hbar\omega_s$ = 40.5 meV obtained by Vlasenko.[50] Equation (4.3) was obtained by assuming that the luminescent centre interacts only with phonons of one energy[51] and is not strictly applicable here.

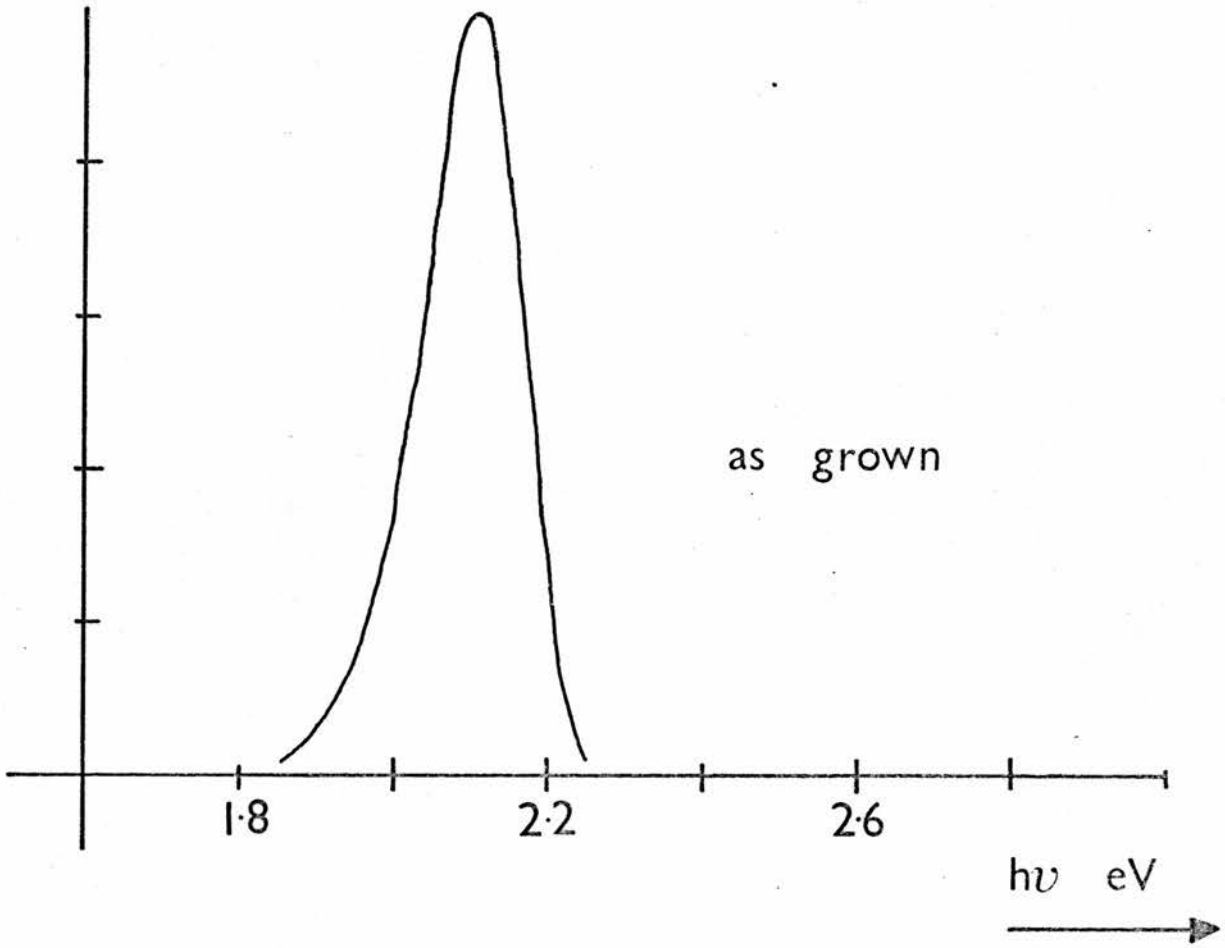

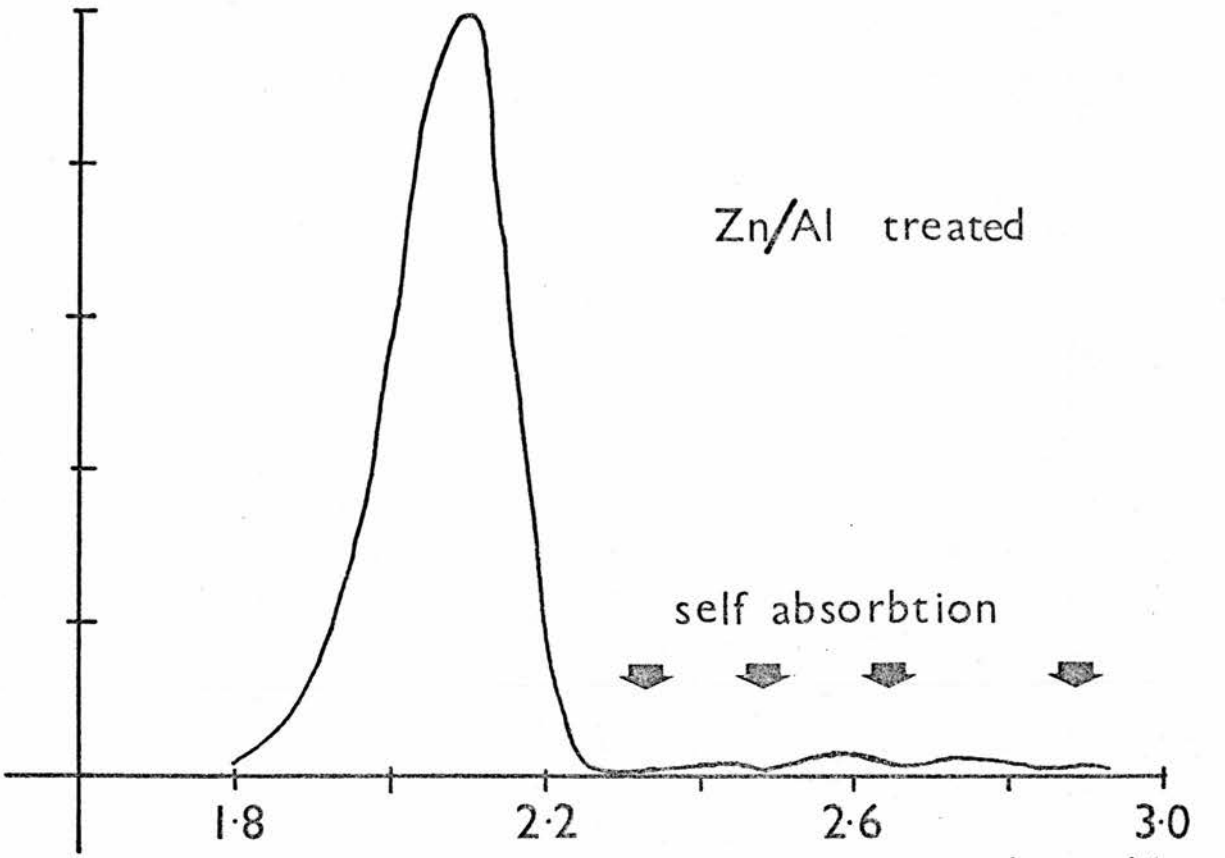

Figure 4.4 Photoluminescence spectrum of Eagle Picher ZnS:Mn excited at 3.4 eV. T = 120 K.

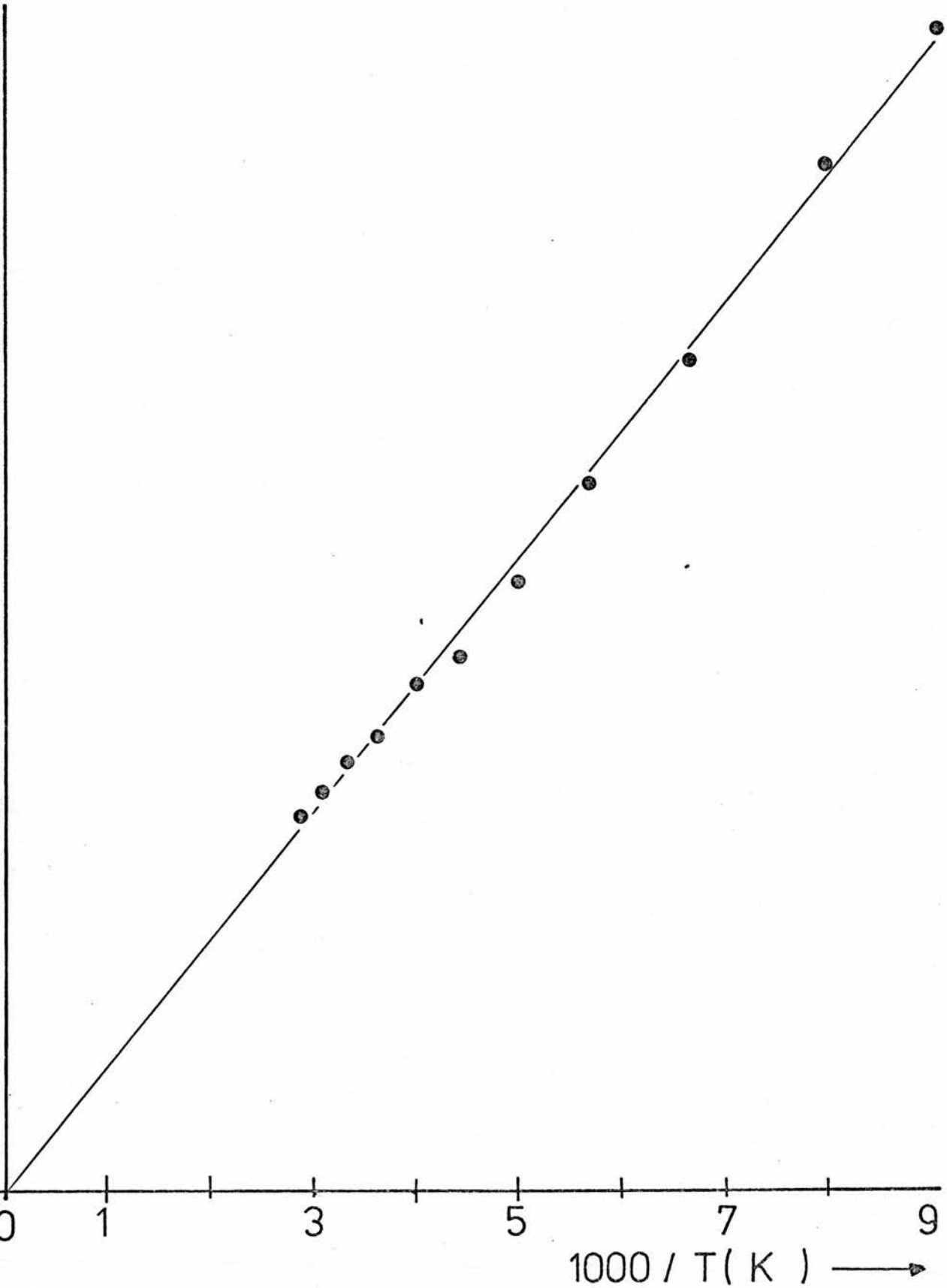

Figure 4.5 The variation of the width of the manganese emission peak with temperature plotted according to equation (4.3).

Figure 4.6 shows how the quantum efficiency of the manganese luminescence varies with temperature in the as-grown Eagle Picher material. It is evident that little quenching takes place below 370 K at which point the luminescence is strongly quenched. The solid line in figure 4.6 is a best fit of the form

$$\eta_{qu} = \frac{\eta_{qu}^{\,o}}{1 + C \exp - \frac{E_A}{kT}} \qquad (4.4)$$

with

$$C = 7.65 \times 10^5$$

$$E_A = 0.89 \text{ eV}$$

The decay of the luminescence was recorded using a boxcar to improve the signal to noise ratio. A typical trace is shown in figure 4.7 from which it can be seen that the decay is not a single exponential. A number of authors[52-53] have observed non-exponential decays in ZnS:Mn. The smaller time constants can either be due to the formation of manganese pairs or to manganese atoms in interstitial positions. As the difference between the time constants for manganese on different lattice sites is small, it is thought that the decay of the luminescence is non-exponential mainly because of the formation of exchange coupled pairs of manganese atoms.[47, 52]

The decay curve of figure 4.7 was analysed using the Manglesdorf method,[54] and it was found that after the initial sharp drop, the time constant tended to about 0.92 ms. This time constant is plotted as a function of temperature in figure 4.8 and remains constant to within experimental error. When the slow decay is subtracted from the total

Figure 4.6 Thermal quenching of the radiative efficiency in

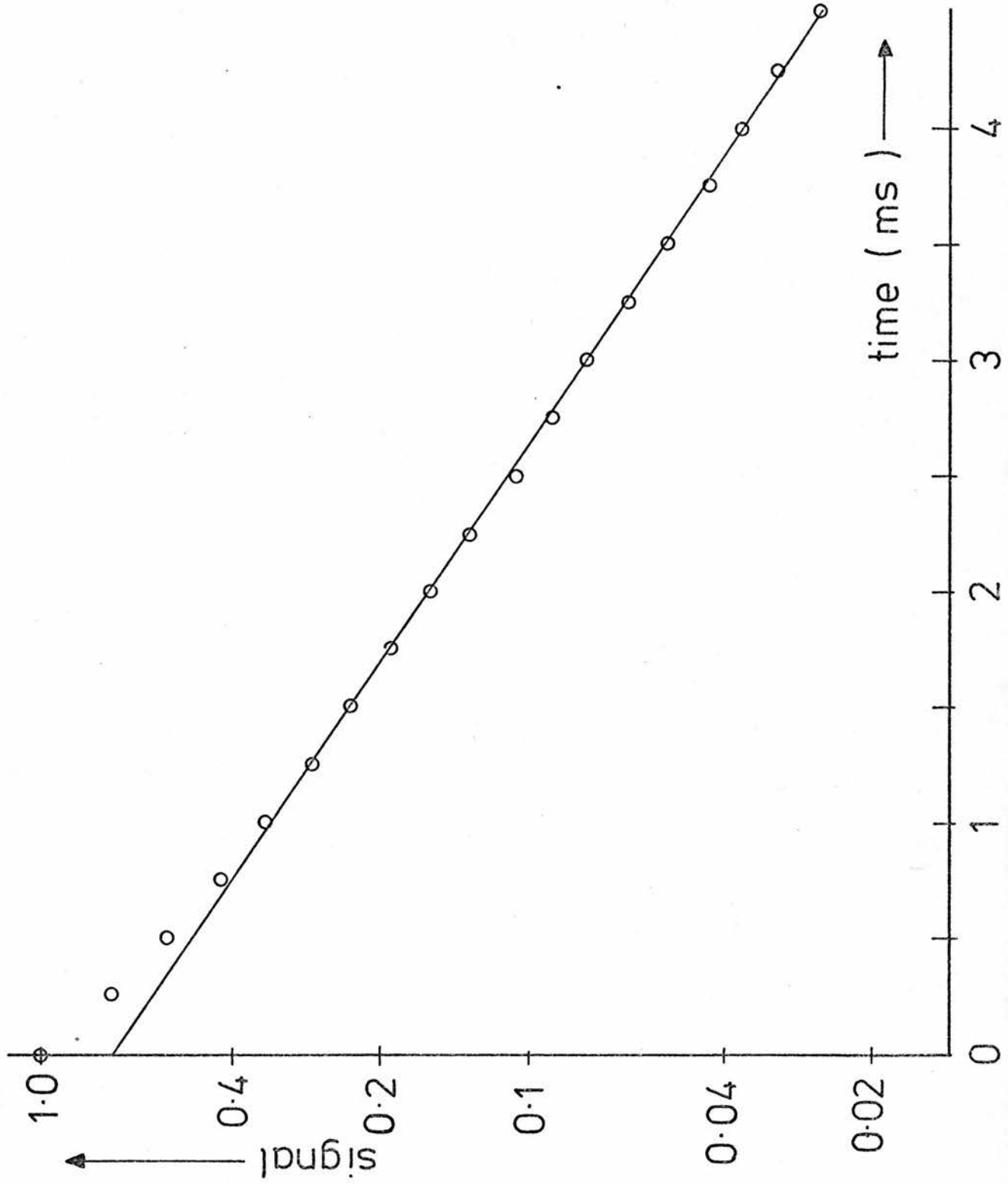

Figure 4.7 Decay of luminescence in as - grown Eagle Picher ZnS:Mn.

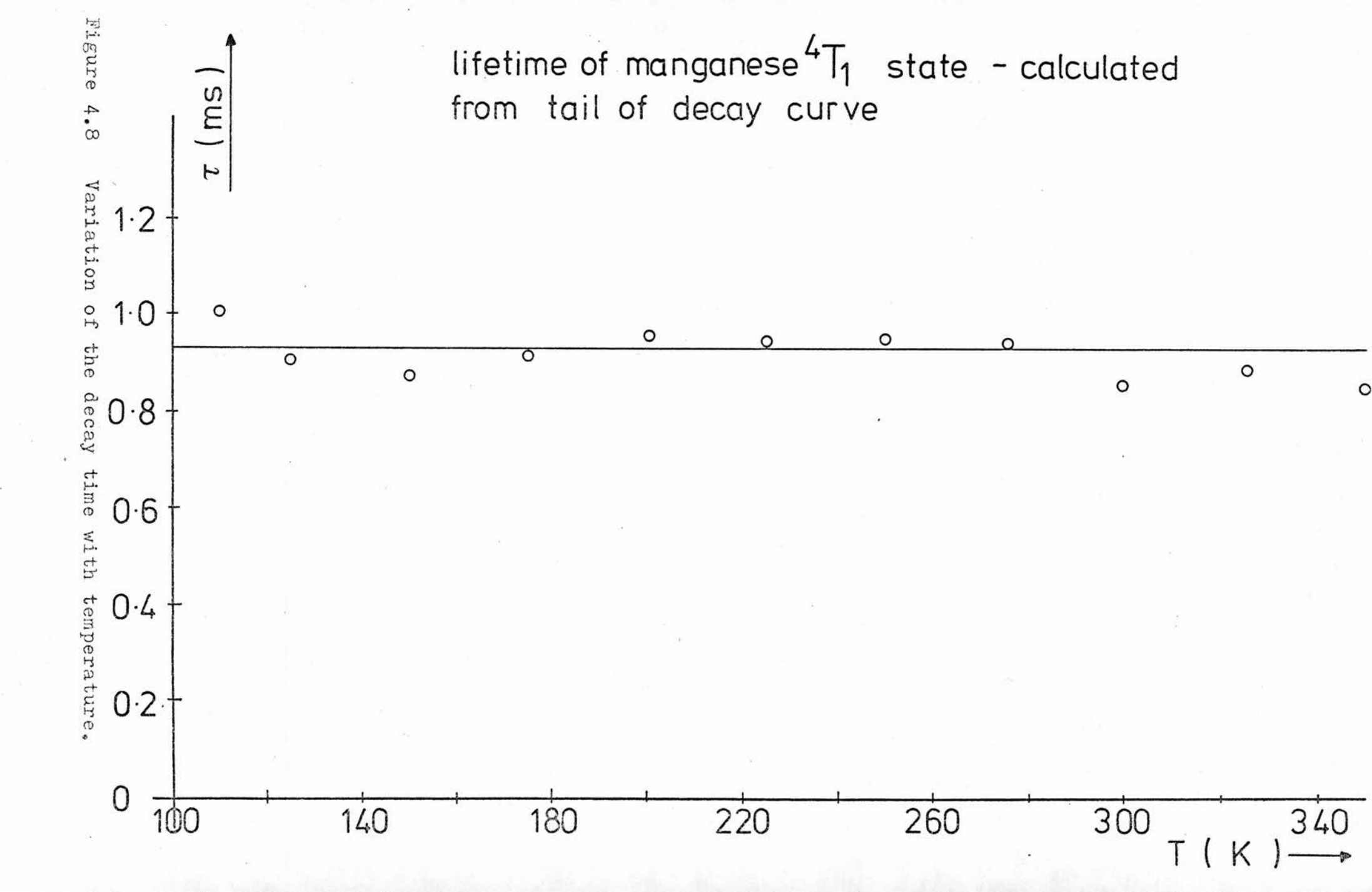

Figure 4.8 Variation of the decay time with temperature.

light output, the remainder can be poorly fitted to an exponential with a time constant of about 0.34 ms. These results are compared with those obtained by Walentynowicz et al[55] from the decay of the electroluminescence in 0.5% ZnS:Mn thin films in table 4.1.

In the fcc lattice, each manganese has 12 cation nearest neighbours (assuming that the manganese is not in an interstitial position). If f is the fraction of the cations which are manganese, then the probability that any manganese atom has no manganese nearest neighbours (i.e. is a single manganese atoms) is $(1 - f)^{12}$, in this case 94.2%. The probability that it is one of a pair is $12f\ (1 - f)^{18}$, i.e. 5.5%. At first sight, it is difficult to see how 5.5% of the atoms can be responsible for 25% of the luminescence. It should be noted, however, that the excitation cross section will be greater for pairs than for isolated atoms.[47] Another complication is that energy transfer could be taking place between the isolated atoms and the pairs during the long radiative lifetime.[56-57]

It would appear reasonable, however, to associate the slow time constant of 0.92 ms with isolated manganese atoms. Busse et al[52] have found three time constants in their analysis of the manganese decay in ZnS:Mn. They tentatively assign the intermediate time constant to the less efficient coupling between manganese on next nearest neighbour sites. Although it has been suggested in the present work that the fast part of the decay was not a single exponential, the experimental data were not sufficiently accurate to justify further analysis.

TABLE 4.1

The decay of the manganese luminescence in 0.5% ZnS:Mn has been fitted to the equation

$$B(t) = B_{01} \exp - \frac{t}{t_1} + B_{02} \exp - \frac{t}{t_2} .$$

The values of B_{01}, B_{02}, t_1 and t_2 are given in the table below,

	B_{01}	B_{02}	t_1	t_2
Photoluminescence (this work)	0.75	0.25	0.92	0.34
Electroluminescence (ref. 55)	0.70	0.30	0.99	0.25

The time constants are in milliseconds.

4.d.ii Electrical Measurements

In order to check equation (4.2) of the introduction, it is necessary to know how the free electron concentration n varies with temperature. This is a particular problem in ZnS because of the difficulty of making good ohmic contacts. The most successful 'recipe' to date is described in chapter 5. This tended to produce non-ohmic contacts, the resistance of which tended to about 10 kΩ as the applied voltage was decreased. Because the samples were often of arbitrary shape, the resistivity was measured by the Van der Pauw technique.[58] The current contacts were connected to a Keithley 225 constant current source and the voltage contacts to a Keithley 616 digital electrometer which had an input impedance greater than 10^{14} ohms. It was possible to alter the impedance of the voltmeter by a switch on the front panel. This proved to be a simple method of checking whether or not a significant voltage was being dropped across the voltage contacts. The resistance of the 'ohmic' contacts increased rapidly as the temperature was lowered and became greater than the voltmeter resistance below about 120 K. It was therefore only possible to obtain reliable resistance measurements above 150 K. At each temperature, current-voltage measurements were taken over as wide a range as possible for both current directions and plotted on log-log paper. These were linear with slope unity at low currents but the resistance tended to drop at high currents. This was probably due to sample heating as a result of the large voltage drop across the current contacts.

Typical results are shown in figure 4.9 from which it can be seen that the conductivity of the ZnS was highly thermally activated over the temperature range of interest. The activation energy varied from

sample to sample and was always between 0.20 and 0.28 eV. The concentration of free electrons was calculated using the relationship

$$\sigma = n e \mu \qquad (4.5)$$

Since the variation in μ is expected to be relatively small over this temperature range,[59] the large thermal activation of the conductivity will be mainly due to the variation in n. Thus, the activation energy for n is expected to be very close to that for σ. A constant mobility of 125 cm^2/Vs[59] was normally assumed. This was checked for one sample in which the temperature dependence of both the Hall coefficient and the conductivity were measured over as large a range as possible. These results are also plotted in figure 4.9 and confirm that the thermal activation energies of n and σ are approximately the same. The calculated mobility is plotted against temperature in figure 4.10 and remained constant at about 65 cm^2/Vs to within the (considerable) experimental error. It was estimated that this value could be out by a factor of 2 due to the poorly defined sample geometry, but, of course, this does not affect the activation energy.

The Hall effect data of figure 4.9 show that over the measured range

$$n \sim (1.02 \times 10^{20}) \exp - 0.27 \left(\frac{e}{kT}\right) \qquad (4.6)$$

There are three regions in which the concentration of free electrons can vary exponentially with 1/T.

(A) The intrinsic region, in which the activation energy is $E_g/2$. This is 1.83 eV for ZnS and hence is not applicable here.

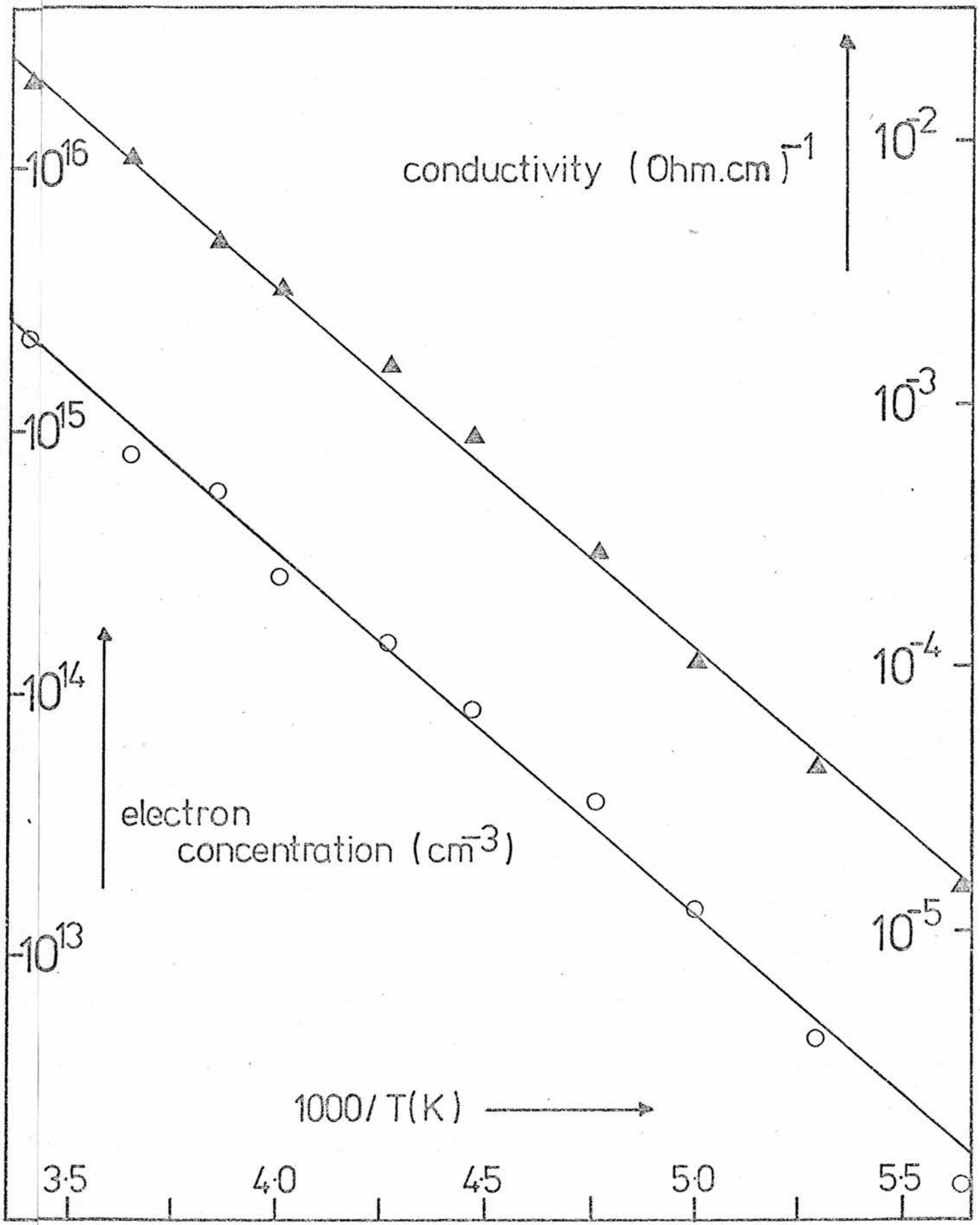

Figure 4.9 Electron concentration and the conductivity of a sample of ZnS:Mn as measured by the Hall effect.

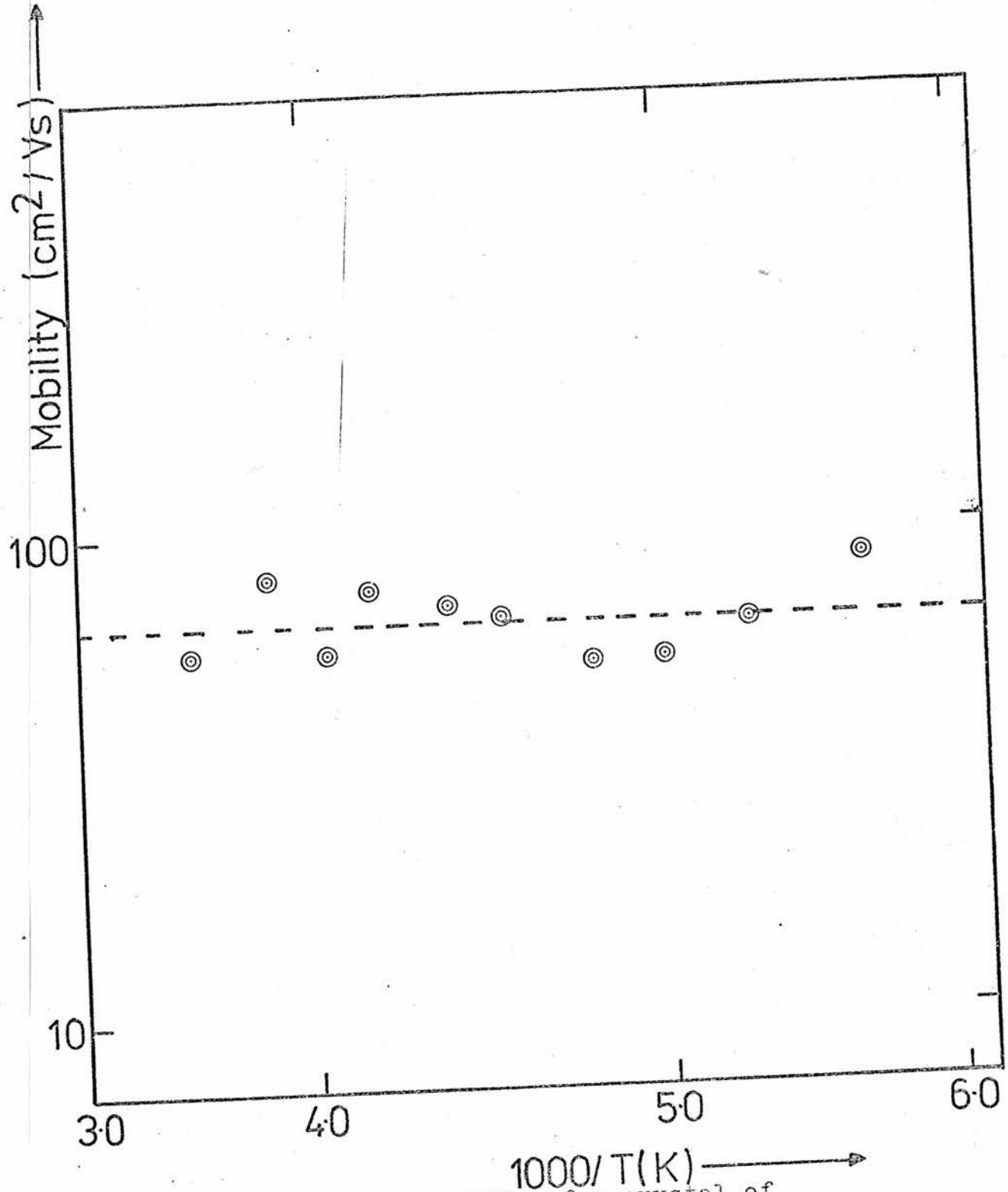

Figure 4.10 The Hall mobility of a crystal of ZnS:Mn as a function of temperature.

(B) $N_a < n < N_d$ in which case,

$$n \sim (N_c N_d)^{\frac{1}{2}} \exp - \frac{\varepsilon_d}{2kT} \qquad (4.7)$$

(C) $n < N_a < N_d$ in which case,

$$n \sim N_c (r-1) \exp - \frac{\varepsilon_d}{kT} \qquad (4.8)$$

where $r = \frac{N_d}{N_a}$ is the compensation ratio.

Thus, depending on whether (B) or (C) is applicable, 0.27 eV is to be interpreted as being either $\varepsilon_d/2$ or ε_d. Substituting $N_c = 5 \times 10^{18}$ cm^{-3} into equations (4.6) and (4.7) gives $N_d = 2.08 \times 10^{21}$ cm^{-3} and $\varepsilon_d = 0.54$ eV. The effective donor concentration, i.e. $(N_d - N_a)$ has been measured by the capacitance-voltage technique to be about 2.0×10^{17} cm^{-3} and hence case (B) is not reasonable.

It would, therefore, appear that equation (4.8) is applicable in this temperature range and hence that the donor depth and compensation ratio are about 0.27 eV and 21 respectively. Note that the measured activation energy is expected to be more reliable than the compensation ratio because of the uncertainty in the absolute value of the conductivity. In addition, if ε_d varies with temperature, the deduced value of r will be wrong and the measured activation energy will be that extrapolated to T = 0 K.

Finally, it should be noted that since $n = n_o \exp - E_A/kT$ (equation (4.6)) over the measured range, the radiative quantum

efficiency should vary with temperature according to

$$\eta_{qu} = \frac{1}{1 + \gamma \tau_R n_0 \exp - \frac{E_A}{kT}} \quad (4.9)$$

This relationship will be compared with the experimental results in the following section. The quantity γ will be taken to be temperature independent, although this will be discussed at greater length in section 4.e.i.

4.d.iii Temperature Dependence of the Luminescent Efficiency

(A) AWRE Material

The photoluminescence spectrum of a slice of Zn/Al treated ZnS:Mn is shown in figure 4.11 for 100 K and 300 K. The photoluminescence was excited at 3.6 eV. It was found that although the intensity of the blue luminescence band remained fairly constant with temperature, the sharper manganese peak became quenched above 200 K. The blue luminescence of this particular sample was separated from the manganese band. This made it a suitable sample for a more quantitive investigation.

The experiment was repeated this time exciting the manganese directly within its absorption bands at 5 000 Å. After the residual high temperature luminescence had been subtracted off, the temperature dependence of the luminescence was as is shown in figure 4.12. A least squares fit to the form of equation (4.9) gave

$$\eta_{qu} = \frac{1}{1 + (2.25 \times 10^5) \exp - 0.18 \left(\frac{e}{kT}\right)}$$

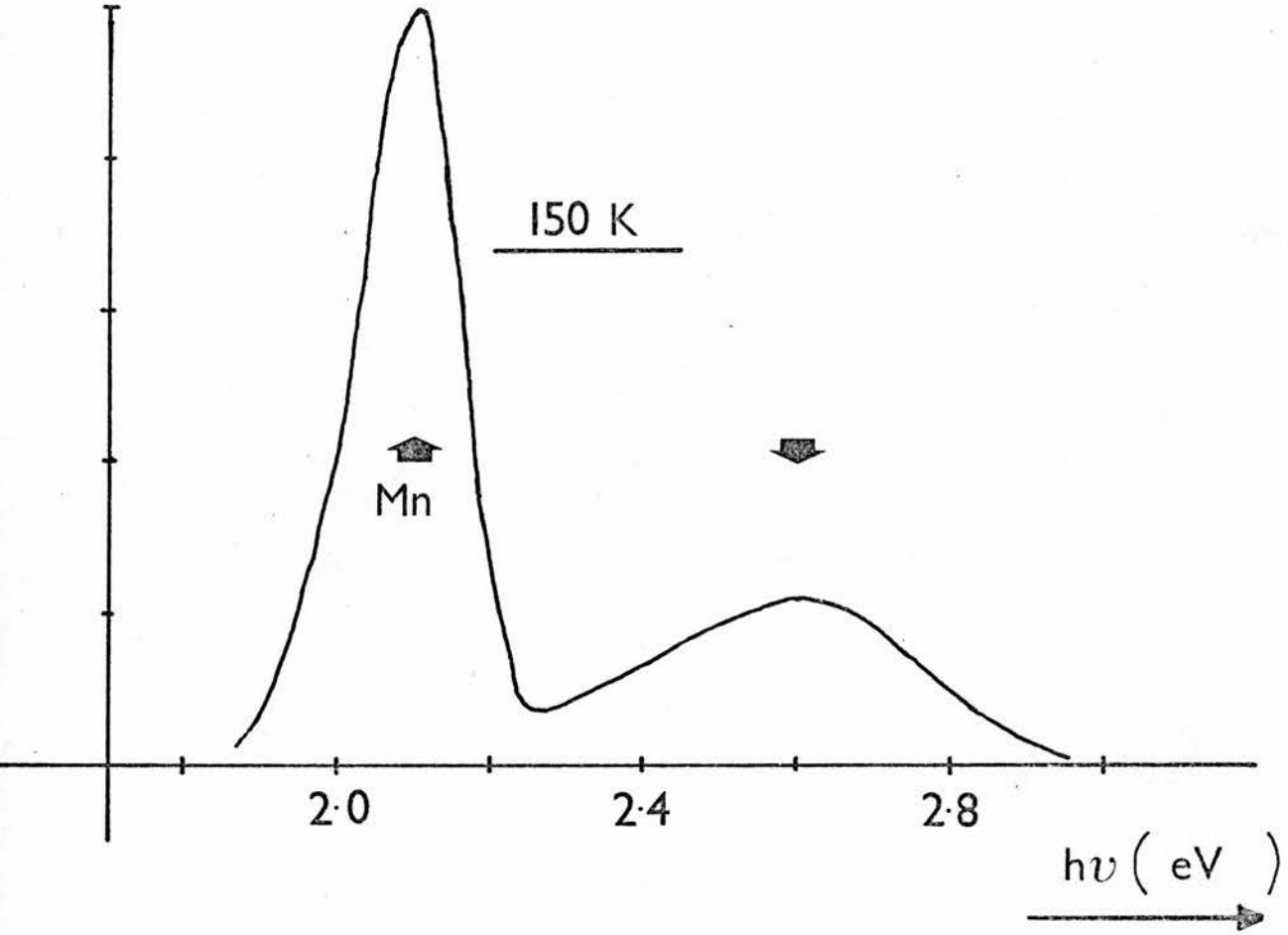

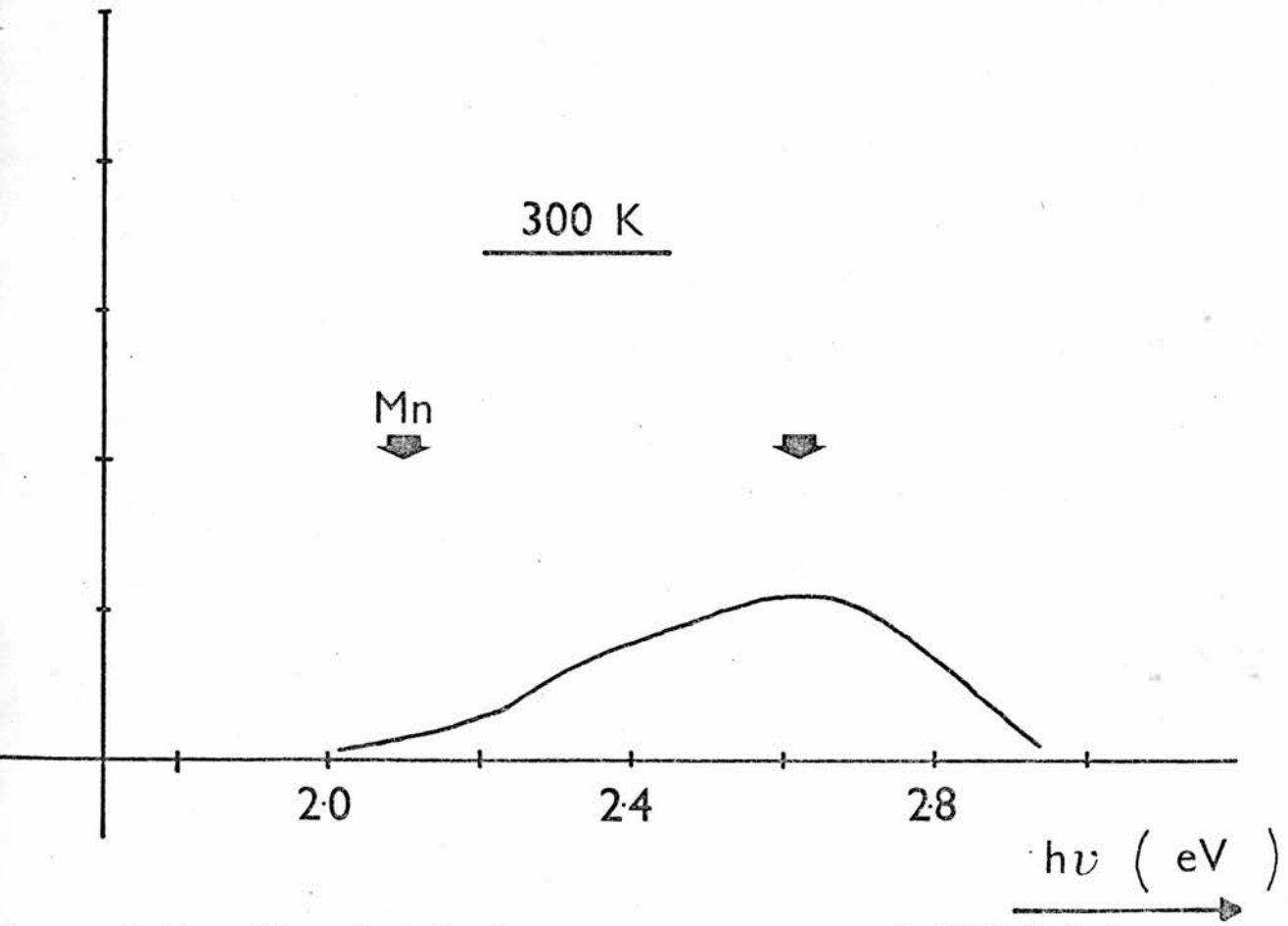

Figure 4.11 The photoluminescence spectrum of AWRE ZnS:Mn excited at 3.6 eV.

which is the solid line in figure 4.12. Although this equation gives a good fit to the experimental points, the activation energy of 0.18 eV is significantly different from the activation energy derived from the conductivity of 0.23 eV.

In general, it was found that the quenching of the luminescence was spread over a larger range than would be predicted from the conductivity measurements. Sometimes, the luminescence persisted to well above room temperature. These anomalous results will be considered at greater length in the discussion section of this chapter.

(B) Eagle Picher Material

The quenching of the luminescence with temperature of a sample of Eagle Picher ZnS:Mn is shown in figure 4.13. It can be seen that the results are qualitatively similar to those obtained for the AWRE material, although in this case there was no blue luminescence to be subtracted. The quantum efficiency was measured at the peak of the manganese luminescence before and after the Zn/Al treatment and the two measurements were divided to give the data shown in figure 4.12. In this way, it was possible to correct for the widening of the emission band with temperature.

4.d.iv The Temperature Dependence of the Lifetime of the $^4T_1$ Excited State

It was noted in section 4.d.i that the decay of the luminescence was not a single exponential, even in the as-grown material. The rate of decay of the luminescence in the conducting material did increase with temperature as expected, although it was only possible to do a

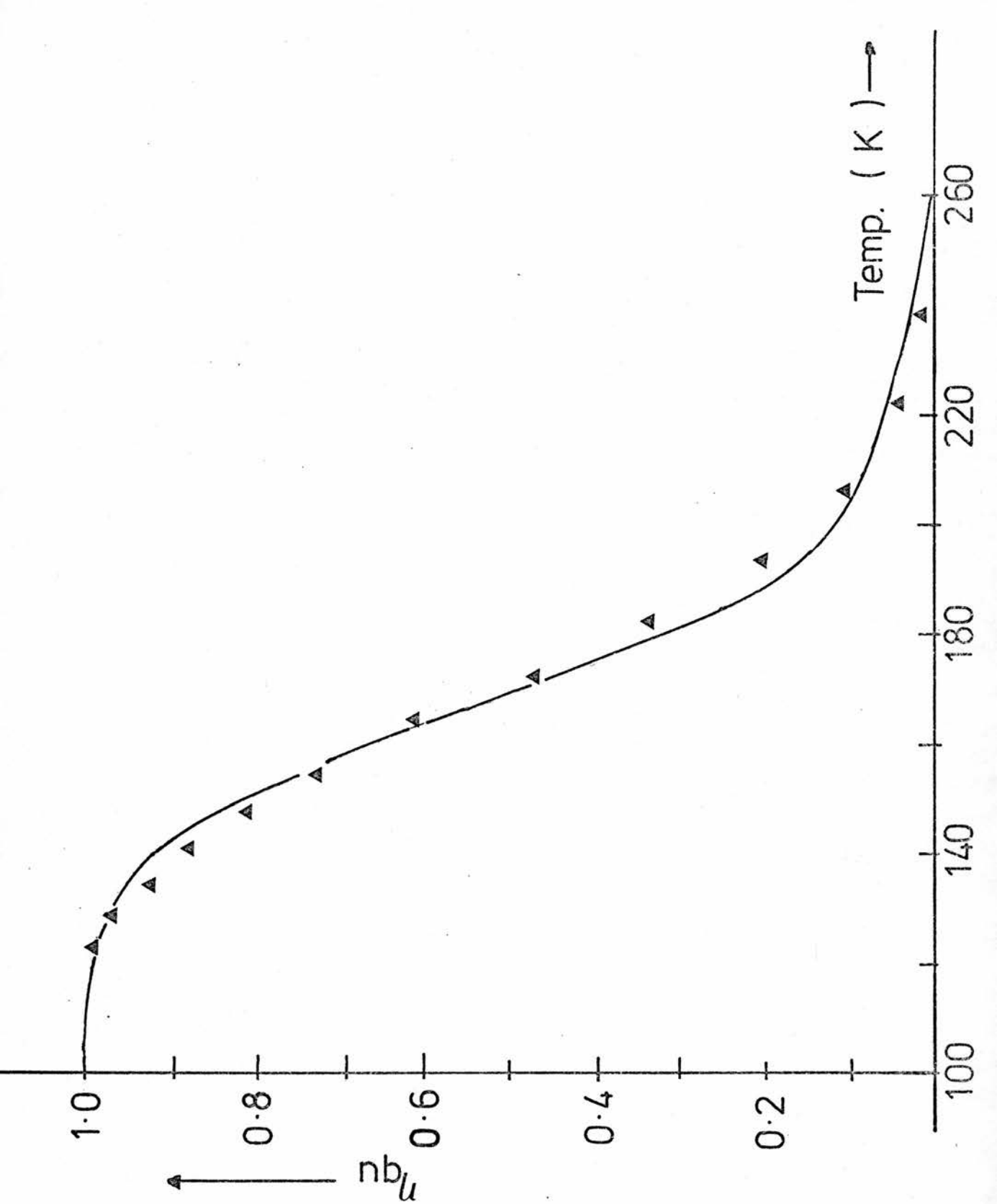

Figure 4.12 The radiative quantum efficiency of AWRE ZnS:Mn as a function of temperature. The solid line is a "best fit " to the experimental points (triangles) using equation (4.9).

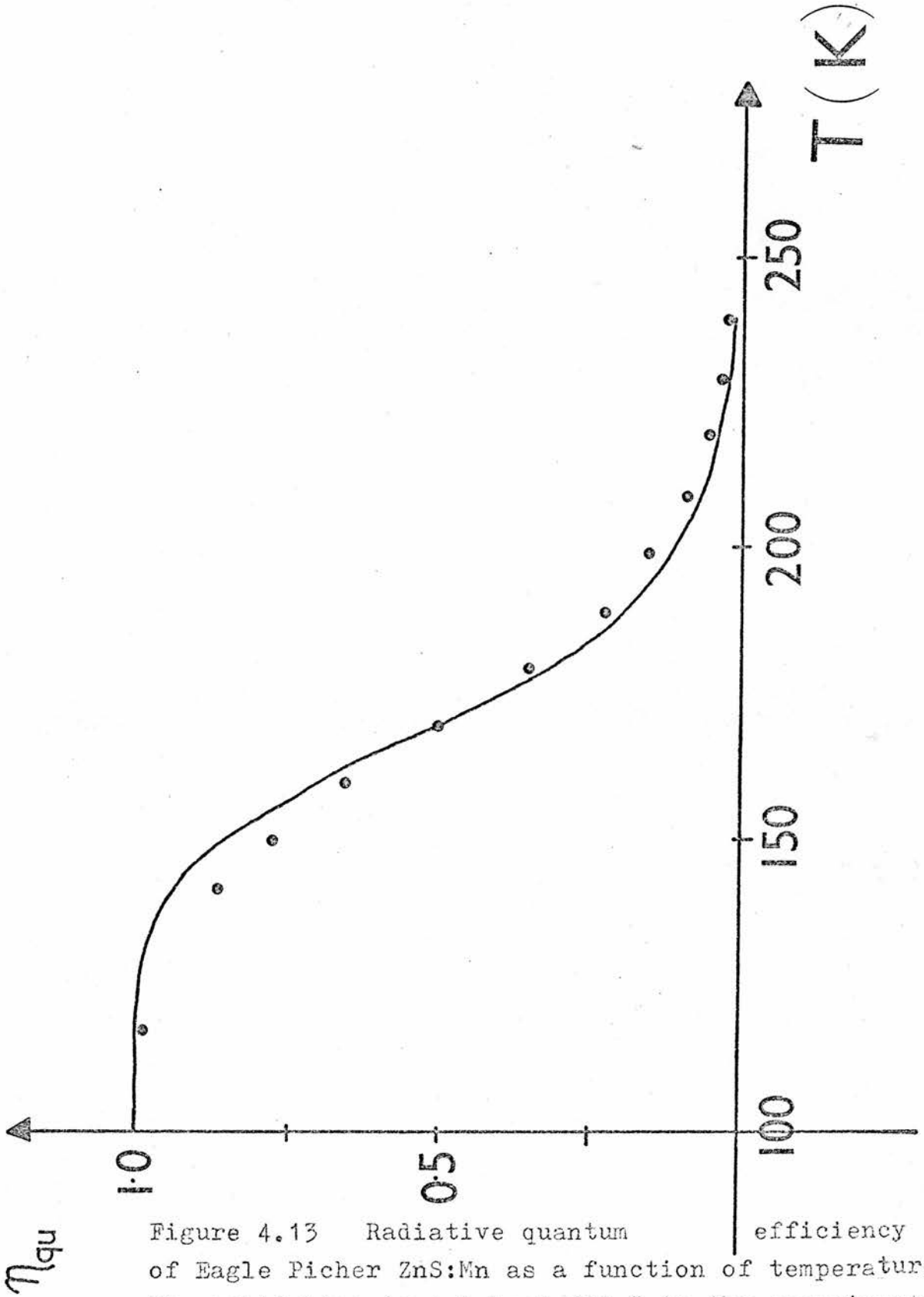

Figure 4.13 Radiative quantum efficiency of Eagle Picher ZnS:Mn as a function of temperature. The solid line is a " best fit " to the experimental points using the activation energy deduced from the conductivity in equation (4.9).

qualitative analysis of the results. In figure 4.14, the time taken for the luminescence to half is plotted as a fraction of the half-life in the insulating material as a function of temperature. From equation (4.2), $\eta_{qu} = \tau/\tau_R$ and hence figures 4.13 and 4.14 should be identical. The lack of detailed agreement between these will be discussed in the next section.

4.e Discussion

4.e.i The Temperature Independence of γ

Changing the temperature of a crystal of ZnS not only changes the number of free electrons but also their energy distribution. It has been assumed so far that the Auger transition probability is independent of the initial energy of the electron. In general, this transition probability will depend on both the density of final states and on the matrix element coupling the initial to the final state (Fermi's rule).

The Auger transitions considered here differ from the more usual two-electron Auger transitions in two important aspects.

(A) As there is only one free electron involved, the Auger rate is proportional to the electron density n rather than n^2.

(B) Because the manganese states are composed of wavevectors from throughout the Brillouin zone, $\underline{k}$ conservation is not required for the Auger electron. The situation is further complicated by the fact that the internal manganese transition produces a number of local phonons which could provide crystal momentum in any case.

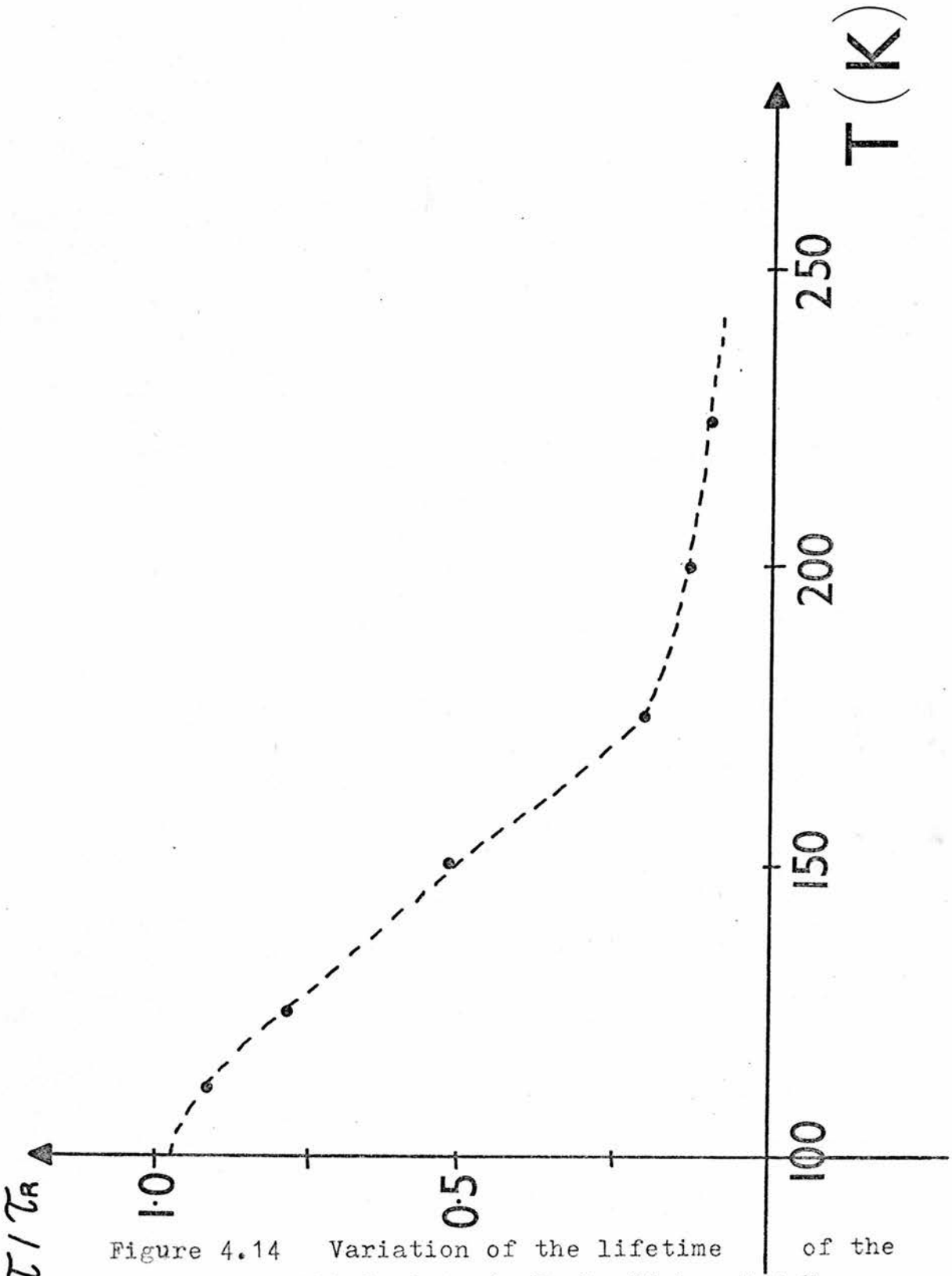

Figure 4.14 Variation of the lifetime of the manganese excited state in Eagle Picher ZnS:Mn as a function of temperature.

These local phonons are also responsible for the broadening of the manganese luminescence. In the absence of phonon broadening, the emission spectrum of ZnS:Mn would consist of photons of only one energy, ΔE_{elect}, the energy difference between the $^4T_1$ and $^6A_1$ states. In practice, however, the energy of the emitted photons is given by

$$h\upsilon = \Delta E_{elect} - n\hbar\omega$$

where n is the number of phonons produced and $\hbar\omega$ is their energy. The emission spectrum in figure 4.4 shows that the energies of the emitted photons are spread out over about 100 meV. Similarly, the energy transferred to the conduction band electron in an Auger process is expected to vary by about 100 meV.

It follows that in order to calculate the Auger transition rate for an electron in a given conduction band state, it is necessary to average both the matrix element and the density of final states over 100 meV. The mean thermal energy of a conduction band electron changes between 16 and 25 meV over the temperature range in which the Auger quenching occurs. As the change in the mean electron energy is much less than 100 meV, neither the averaged matrix element nor the averaged density of final states is expected to vary much with temperature.

There is, therefore, no reason to expect the coefficient δ to be strongly temperature dependent, especially in comparison with the large thermal activation of the electron concentration.

4.e.ii Disagreement Between Theory and Experiment

It was noted in section 4.d.iii that for a number of samples, the photoluminescence did not quench as rapidly with temperature as would be expected from Hall effect measurements. This is believed to be due to inhomogeneous doping of the material. If the sample contains regions of different donor concentrations, then the quenching of the luminescence will occur over different temperature ranges for the different regions. The result is that an inhomogeneous sample has a wider range of temperature quenching than a homogeneous one, and the apparent values of E_A and γ are then not the true ones. For some samples, the manganese luminescence was clearly visible, even at room temperature. Sometimes, the regions of low doping density could be picked out, although the light normally appeared to be emitted uniformly from the sample. The large refractive index of ZnS has the effect that most of the light which is emitted from a polished surface has undergone at least one reflection. This has two important consequences. The first is that it can be difficult to determine the position of the light emitting regions, and the second is that a lot of light will be emitted from edges and corners where the surface is rougher.

Despite this drawback, the measurement of the luminescent efficiency of ZnS:Mn as a function of temperature could be a useful technique for investigating, and hence improving the Zn/Al treatment which is used to produce n-type material. In one experiment, a thin slice was cut from the surface of a lump of Zn/Al treated Eagle Picher material. This was carefully lapped with carborundum to a thickness of about 0.2 mm. The sample was roughly powdered (to increase the efficiency of the photoluminescence) and painted on to the cryostat

cold finger with potassium silicate solution. Care was taken not to powder the sample too finely as the large dislocation density which would result could compensate the sample. The activation energy for the Auger quenching in the powder was 0.17 eV whereas that for the sample as a whole was 0.10 eV. These energies have to be compared with the activation energy of the conductivity, which was about 0.23 eV.

As this sample had only the minimum Zn/Al treatment of 10 hours, it would appear that a treatment of this time does not produce a uniformly conducting sample, the material with the highest conductivity being closest to the surface.

Finally, it should be noted that non-uniform doping has two consequences which affect the interpretation of the $^4T_1$ lifetime measurements.

(A) Even in the case of a single radiative time constant, the decay of the luminescence in the conducting material will no longer be exponential.

(B) The averaged quantum efficiency and τ / τ_{rad} are no longer exactly equal.

If $P_r(N_d)\, dN_d$ is the fraction of the crystal which has a donor density between N_d and $N_d + dN_d$ and $\tau(N_d)$ is the lifetime of the manganese excited state then

$$\eta_{qu} = \int_0^\infty P_r(N_d) \frac{\tau(N_d)}{\tau_R} \, dN_d .$$

When the excitation is switched off, the light output is

$$L(t) = \int_0^\infty P_r(N_d) \frac{\tau(N_d)}{\tau_R} \exp -\frac{t}{\tau(N_d)} \, dN_d$$

The weighting factor of exp - $t/\tau(N_d)$ in the second expression produces a slightly different temperature dependence in the two cases and explains the difference between figures 4.13 and 4.14.

4.e.iii Estimation of γ

It is not possible without further improvement of the materials to get an accurate estimate of the Auger coefficient. The fact that the conductivity measurements are sensitive to the low resistivity regions of the sample whereas luminescence efficiency measurements are sensitive to the high resistivity regions tends to amplify the effects of non-uniform doping. As the conductivity is activated with a different energy to the luminescence, the best procedure is to choose γ so that the theoretical quenching curve (i.e. that calculated from the conductivity) intersects the experimental curve at some suitable matching temperature . The correct matching temperature will depend on the distribution $P_r(N_d)$. As this is not known, γ was chosen so that the two curves intersect at half the low temperature value.

The value of γ deduced in this way was

2×10^{-9} cm^3/s from figure 4.12

and 4×10^{-10} cm^3/s from figure 4.11

4.f Some Theoretical Considerations

4.f.i The Value of γ

We know of no theory with which this value of γ can be compared. It is interesting to note, however, that the Auger process is the inverse (time reversal) of an impact excitation process in which an energetic electron transfers its energy to a manganese impurity. A crude comparison of the two processes is given in appendix B of chapter 5. This shows that to a first approximation

$$\sigma \sim \frac{\gamma}{v_d} \qquad (4.10)$$

where σ is the cross section for impact excitation and v_d is the electron drift velocity. Taking v_d to be 10^7 cm/s (see chapter 5) gives $\sigma = 2 \times 10^{-16}$ cm^2.

This is a reasonable value as it is comparable with the geometrical area of the manganese d^5 shell.

4.f.ii Neutral Donor Quenching

When the temperature of a slice of conducting ZnS:Mn is lowered, the electrons will condense on to the donors leaving insulating material. Although there are still the same number of electrons per unit volume in the insulating material, the electrons are now in localised rather than extended states. It is not immediately obvious that this rearrangement of the electron probability density from a uniform to a non-uniform distribution will result in a decrease in the Auger quenching rate.

An estimate of the effects of neutral donor quenching is given in appendix 4.A. It will be shown that the donors have a negligible effect for the whole range of parameters considered here. This will not be the case, however, for systems with a sufficiently large donor concentration or donor radius. For such systems, the luminescence will be quenched at all temperatures. It has been brought to the attention of the author that this could be the case in CdF_2:Mn.[60]

4.f.iii The Importance of the Auger Effect in ZnS:Mn

There is an interesting problem concerned with the fact that the Auger effect is important in ZnS:Mn and ZnSe:Mn but has not been observed in other systems. Clearly, the importance of the Auger effect depends on the ratio of the Auger transition rate to the radiative transition rate. By Fermi's rule, the radiative transition rate will be proportional to the matrix element squared i.e.

$$R_{RAD} = \frac{2\pi}{\hbar} \left| \langle {}^4T_1 | H_1 | {}^6A_1 \rangle \right|^2 \rho(E_F)$$

where $H_1 \propto \underline{A}.\underline{p}$ is the interaction with the radiation. As this does not mix states of different spin, the above matrix element might be expected to be zero. However, the spin-orbit interaction mixes states of different spin, hence making the matrix element non-zero.

In ZnS:Mn, the spin-orbit interaction is largest where the tail of the manganese wavefunction overlaps on to the neighbouring sulphur atoms. Similarly in ZnSe:Mn the spin forbiddenness will be partially removed because the manganese wavefunctions overlap on to the selenium atoms. As the spin-orbit interaction is larger in selenium than in

sulphur, the lifetime of the manganese $^4T_1$ state is about ten times less in ZnSe than in ZnS.

The rate of the Auger transitions will also depend on the appropriate matrix element squared i.e.

$$R_{AUGER} = \frac{2\pi}{\hbar} \left| \langle X_3, \sigma' : {}^6A_1 | H_2 | \Gamma_1, \sigma : {}^4T_1 \rangle \right|^2 \rho(E_F)$$

where $H_2 = \sum_i \frac{e^2}{|\underline{r} - \underline{r}_i|}$ is the Coulomb interaction between the conduction band electron and the manganese d-electrons.

Here, the initial state is labelled by $| \Gamma_1, \sigma : {}^4T_1 \rangle$ which implies that the manganese centre is in the excited $^4T_1$ state and that there is a conduction band electron in the Γ_1 minimum with spin σ. In this case, however, there are two possibilities.

1. $\sigma = \sigma'$. Since the interaction H_2 does not mix states of different total spin, the matrix element will once again depend on the mixing of different states via the spin-orbit interaction. Let the rate of these transitions be R(1).

2. $\sigma \neq \sigma'$. In this case, the total spin is conserved as the incident conduction band electron is exchanged with one of the manganese d-electrons. Normally, an exchange process of this type would be expected to have a low probability. However, its probability does not depend on the mixing of the spin states. Let the rate of these transitions be R(2).

The importance of the Auger effect depends on the ratio

$$r = \frac{R_{AUGER}}{R_{RAD}} = \frac{R(1) + R(2)}{R_{RAD}} .$$

For a system in which the radiative transition is only slightly spin forbidden, R(1) will be much greater than R(2) and much less than R_{RAD}. Hence, Auger transitions will be unimportant. As the spin forbiddenness is increased, R(1) and R_{rad} will decrease approximately in proportion and hence r will remain small. However, R(2) is not affected by the spin forbiddenness. For a system which is very spin forbidden, R(1) will become less than R(2) and the relative importance of the Auger process will increase. It is possible that this is the case in ZnS:Mn and ZnSe:Mn.

4.g Summary

In the introduction, it was noted that Allen, Ryall and Wray[46] had found that the manganese luminescence was quenched in conducting ZnSe:Mn and that this was attributed to an Auger process. There is now a considerable amount of evidence that the quenching of the luminescence in ZnS:Mn is also due to an Auger process.

An important piece of evidence is the observation of manganese electroluminescence in Zn/Al treated ZnS:Mn crystals (see chapter 5). This shows that the quenching depends on the position of the Fermi level, as the luminescence is not quenched in the depletion region, rather than being due to the diffusion of impurities into or out of the crystal as a result of the Zn/Al treatment. The temperature dependence of the quantum efficiency shows that the quenching varies linearly with n. This implies that the interaction is between the manganese and free electrons rather than between the manganese and neutral donors introduced by the Zn/Al treatment. The results are consistent with a temperature independent Auger coefficient of about 2×10^{-9} cm^3/s which is a reasonable value for this type of process.

During the course of this work, it was noted that the results were sensitive to doping inhomogeneities in the crystal and that the homogeneity of some of the crystals was poor. It is possible that photoluminescence could be a useful contactless technique for investigating these inhomogeneities, or for measuring the mean electron density.

APPENDIX 4A

4A.i Quenching due to Electrons bound on Shallow Donors

In this section, the quenching efficiency of an isolated neutral donor will be compared with that of a free electron. This will make it possible to estimate the concentration of donors which will halve the quantum efficiency of a doped relative to an undoped crystal at absolute zero. It will be shown that free electrons are at least 10^5 times more efficient than neutral donors and that a donor concentration greater than 10^{17} cm^{-3} is required to quench the luminescence of a crystal at all temperatures.

If a donor wavefunction is expanded in the complete set of Bloch wavefunctions i.e.

$$\psi_d = \sum_{n,\underline{k}} a_{n,\underline{k}} \phi_{n,\underline{k}}$$

then $a_{n\underline{k}}$ will be large throughout most of the Brillouin zone because of the smallness of the donor wavefunction. (This is equal to 6.4 Å for a donor energy of 0.27 eV.) It follows that the donor states are composed of a larger range of $\underline{k}$ values than are free electrons. It was noted in section 4.e.i that the Auger transition probability is not expected to be strongly $\underline{k}$ dependent and hence it will be assumed that the non-radiative rate depends only on the local probability density $|\psi|^2$.

The approximations and assumptions used in the following calculation are listed below.

(A) The Auger transition rate is proportional to the local electron probability density, i.e. $R = \gamma |\psi|^2$.

(B) The manganese atoms are uniformly distributed.

(C) The donors have hydrogen-like wavefunctions

$$\psi(r) = \frac{1}{\pi a^3} \exp - \frac{r}{a} \quad . \tag{4A.1}$$

These approximations are made to overestimate the effect of the neutral donors.

Consider the effect of one isolated donor. The radiative efficiency of a manganese centre at a distance r from the donor is given by

$$\eta_{qu}(r) = R_{RAD} / (R_{RAD} + R_{AUGER}(r))$$

$$= \frac{1}{1 + \gamma \tau_R |\psi|^2} \quad . \tag{4A.2}$$

using assumption A. The radiative lifetime τ_R is defined as the reciprocal of the radiative rate. The probability that a manganese atom placed at r will decay non-radiatively is therefore

$$1 - \eta(r) = \frac{\gamma \tau_R |\psi(r)|^2}{1 + \gamma \tau_R |\psi(r)|^2} \quad . \tag{4A.3}$$

Integrating the above expression over all space gives the 'dead volume' V_b of one bound electron. This is defined so that the total light output from a crystal of volume V with one donor is the same as the light output from a crystal of volume $(V - V_b)$. Hence

$$V_b = \int_0^\infty \left(1 - \eta(r)\right) 4\pi r^2 \, dr$$

$$= \frac{4\gamma\tau_R}{a^3} \int_0^\infty \frac{r^2 \, dr}{e^{r/a} + \frac{\gamma\tau_R}{\pi a^3}} \qquad (4A.4)$$

putting $t = r/a$ gives

$$V_b = \frac{\gamma\tau_R}{4} \int_0^\infty \frac{t^2 \, dt}{e^t + \frac{\gamma\tau_R}{\pi a^3}} \qquad (4A.5)$$

Letting a tend to infinity in equation (4A.5) shows that

$$V(\text{one free electron}) = V_f = \gamma\tau_R \qquad (4A.6)$$

The ratio $r = V_b/V_f$ gives the quenching efficiency of a bound relative to a free electron. This is plotted for various values of γ and a in figure 4A.1. The relevant values for ZnS are given below.

	ε_d(meV)	a(Å)
experimental	270	6·4
effective mass	59	13.8

It can be seen that $r \sim 10^{-5}$ in the range of interest and hence bound donors are sufficiently inefficient non-radiative centres for their effect to be negligible on the temperature dependence of the quantum efficiency.

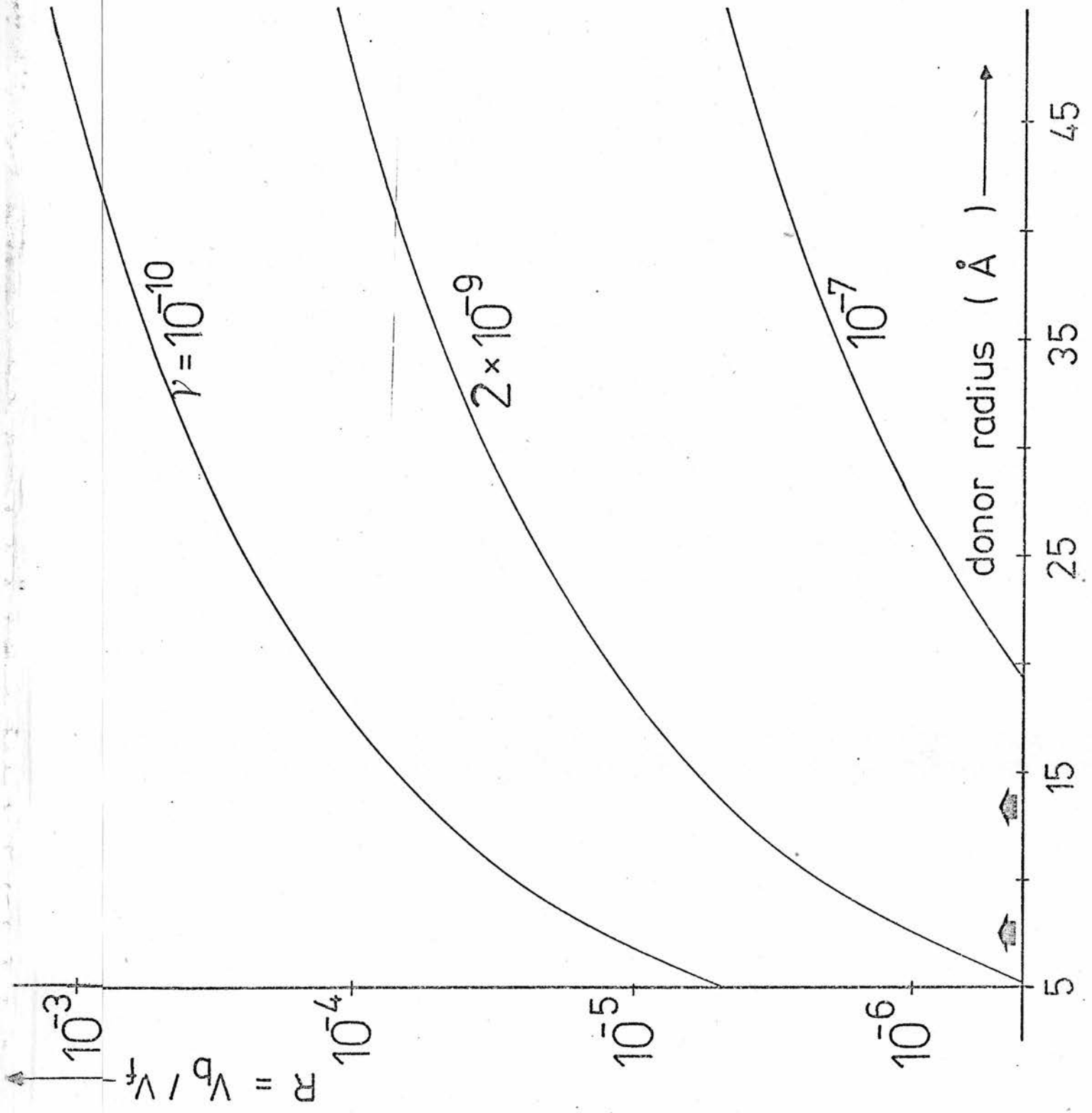

Figure 4A.1 The relative quenching efficiency of bound donors as a function of the donor radius.

In order to estimate the radiative quantum efficiency of a crystal containing N_d donors, it is necessary to calculate the total dead volume. At first sight it would appear that this is $N_d V_b$ and hence that the radiative efficiency is

$$\eta = 1 - N_d V_b \quad . \tag{4A.7}$$

However, this is only true if there is no overlap of the donor wavefunctions. When overlap occurs, the Auger rate which results from two electrons is always less than the sum of the rates which would have resulted from isolated electrons. There are, however, two limiting cases. The first is correct for zero overlap of the donors and is given by equation (4A.7). The second is for a uniform overlap for which it has been shown in equation (4.2) that

$$\eta = \frac{1}{1 + n V_f} \quad . \tag{4A.8}$$

Hence, the efficiency of the phosphor drops to 0.5 when

$$N_d V_b = 0.5$$

$$\text{or} \quad N_d V_b = 1$$

depending on whether (4A.7) or (4A.8) is the better approximation. Figure 4A.2 shows how this quantity varies with the donor radius and γ assuming equation (4A.7), which overestimates the donor efficiency. It can be seen that in the range of interest, the required donor density is greater than 10^{17} cm^{-3}. As the concentration of donors required varies fairly rapidly with the donor radius, it is likely that a crystal with a donor concentration of (say) 10^{18} cm^{-3} and a shallower donor will be quenched at all temperatures. However, the following points should be noted.

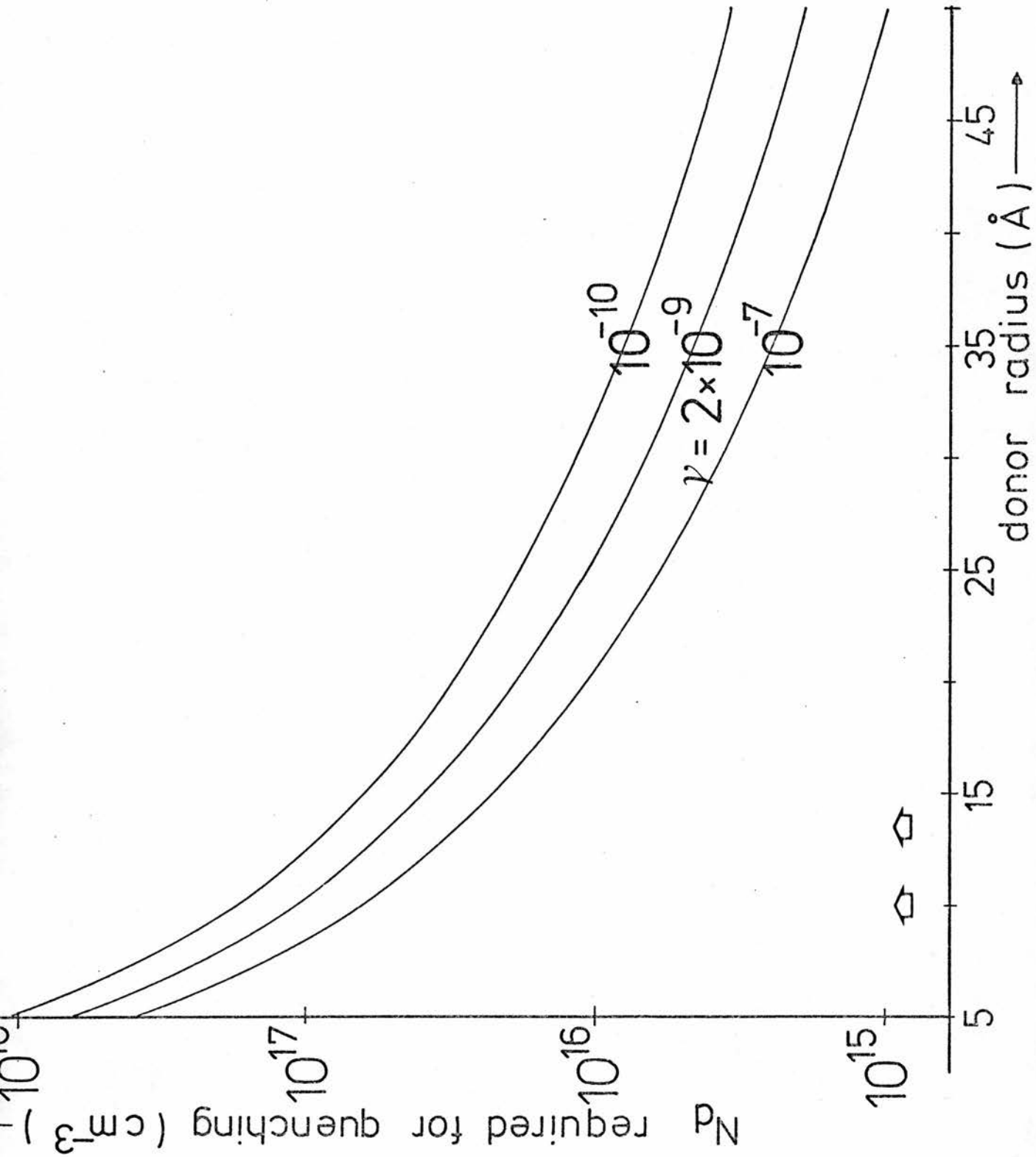

Figure 4A.2 The density of bound donors required to half the efficiency of a ZnS:Mn phosphor as a function of the donor radius.

(A) As the donors have a large central cell correction, the electron density near the donor will be larger than would be predicted from the assumed hydrogenic wavefunctions.

(B) A uniform distribution of manganese atoms was assumed whereas, in practice, there is no possibility of finding an atom within one lattice constant of the donor, i.e. where the electron concentration is greatest. This, together with point (A), shows that the quenching efficiency of the donors has been overestimated as was required.

(C) If energy transfer occurs between the manganese centres, the manganese excitation will be mobile. This will effectively increase the donor concentration and hence the importance of donor quenching. As this complication would introduce a large number of new (and unknown) variables into the problem, it will not be considered here. Note, however, that energy transfer will only be important for large manganese concentrations.

4A.ii Excited State Quenching

The analysis given in the previous subsection estimates the quenching efficiency of neutral donors at T = 0 K. At any non-zero temperature, some of these donors will be in excited states which will be more efficient at quenching the luminescence because of their larger size. In general, the temperature dependence of the quantum efficiency will be due to the excitation as well as the ionisation of the donors. If the quenching due to excitation is at all comparable to that due to the free electrons, then the analysis given in this chapter will be incorrect.

It will be shown, however, that the quenching due to electrons in excited states is about 600 times smaller than that due to free electrons, even in the worst possible case. Thus, excited state quenching will not affect any of the results quoted earlier.

The probability that an electron is in the nth donor energy level is given by

$$P_r(\varepsilon_n) = g(\varepsilon_n) \exp\left(-\frac{\varepsilon_n}{kT}\right) \Big/ Z$$

where ε_n is the energy of the nth energy level, i.e.

$$\varepsilon_n = \varepsilon_i \left(1 - \frac{1}{n^2}\right)$$

ε_i is the ionisation energy

$g(\varepsilon_n)$ is the degeneracy of the nth state $= 2n^2$

and Z is the partition function, defined by

$$Z = \sum_n g(\varepsilon_n) \exp\left(-\frac{\varepsilon_n}{kT}\right)$$

where the sum is over all energy levels. There is a problem here in that the formula for ε_n is only applicable when the donor radius is less than the separation between the donors. The higher energy states are no longer localised and belong to the conduction band. In the following, a sufficient number of excited states will be considered to give an overestimate of the excited state quenching.

As the energies of the excited states are less than the ionisation energy of the donor, the ratio of the quenching efficiency of the excited states to that of free electrons will be greatest for large donor energies and small temperatures. The largest encountered donor energy was 0.27 eV, and the lowest temperature of which there was significant quenching was about 120 K ($kT = 10.4$ meV).

The probability of occupation of all the possible excited states has been estimated in table 4A.1. Note that the mean donor separation was about 200 Å. The probability of the electron being ionised was calculated by dividing the electron concentration (as measured by the Hall effect) by the total concentration of donors.

From this table, the relative effectiveness of the excited states is given by

$$\sum_{i=2}^{6} P_r(\varepsilon_i)\, r(\varepsilon_i) \simeq 3.14 \times 10^{-12}$$

whereas that of the electrons in the conduction hand is

$$P(CB)\, r(CB) \simeq 1.9 \times 10^{-9}$$

Thus, even in this extreme case, the quenching produced by the small number of free electrons is at least 600 times as great as that produced by electrons in excited states. This ratio will, of course, increase as the temperature is increased.

N.B.

In the preceeding calculation, no account has been taken of the fact that the form of the wavefunction is different from equation (4A.1) for the excited states, i.e. the wavefunction has been taken as equation (4A.1) with $a_n = a_1 \times n^2$. It has already been noted that the donors have a large central cell correction. For some of the excited states $\psi \sim 0$ close to the nucleus and hence these states will be less affected by the potential in the central cell. It follows that their energies will be closer to those predicted by the effective mass theory, i.e. closer to the conduction band edge. This will therefore

TABLE 4A.1

The relative quenching efficiencies of the donor excited states

Level Number	Degeneracy	Radius (Å)	Occupation Probability	$r = \frac{V_b}{V_f}$
1	2	6.4	1.0	8.0×10^{-7}
2	8	25.8	1.21×10^{-8}	2.3×10^{-5}
3	18	58.0	7.65×10^{-10}	1.8×10^{-4}
4	32	103	3.87×10^{-10}	7.1×10^{-4}
5	50	161	3.83×10^{-10}	2.0×10^{-3}
6	72	232	3.75×10^{-10}	4.5×10^{-3}
CB	358	infinity	1.90×10^{-9}	1.0

have the net effect of reducing the efficiency of the excited states at quenching the luminescence.

APPENDIX 4B

Photographs of some crystals which exhibit the Auger effect

These photographs are shown in figure 4B.1. In figure 4B.1(a), the crystals are at room temperature while those in figure 4B.1(b) have been immersed in a liquid nitrogen bath. Unfortunately, the colours have not come out very well in the printing of these photographs. The crystals are numbered from bottom left to top right and are in the same order in the two photographs. Note that the luminescence is being excited with the 3,650 Å mercury line.

Crystal Number

1. Eagle Picher ZnS:Mn, as-grown. This is included for reference as it luminesces equally strongly at both temperatures. Comparison of figures 4B.1(a) and (b) shows that the camera sensitivity was less in the latter case.

2. Eagle Picher Zn/Al treated ZnS:Mn. Comparison with crystal 1 shows that both crystals luminesce equally strongly at liquid nitrogen temperature, but that the luminescence in the conducting material is quenched at room temperature. It is perhaps also possible to see that the colour of the luminescence in the conducting material is slightly shifted towards the red (section 4.d.i) as the eye is very sensitive in this part of the spectrum.

3. AWRE, Zn/Al treated ZnS:Mn. This crystal luminesces predominantly in the yellow at liquid nitrogen temperature but luminesces in the blue at room temperature when the manganese luminescence is quenched (see figure 4.11).

Figure 4B.1(a) The photoluminescence of ZnS:Mn crystals at room temperature

Figure 4B.1(b) The photoluminescence of ZnS:Mn crystals at 77 K.

4. B.D.H., Zn/Al treated ZnS:Mn. This luminesces less strongly than crystal 1 at room temperature but is the brightest at liquid nitrogen temperature. This material was fairly polycrystalline and hence an efficient light emitter due to cracks and grain boundaries (section 4.e.ii).

CHAPTER 5

HIGH FIELD ELECTROLUMINESCENCE IN ZnS:Mn

5.a Introduction

Light is emitted when a sufficiently large electric field is applied across a layer of ZnS:Mn. It is found that this phenomenon can be used to obtain bright electroluminescent panels from thin layers of ZnS:Mn. The initial pioneering work was performed by Destriau[3] in 1936 and research is currently centred on two different types of device.

Electroluminescent d.c. powder panels[4] are produced by sandwiching a layer of copper coated ZnS:Mn particles between two conducting plates one of which is transparent (figure 5.1(b)). The copper coating provides a conducting path between the electrodes. The panel is put through a so called forming process[61] which produces an insulating copper-free region adjacent to the anode. When a d.c. voltage of about 100 V is applied, the breakdown field of the insulating region is exceeded and light is emitted from the device.

Recently, there has been renewed interest in thin film devices following reports by Mito and co-workers[5, 62] that a new type of thin film device has excellent ageing characteristics. The basic device is shown in figure 5.1(a) and consists of a thin film of ZnS:Mn sandwiched between two oxide layers. The oxide chosen should have a large breakdown field and dielectric constant. Normally either Y_2O_3[63] or $BaTiO_3$[64] is chosen. On the application of about 100 V to the device, the ZnS breakdown field is exceeded and a pulse of current flows. In

a) thin film electroluminescence

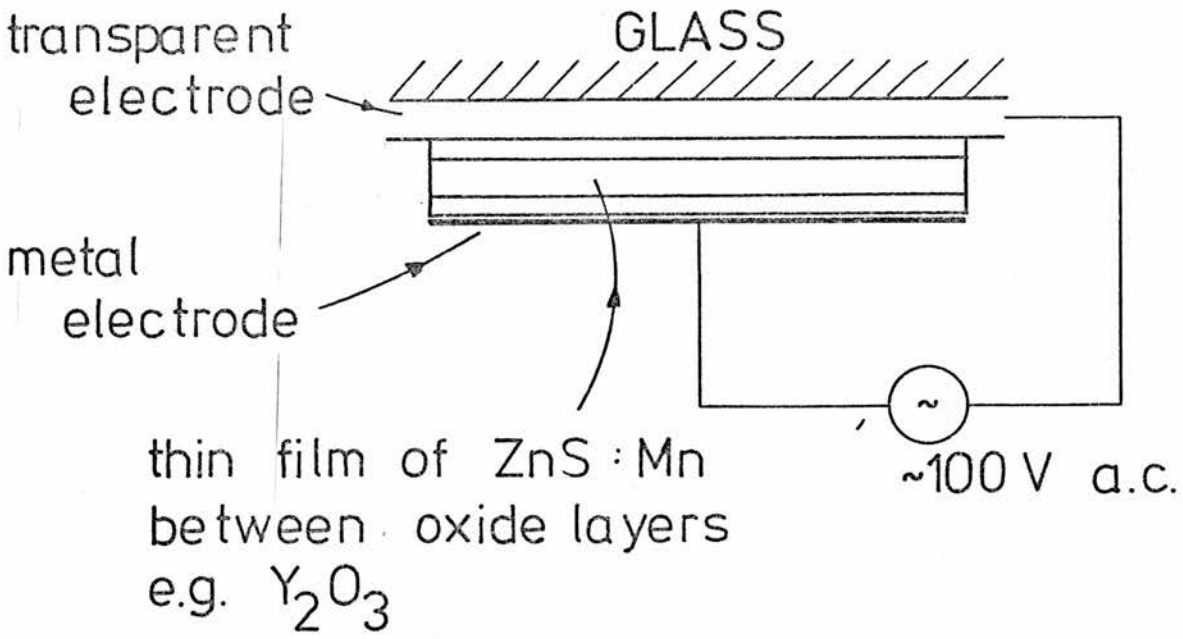

b) d.c. powder panel

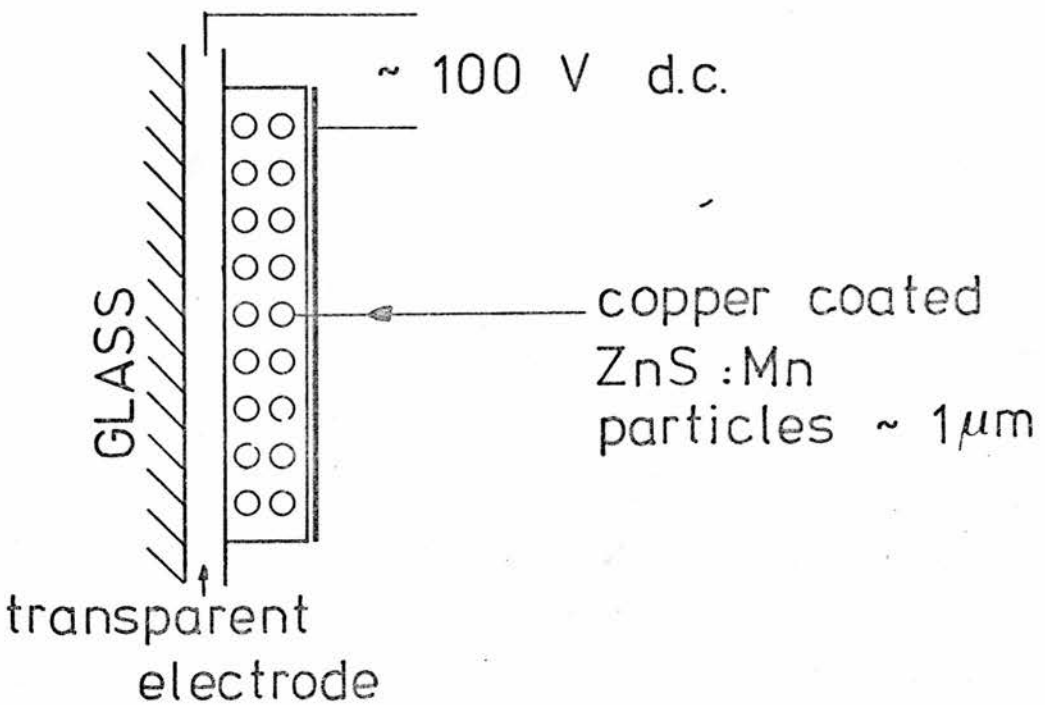

Figure 5.1 Two devices for exciting electroluminescence in ZnS:Mn.

practice, an a.c. current is used to couple capacitively to the ZnS:Mn through the insulating oxide layer.

For a number of applications, these panels can be more useful than conventional $GaAs_xP_{1-x}$ LEDS as electroluminescent displays. The main advantage of the ZnS panels is that since zinc is over an order of magnitude cheaper than gallium large area displays are economically possible. In addition, the peak emission from a ZnS:Mn panel is at 5 900 Å which is close to where the eye is most sensitive. Because of this a considerable amount of effort has gone into producing efficient and reliable panels for commercial applications. Unfortunately, this research has had to proceed on a fairly empirical basis because the fundamental properties of ZnS were not known and the commercial devices did not provide a sufficiently well-defined structure for these properties to be deduced from those of the panels.

In the powder panels, there is the problem that the electric field distribution in the active region is not known. In addition, there is some evidence that the current flows preferentially through the copper rich areas between the particles hence making the current distribution unknown.[65] The thin film devices require an a.c. voltage. This produces other complications which can make the light output dependent on the history of the film (the memory effect).[66] Both devices require breakdown in the active region before any current can flow. Thus the light output depends on the breakdown as well as the electroluminescent properties of the ZnS:Mn and it is difficult to separate the two processes.

Clearly, the observation of electroluminescence in a more well-defined structure such as a Schottky diode on conducting ZnS:Mn would

help to clarify the situation. In this case, the light emission would be from the depletion region below the Schottky contact in which the electric field distribution can be determined by capacitance-voltage measurements. The main problem in obtaining such a structure is the difficulty in producing conducting ZnS:Mn.

ZnSe is a semiconductor with similar chemical and electrical properties to ZnS. The chemical similarity arises because sulphur and selenium are adjacent elements in group VI of the periodic table. Electrically, both are direct band gap semiconductors with very similar band structures.[67-68] The main difference is that the band gap of ZnSe is 2.72 eV at room temperature whereas that of ZnS is 3.65 eV. Similar semiconductors with an intermediate band gap can be produced by growing mixed crystals of the form $ZnSe_xS_{1-x}$.

There is a general rule that technological problems associated with the electrical properties of a semiconductor increase with its band gap. This is also the case here as ZnSe is easier to work with than ZnS. The main problems with ZnS are in producing conducting material and making electrical contact to it. It is only comparatively recently that it has been possible to produce conducting material reliably.[49]

In 1972, Allen, Livingstone and Turvey investigated electroluminescence in ZnSe:Mn using a Schottky structure.[69] Unfortunately, it was not obvious from these experiments how the luminescence was excited or even how it arose. The confusion was due to the fact that the manganese $^4T_1$ first excited state was thought to be almost degenerate with the conduction band. It was therefore possible that the electroluminescence could either be due to electrons being radiatively

captured by the ionised manganese or due to the internal $^4T_1 - {}^6A_1$ transition. A series of measurements of the absorption and emission spectra of ZnS:Mn and ZnSe:Mn[46] led to this problem being resolved. The electroluminescence of the ZnSe:Mn was shown to be due to the internal $^4T_1 - {}^6A_1$ transition within the manganese d^5 shell. The excitation process was thought to be direct impact excitation of the manganese impurities by hot electrons in the depletion region. This process is shown schematically in figure 5.2. In a later publication,[70] a simple theory was produced for this process which was thought to be generally applicable to other systems such as ZnS:Mn. By making the assumption that the electroluminescence in ZnS:Mn was due to the same mechanism as in ZnSe:Mn it was possible to use the data obtained from the ZnSe:Mn measurements to predict the behaviour of ZnS:Mn. Hence, it was possible to estimate such parameters as the maximum power efficiency of such a device.

This chapter reports an investigation into the fundamental electroluminescent properties of ZnS:Mn by direct measurement with a Schottky diode evaporated on to a crystal of conducting ZnS:Mn. It will be shown that the properties of ZnS:Mn are indeed very similar to those of ZnSe:Mn and are consistent with the mechanism of figure 5.2.

Electroluminescence in conducting ZnS:Mn is also of some theoretical interest due to the extreme conditions which exist in the active region. For the diodes studied here, the electric field can reach 10^6 V/cm in the depletion region. The mean energy of electrons injected into this region is determined by competition between this field and scattering processes. Because of the magnitude of this field, the electrons can have a mean energy of greater than 2 eV (this is equivalent to an electron temperature of 15 000 K, using $E = 3/2\ kT_e$).

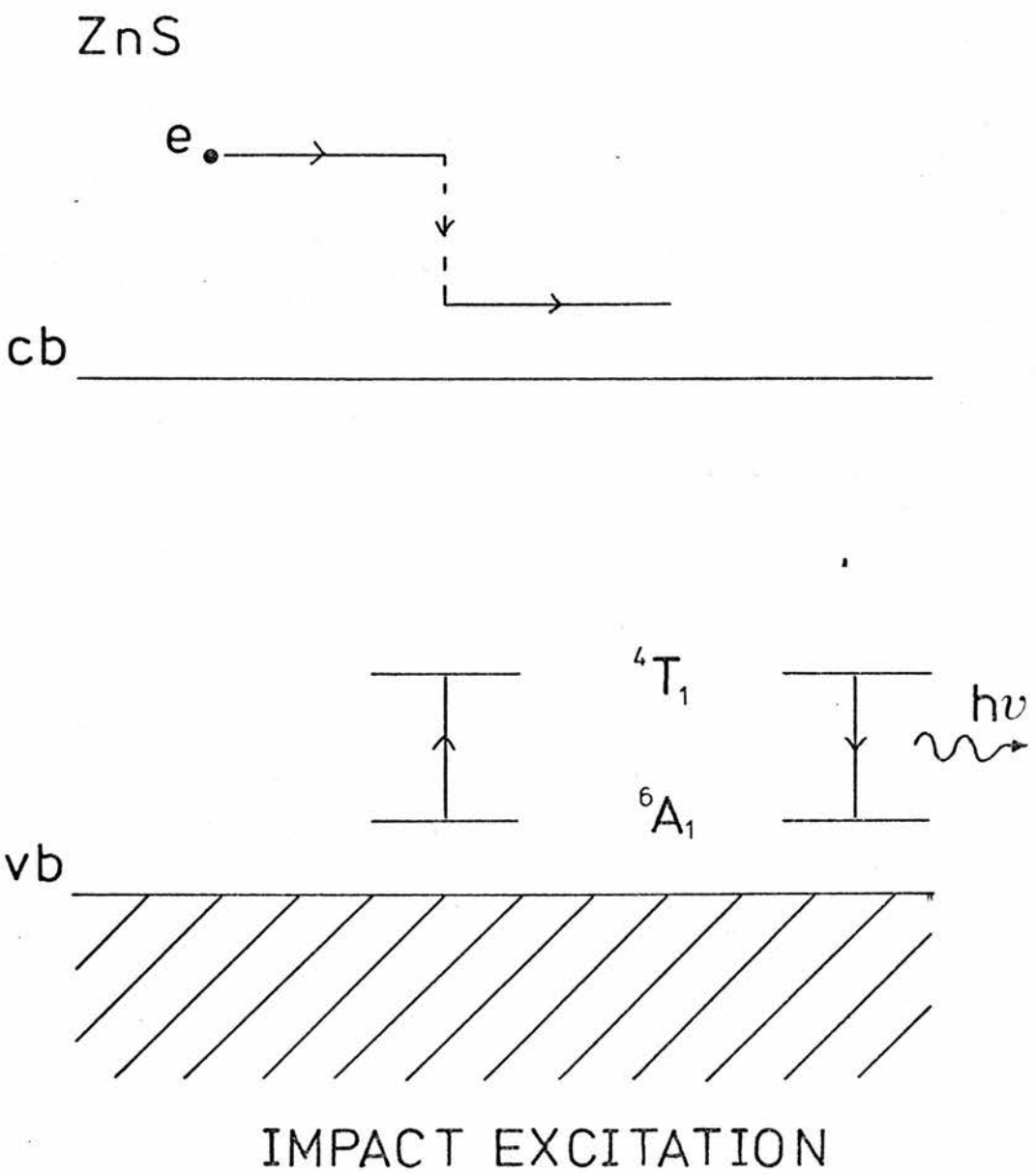

Figure 5.2 The mechanism thought to be responsible for the electroluminescence.

In a well-defined structure such as a Schottky diode electroluminescence can be used as a probe to measure the number of hot electrons. Normally, it would be expected that the number of hot electrons would be determined by optical phonon scattering, although some experimental evidence will be presented that ionised impurity scattering is of more importance here. It is thought that this is related to the nature of the band structure of ZnS. Finally, it will be shown that the quantum efficiency of a ZnS:Mn Schottky diode goes through a maximum at high fields. This is thought to be a fundamental effect and device implications will be considered.

5.b Experimental

5.b.i Introduction and Materials Used

Although ZnS:Mn phosphors have been extensively studied during the last 50 years, conducting ZnS:Mn has only recently been investigated. This is mainly due to the problems of doping and contacting associated with its large band gap. The work reported in this chapter is the first investigation of electroluminescence in conducting crystalline ZnS:Mn.

The ZnS:Mn was made conducting using a Zn/Al treatment as described by Kukimoto.[49] The details of the conductivity treatment were presented in chapter 4. A variety of etches and contacts were used in an effort to produce low resistance contacts on to the resulting material. The quality of these contacts improved significantly throughout the course of this work as better techniques were discovered, largely by trial and error. Typical values of the contact resistance

dropped from 1 MΩ to 4 kΩ . However, most of these results were obtained using contacts with a large resistance for which some allowance had to be made.

The ZnS:Mn used for these experiments was obtained from two separate sources, B.D.H. and AWRE. Its preparation has already been described in chapter 4. No systematic differences were observed between the electroluminescent properties of the ZnS:Mn obtained from these sources.

5.b.ii Device Structure and Contacts

Devices were normally fabricated on chips of dimensions - 6 mm x 4 mm x 1 mm which were cut from a slice of Zn/Al treated ZnS:Mn. These dice were polished with carborundum and jeweller's rouge in order to remove any surface layer leaving a smooth, clean surface and then etched in pure bromine for about 30 seconds. The bromine was removed by rinsing in methanol and then the sample was left in carbon disulphide for about 20 minutes to remove any etch products. The contacts were usually indium dots which were cut from a length of clean indium and then squashed on to the surface with a warm indium soldering iron. This procedure ensured that the indium wetted the crystal surface on melting which was found to be essential for obtaining mechanically good contacts. The contacts were formed by heating the crystal in a reducing atmosphere of nitrogen : 10% hydrogen to 420°C, and then cooling rapidly to room temperature.

Finally, a 1 mm diameter Schottky contact of either gold or aluminium was evaporated on to the opposite face of the device to produce a similar structure to that illustrated in figure 2.1. The

surface of the crystal had to be re-etched as before prior to the evaporation which was performed in a diffusion pumped, liquid nitrogen trapped chamber at a pressure of about 10^{-6} Torr.

When a reverse bias of about 50 V was applied to this structure (i.e. the Schottky contact negative and the indium positive) it lit up with a characteristic yellow-orange colour. The electroluminescence comes entirely from the depletion region which extends for about 600 Å below the evaporated contact. Information about this important region can be obtained from a measurement of the Schottky barrier capacitance as a function of voltage, as described in chapter 2. Briefly, the model is based on the depletion approximation which assumes that there is an electron-free region of change density $\ell (N_d - N_a)$ below the Schottky contact (figure 2.3). The width of this insulating layer increases with reverse voltage and can easily be determined from the capacitance using

$$C = \varepsilon_o \varepsilon_s A / W \quad . \qquad (5.1)$$

The average electric field can be calculated using

$$\mathcal{E}_{AV} = \frac{V_{TOTAL}}{W} = \frac{V_a + \phi}{W} \qquad (5.2)$$

where ϕ is the barrier height and V_a the applied reverse voltage. The barrier height could often be neglected in equation (5.2) because of the large reverse voltages which were required for electroluminescence. It should be noted that the electric field is not uniform in the depletion region. In fact it can be shown that the electric field varies linearly across the depletion region as will be discussed in section 5.c.iii. Finally, the effective donor concentration could be

measured from the variation of the capacitance with voltage i.e.

$$\frac{A^2}{C^2} = \left(\frac{2}{\varepsilon_0 \varepsilon_s (N_d - N_a) e}\right)(V_a + \phi) \quad (5.3)$$

Thus it is possible, in principle, to obtain a lot of useful information about the light emitting region by measuring the capacitance of the Schottky contact as a function of voltage. In practice, the large resistance of the ohmic contacts produced two separate problems. The first was that any voltage applied to a device like that shown in figure 2.1 will be divided between the Schottky and the indium contact. Thus, the voltage dropped across the depletion region is not known. The second problem is that at the measuring frequency of 1 MHz , the impedance of the Schottky contact ($|X| = 1/\omega C$; $C \sim 600$ pF) is of the order of 300 ohm, which is much smaller than that of the ohmic contact. It was only possible to measure the impedance of the two contacts in series which was equal to the impedance of the indium contact to a good approximation. Both problems could be solved by using a device structure as shown in figure 5.3. Here, the capacitance of two Schottky contacts in series is measured. If one contact is about ten times as large as the other, the total capacitance at zero bias is

$$C_T = \frac{C_s C_L}{C_s + C_L} = \frac{C_s \, 10C_s}{11 C_s} = \frac{10}{11} C_s \sim C_s \quad (5.4)$$

Thus, the total capacitance is equal to the capacitance of the small contact to a good approximation. On the application of a reverse bias to this contact its capacitance decreases and the

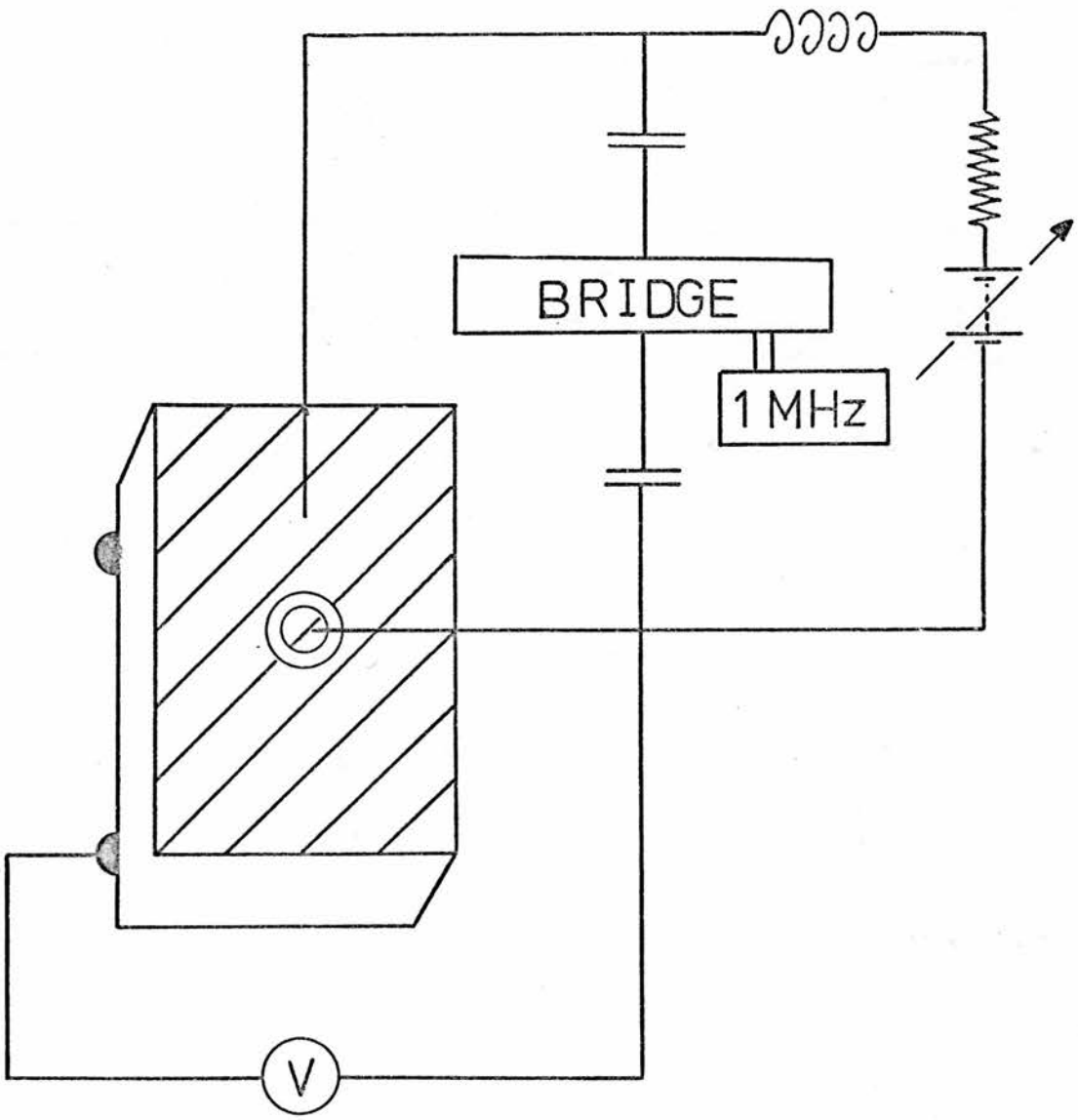

Figure 5.3(a) Device structure used for the C-V measurements.

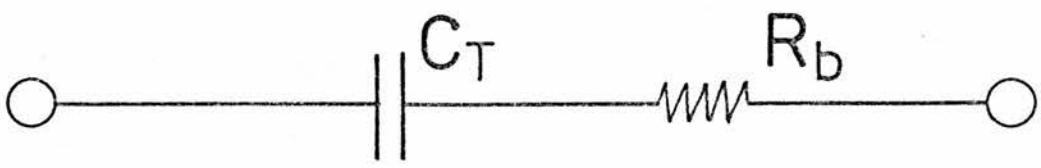

Figure 5.3(b) The equivalent circuit.

capacitance of the large contact increases making equation (5.4) an even better approximation. It was possible to measure the voltage dropped across the small Schottky contact by using one of the alloyed contacts as a probe electrode, as is shown in figure 5.3.

The resistivity of the ZnS was measured by the Van der Pauw technique to be between 10 and 100 ohm cm for all the crystals measured here and hence the equivalent a.c. circuit for a ZnS diode is C_T in series with a bulk resistance R_S. The impedance of this circuit was measured with a Wayne Kerr bridge which compared the unknown impedance with a parallel R-C circuit. This was converted into an equivalent series circuit using the standard formulae. The value of R_S so obtained is plotted as a function of voltage in figure 5.4. It can be seen that this is independent of voltage to within experimental error. Also plotted in figure 5.4 is $1/C_T^2$ against V, which is a straight line as predicted by equation (5.3). The equivalent circuit of figure 5.3 is only valid if the resistance of the Schottky contact is larger than the reactance of the depletion region with which it is in parallel. At large applied voltages, the Schottky contact begins to draw a significant amount of current which causes both curves of figure 5.4 to deviate from straight line behaviour. For small voltages, the effect of the large capacitance on the measured capacitance is greatest. A computer program was written to correct for this by an iterative technique, which showed that the correction was small provided that one contact was at least six times larger than the other.

For one sample, the bulk resistance, as determined from the a.c. impedence at 1 MHz, was measured as a function of temperature using the sample geometry shown in figure 5.5. This varied with temperature

Figure 5.4 A typical C-V plot. The series resistance is also shown.

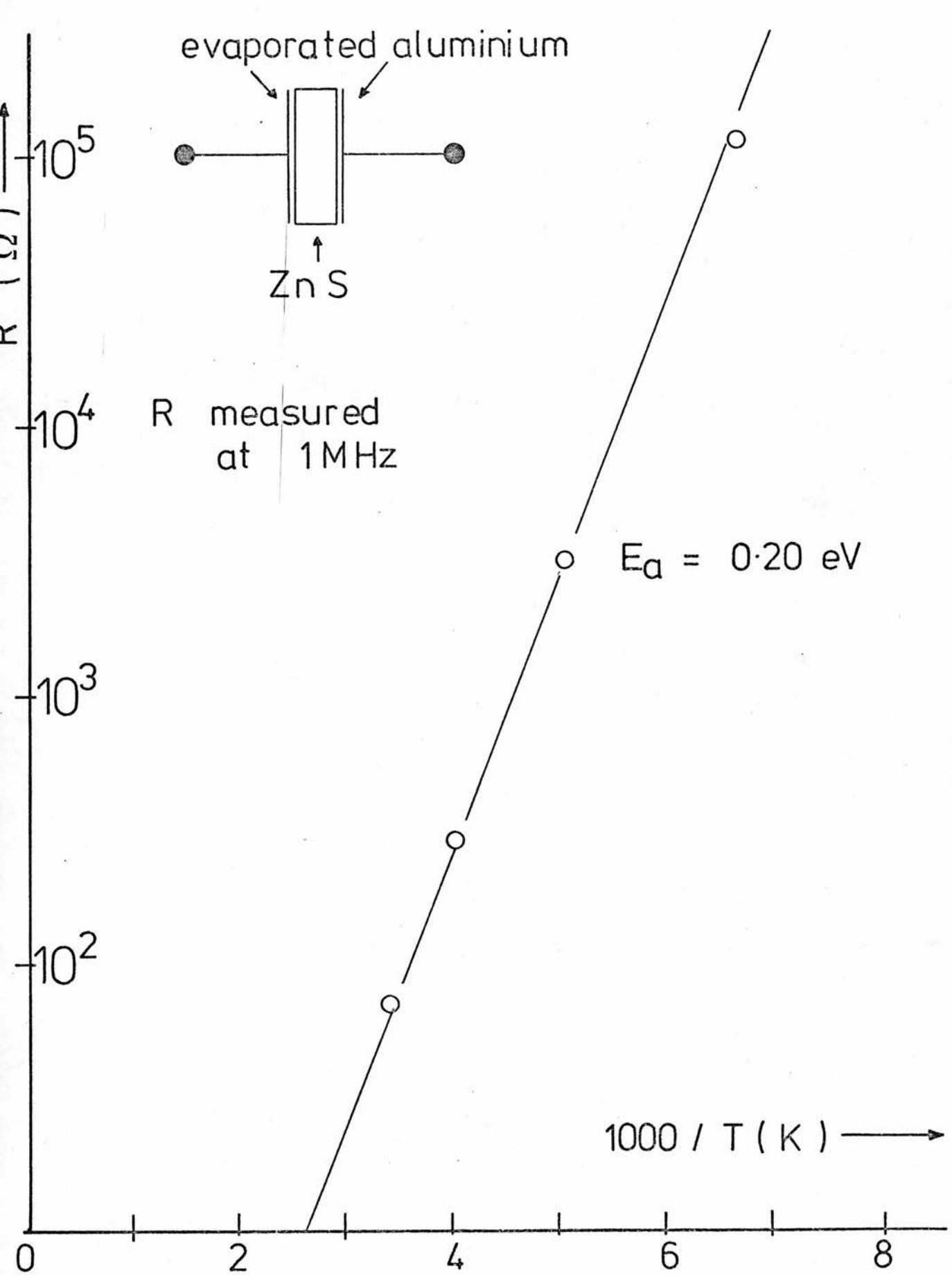

Figure 5.5 The variation of the bulk resistance with temperature.

according to

$$R = R_o \exp\left(\frac{e\phi}{kT}\right)$$

with ϕ = 0.20 eV which is close to that obtained by the more conventional Van der Pauw technique described in chapter 4.

5.b.iii Results

The device structure shown in figure 5.3 is also very suitable for measuring the light output and the current density as a function of voltage. Because of the closeness of the two Schottky contacts, the bulk resistance is small ($<$ 100 ohms) and hence it was not necessary to correct for the bulk resistance of the sample even for the largest currents used (10^{-2} A). The voltage dropped across the small Schottky contact could then be conveniently measured using a probe electrode as before.

The current was supplied with a Keithley 225 current source and the light measured with a S-4 response photomultiplier type RCA 931 A which was mounted directly above the sample. The voltage was measured with a Keithley 616 digital electrometer which had an input impedance of greater than 10^{14} ohms. As both the voltage drop across the Schottky contact and the measured light output should not depend on whether the alloyed contact or the large Schottky contact is used as the probe electrode, a switch was incorporated which could change their relative positions in the circuit. The device was remade if there was any difference between these readings. The current-voltage and light-voltage curves are plotted for two different devices in figures 5.6 and

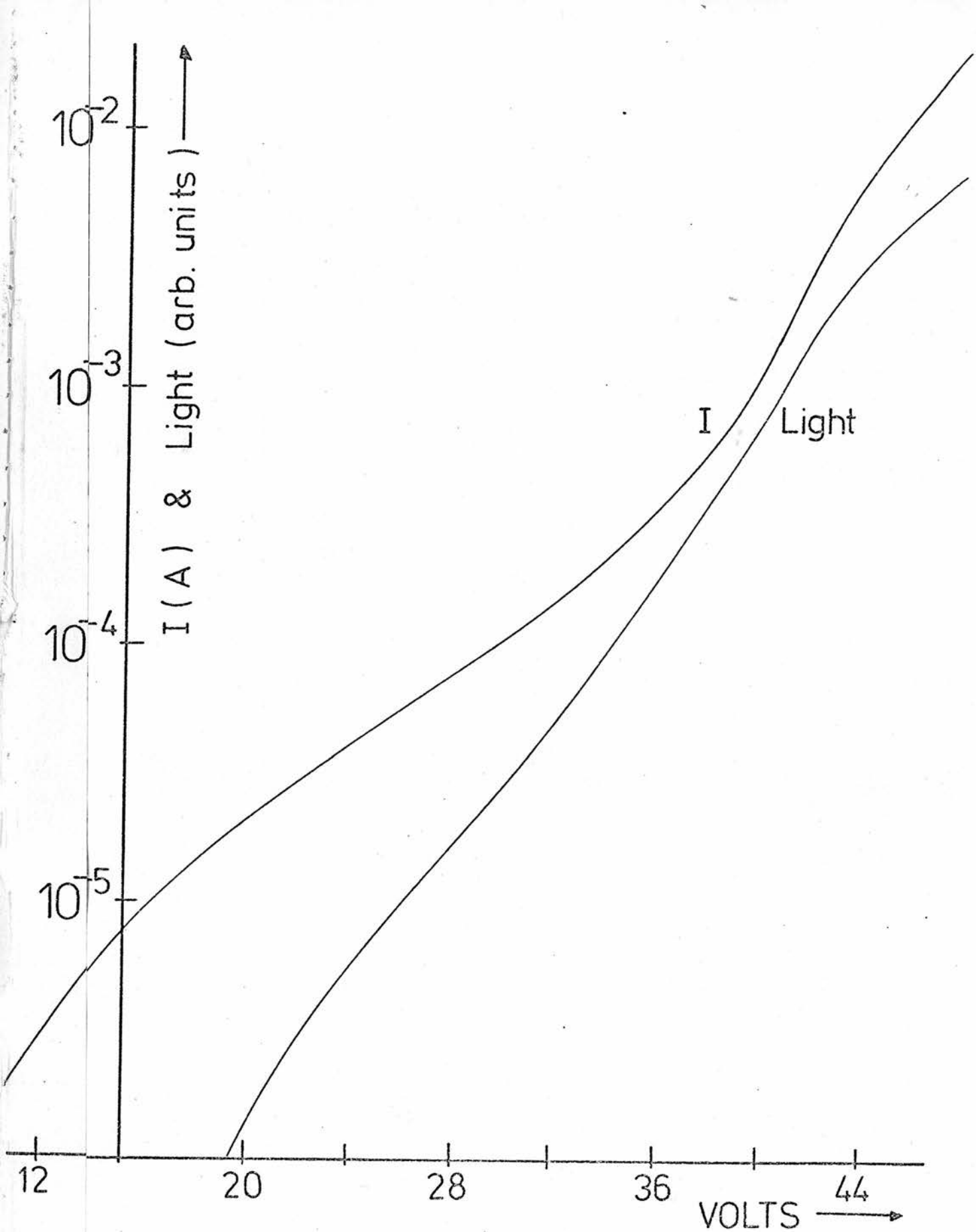

Figure 5.6 The variation of the light and current with voltage for a typical diode.

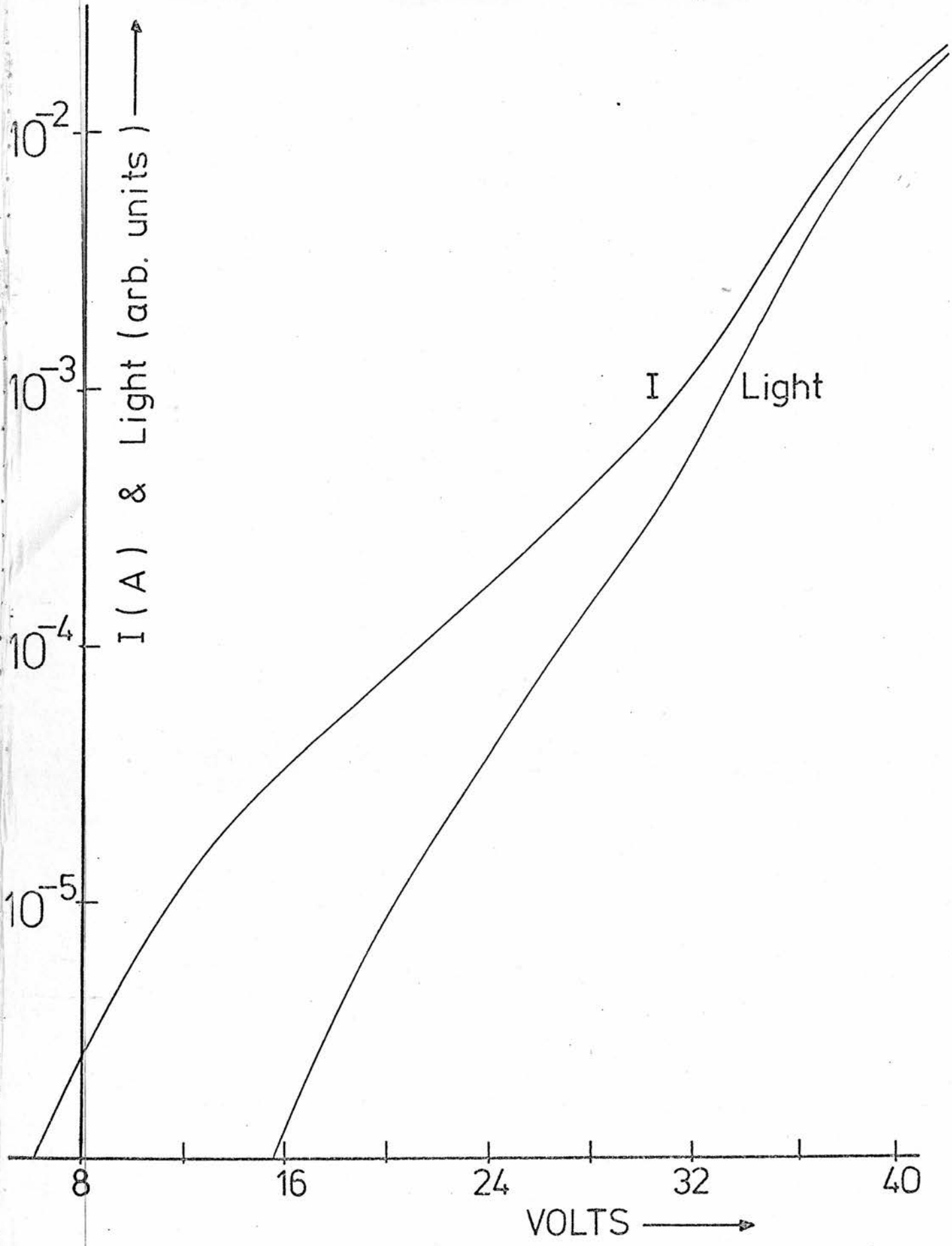

Figure 5.7 The variation of the light and current with voltage for a typical diode.

5.7. The electroluminescence spectrum of a ZnS:Mn device is shown in figure 5.8(b) which is to be compared with its photoluminescence spectrum excited at 5 000 Å in figure 5.8(a).

5.c Theory of Electroluminescence

5.c.i Mechanism of Electroluminescence

From the similarity of the two spectra in figure 5.8, it is evident that the electroluminescence is from the $^4T_1$ - $^6A_1$ transition within the manganese d^5 shell. The mechanism by which this is excited will now be considered.

Under reverse bias, electrons are injected from the metal Schottky contact into the depletion region where they are accelerated by the depletion region field. Once the energy of an electron exceeds a certain threshold, it can transfer its energy to a manganese impurity leaving it in an excited state. Figure 5.9 shows three possible mechanisms by which energetic electrons can excite the manganese luminescence (note that the position of the manganese levels relative to the conduction and valence bands is purely schematic). In the impact process (figure 5.9(a)), the energy of the electron is transferred directly to the impurity. This process is the simplest of the three, requires the least energy, and is thought to be responsible for most of the luminescence. The second process involves impact ionisation of the manganese followed by the capture of another electron into the excited state. Impact ionisation is thought to occur at high fields in ZnSe:Mn as it produces a detectable amount of multiplication.[71] However, this also suggests that the ionised manganese is more likely

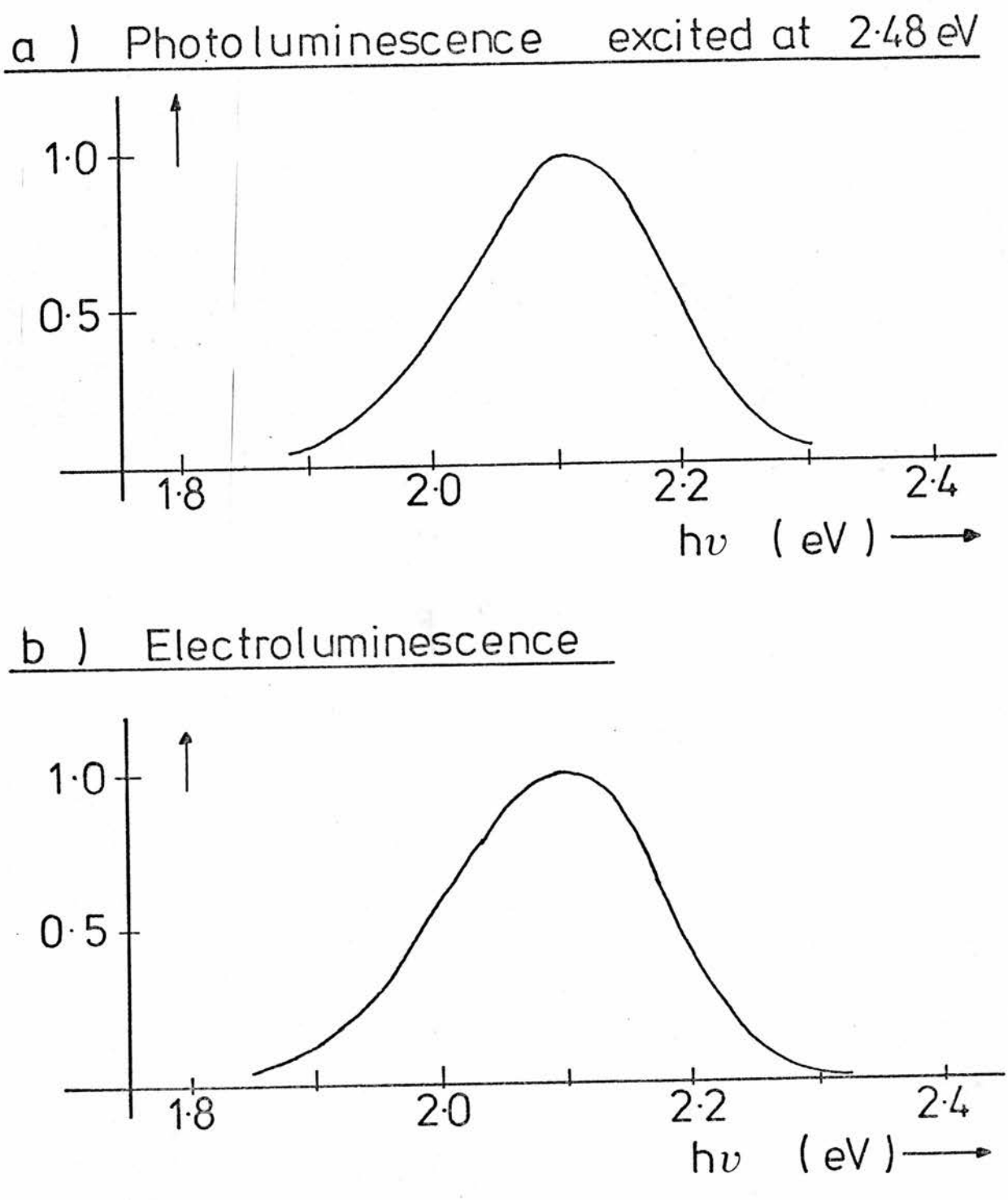

Figure 5.8 The photoluminescence and electroluminescence spectra of ZnS:Mn.

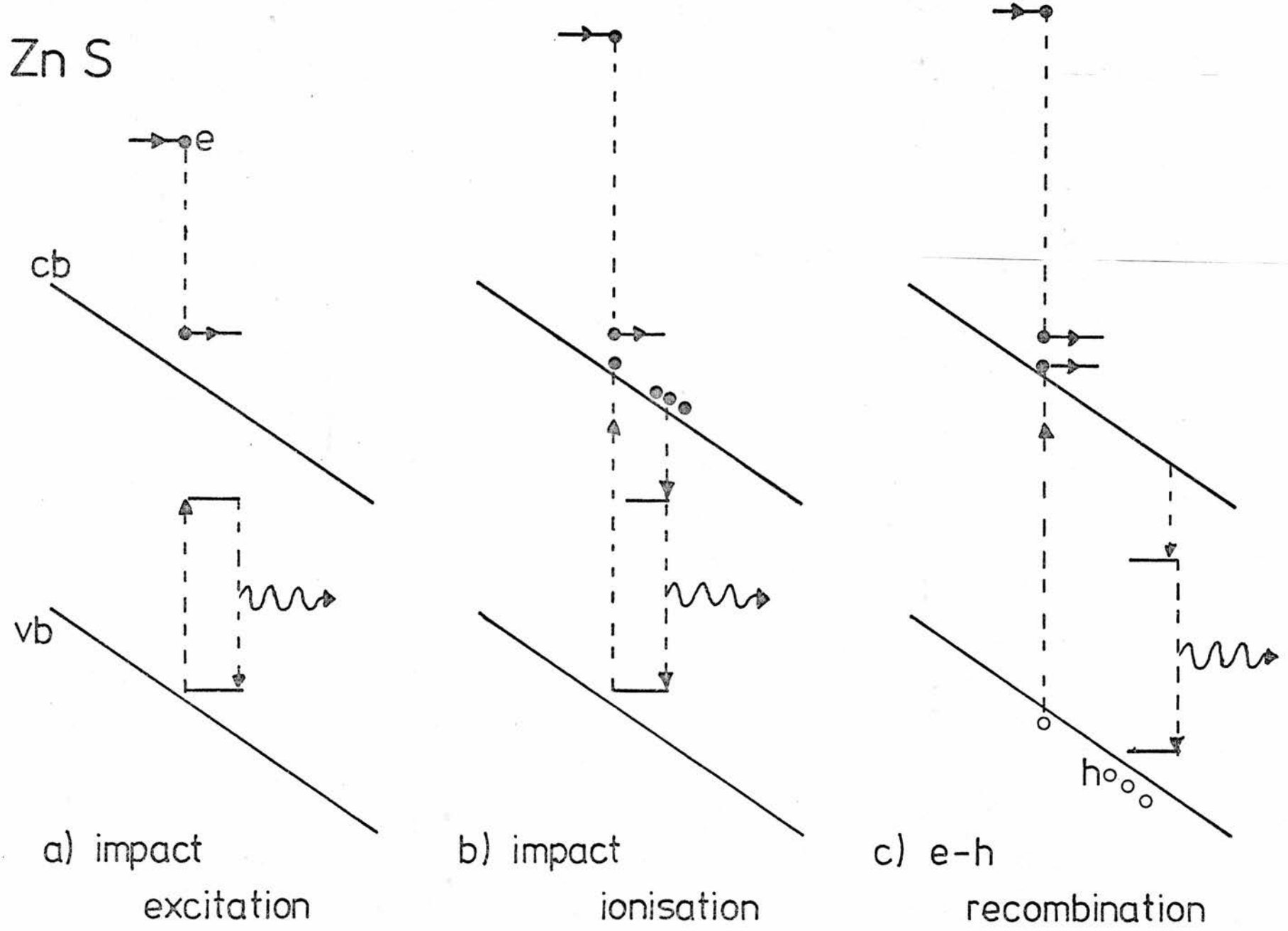

Figure 5.9 Three possible excitation processes.

to capture an electron from the valence band than from the conduction band as the latter process would not produce multiplication. In fact, the capture of an electron from the conduction band is expected to be a very inefficient process. This is because the mean energy in the depletion region is of the order of 2 eV, and hence the electron capture involves a radiationless transition of greater than 2 eV.

In the third process, the excitation is due to avalanching followed by recombination of the resulting electrons and holes at an impurity centre. It should be noted that the threshold energy for electron-hole pair production is expected to lie between E_g and $3/2\ E_g$ which is significantly larger than that required for impact excitation ($E_g \sim 3.65$ eV for ZnS at room temperature). In fact, electroluminescence in ZnSe:Mn occurs at lower fields than is necessary for avalanching.[70] In addition, the process which is illustrated in figure 5.9(c) involves the capture of a conduction band electron into the manganese excited state. In this respect, it is similar to the second process and hence equally unlikely.

Further evidence for the importance of impact excitation comes from the investigation of the electroluminescence in $ZnS:Tb^{3+}$ by Krupka.[72] This material has two luminescing bands at 2.54 eV and 2.83 eV. The spectrum of a thin film of $ZnS:Tb^{3+}$ was measured as a function of applied voltage and it was found that the relative intensity of the high energy emission increased with increasing voltage. Figure 5.10 shows the energy level diagram for $ZnS:Tb^{3+}$ together with the variation of the ratio of the emission intensities of the two bands with voltage for a typical device. Krupka suggests that the terbium is excited directly by an impact process and hence the $^5D_3$

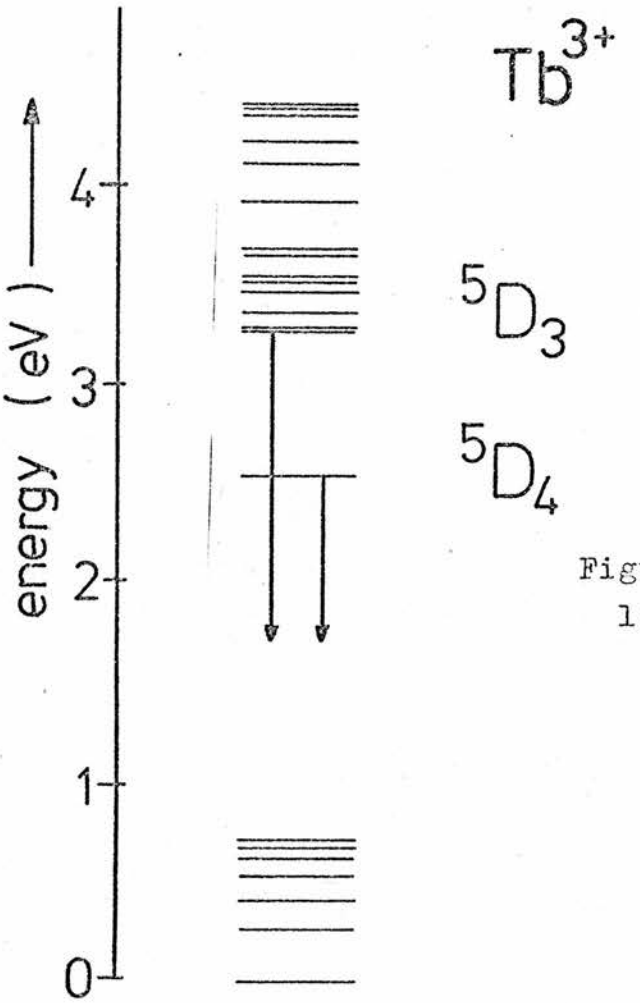

Figure 5.10(a) The energy level diagram for ZnS:Tb^{3+}.

Figure 5.10(b) The variation of the ratio of the intensities of the two transitions with voltage.

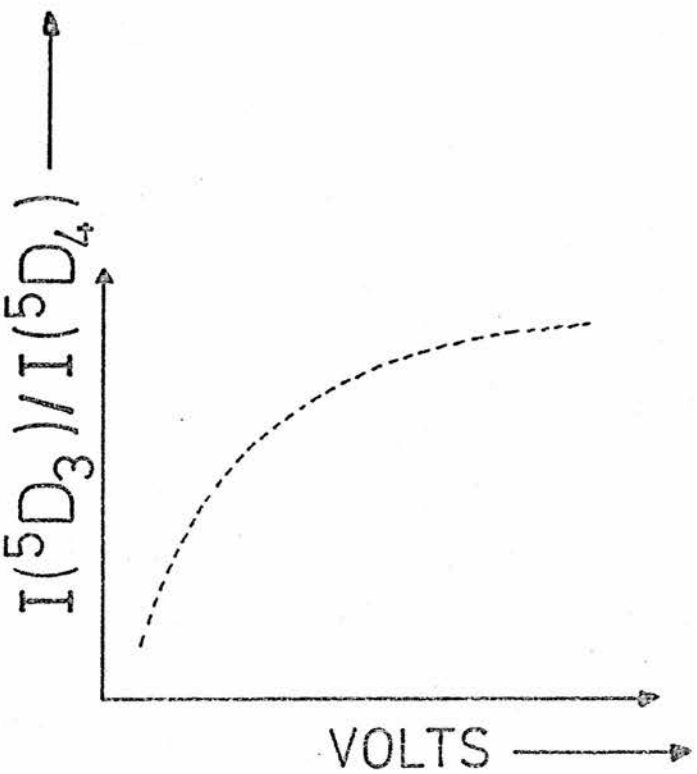

emission is proportional to the fraction of the electrons which have an energy greater than 2.83 eV. Thus, the increase of I ($^5D_3$) / I ($^5D_4$) with voltage is due to the increase of the mean electron energy with voltage. If the terbium was being excited by either of the processes illustrated in figures 5.9(b) and (c), then I ($^5D_3$) / I ($^5D_4$) would not be expected to vary with voltage as the energy transferred to the terbium would always be greater than 2.83 eV.

Finally, some evidence concerning the excitation mechanism comes from the work of Tanaka, Kobayashi, Sarsakina and Hamakana.[63] Here, the response of a ZnS:Mn thin film to a N_2 laser pulse of 3 371 Å was measured. It was found that after applying the 10 ns pulse, the manganese 5 800 Å emission grew to a maximum in about 30 μs. The interpretation is that the laser light produces electron-hole pairs in the ZnS which can excite luminescent centres of unknown origin. Subsequently, luminescent manganese centres are excited through non-radiative energy transfer from these centres with a time constant of about 30 μs.

After applying an electrical pulse to the film, however, the manganese emission appears to decrease monotonically with time. It follows that the manganese centres are not being excited once the electric field has been switched off. It is suggested that in electroluminescence, the manganese is being excited directly by electrons which have been accelerated by the high field. After switch off, the number of hot electrons decreases very rapidly because of scattering.

It is therefore reasonable to conclude that the dominant excitation mechanism is the impact process illustrated in figure 5.9(a).

5.c.ii Theory of Electroluminescence by Impact Excitation

It will be shown in section 5.e that the band structure of ZnS plays an important role in the electroluminescence of ZnS:Mn. In this section, the theory will initially be developed for an arbitrary band structure and then simplified by assuming parabolic bands. This produces a simple equation which describes the electroluminescence in ZnSe:Mn as reported by Allen[70] in a review paper on impact excitation. It will be shown in section 5.d that electroluminescence in ZnS:Mn is also described by this equation except at very high fields, and deviations from the expected behaviour will be examined.

The quantum efficiency is defined as the number of photons produced by one electron crossing the depletion region and hence is proportional to the light intensity divided by the current. For a general band structure, the electron states are described by $|\, n, \underline{k} \,\rangle$ where n is the band number and $\underline{k}$ is the wavevector. Let $R'(n, \underline{k})$ be the rate at which an electron in $|\, n, \underline{k} \,\rangle$ impact excites a manganese atom, i.e. $R'(n, \underline{k})$ is the reciprocal of the lifetime of an electron in $|\, n, \underline{k} \,\rangle$ due to impact excitation. Then the quantum efficiency is given by

$$\eta_{qu}(\mathcal{E}) = \eta_{RAD} \frac{\sum_n \int_{B.Z.} R'(n,\underline{k}) f(n,\underline{k},\mathcal{E}) d^3\underline{k}}{v_d(\mathcal{E})/W} \quad (5.5)$$

where

$v_d(\mathcal{E})$ is the drift velocity

W is the depletion region width

$f(n, \underline{k}, \mathcal{E})$ is the probability of $|\, n, \underline{k} \,\rangle$ being occupied which will depend on the electric field

η_{RAD} is the probability that an excited manganese atom will decay radiatively and is expected to be about 1.

The rate R' (n, $\underline{k}$) will be proportional to the concentration of manganese atoms in the $^6A_1$ state i.e.

$$R'(n,\underline{k}) = (N_{Mn} - N_{Mn^*})\, R(n,\underline{k}) \qquad (5.6)$$

It has been estimated in reference [70] that only a small fraction of the manganese centres are ever excited and hence to a good approximation

$$\eta_{qu}(\xi) = \eta_{RAD}\, W\, N_{Mn}\, \sigma \qquad (5.7)$$

where σ is the averaged cross section defined by

$$\sigma = \frac{\Sigma_n \int_{B.Z.} R(n,\underline{k})\, f(n,\underline{k},\xi)\, d^3\underline{k}}{v_d(\xi)} \qquad (5.8)$$

The distribution function f (n, $\underline{k}$, ξ) has been calculated by Baraff[73] assuming parabolic bands and predominant optical phonon scattering. The interaction between the electrons and the phonons was described by a constant mean free path λ and a phonon energy E_R. For large electric fields, the distribution function tends to a Maxwellian of the form

$$f(E,\xi) \propto E^{\frac{1}{2}} \exp -\frac{E}{kT_e}$$

where T_e is the electron temperature given by

$$k T_e = \frac{(e \xi \lambda)^2}{3 E_R} \qquad (5.10)$$

The functional form of the excitation rate is not known and hence it will be assumed that

$$R(E) = R_0 U(E - E_{th}) \qquad (5.11)$$

where U is the Heaviside function and E_{th} is the threshold energy for impact excitation.

It is shown in appendix 5A that the approximations given by equations (5.9) and (5.11) reduce the equation for the cross section to

$$\sigma = \sigma_0 \exp -\left(\frac{\xi_0}{\xi}\right)^2 \qquad (5.12)$$

where

$$\xi_0 = \left(\frac{3 E_{th} E_R}{(e \lambda)^2}\right)^{1/2} \qquad (5.13)$$

and hence, equation (5.7) becomes

$$\eta_{qu}(\xi) = \eta_{RAD} W N_{Mn} \sigma_0 \exp -\left(\frac{\xi_0}{\xi}\right)^2 \qquad (5.14)$$

Allen[70] has found that equation (5.14) describes the behaviour of ZnSe:Mn Schottky diodes except at very high fields. The results for ZnS:Mn will be compared with this equation in section 5.d. The variation of the quantum efficiency with applied field is determined by a characteristic field ξ_0. Equation (5.13) shows that ξ_0 depends

on E_{th}, E_R and λ and is therefore not expected to vary from diode to diode provided that optical phonon scattering is predominant in determining the electron temperature.

5.c.iii Effect of Non-Uniform Field

It was noted in section 5.b that the electric field in the active region of a Schottky diode is not uniform, but varies linearly across the depletion region. Provided that the electron mean free path is short enough, it is possible to average the cross section of equation (5.12) across the depletion region. Hence

$$\langle\sigma\rangle = \int_0^W \sigma_0 \exp -\left(\frac{\xi_0}{\xi}\right)^2 \Big/ W \qquad (5.15)$$

Changing the variable from x to ξ, it follows from the linear variation of ξ with x that $\xi = \xi_{max}\, x/W$ and

$$\langle\sigma\rangle = \frac{\sigma_0}{\xi_{max}} \int_0^{\xi_{max}} \exp -\left(\frac{\xi_0}{\xi}\right)^2 d\xi \qquad (5.16)$$

$$= \sigma_0 \frac{\xi_0}{\xi_{max}} \Gamma_{\frac{1}{2}}\left(\frac{\xi_0}{\xi_{max}}\right)^2$$

where $\Gamma_{\frac{1}{2}}(x)$ is the incomplete gamma function which is tabulated in, for example, reference [74]. This is plotted in figure 5.11 from which it can be seen that over the range of ξ_0/ξ_{max} encountered experimentally in ZnS:Mn

$$\langle\sigma\rangle = 0{\cdot}23 \exp -1{\cdot}20\left(\frac{\xi_0}{\xi_{max}}\right)^2 \qquad (5.17)$$

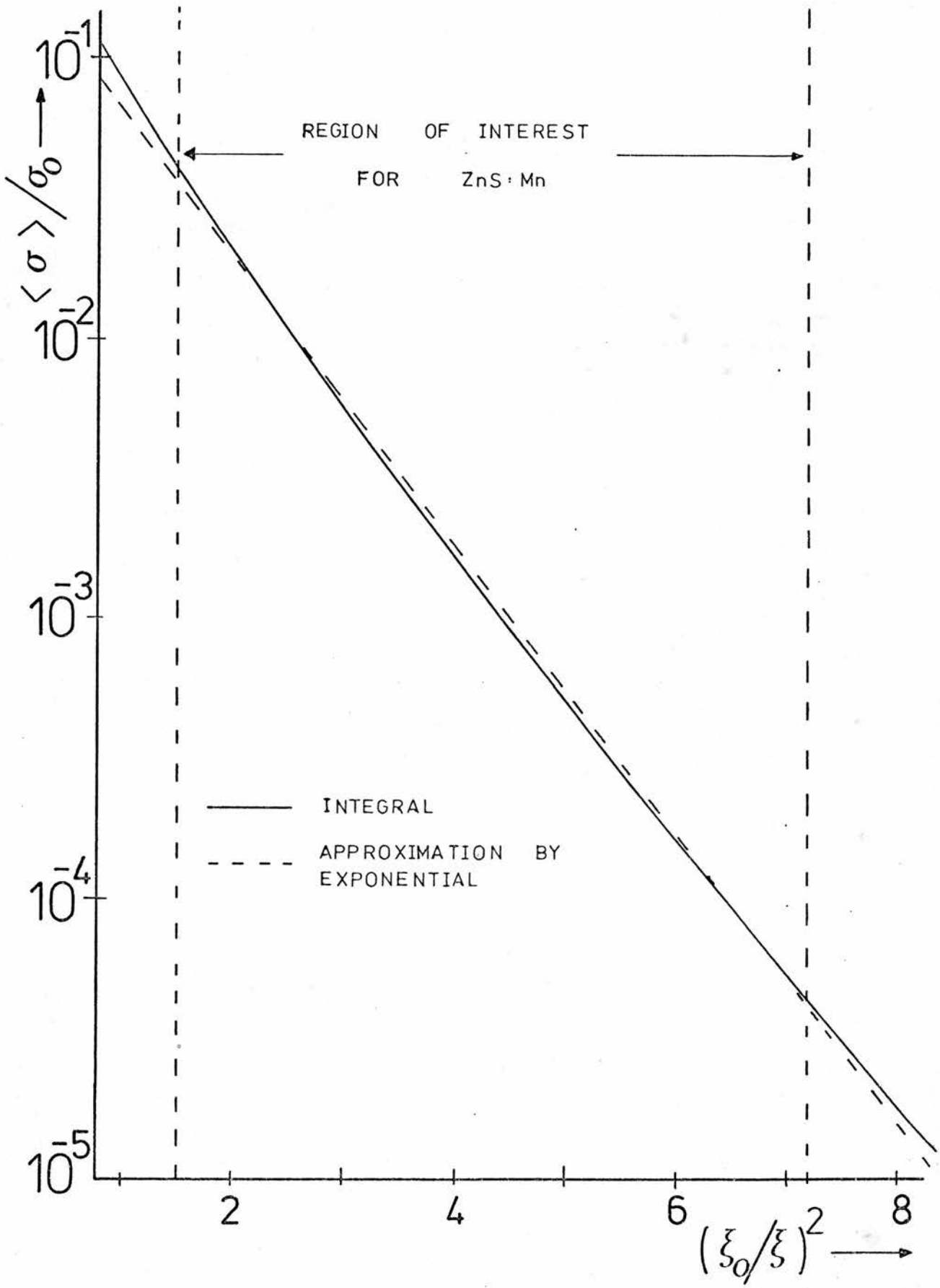

Figure 5.11 The variation of the averaged cross section with field.

to a good approximation. The experimental results were normally fitted to the formula

$$\langle \sigma \rangle = \sigma_o' \exp - \left(\frac{\xi_o'}{\xi_{av}} \right)^2 \quad (5.18)$$

Since $\xi_{av} = \xi_{max}/2$, a comparison of equations (5.17) and (5.18) shows that

$$\begin{aligned} \sigma_o &= 4.35\ \sigma_o' \\ \xi_o &= 1.82\ \xi_o' \end{aligned} \quad (5.19)$$

Thus, if equation (5.14) holds for a device with a uniform field, it is also expected to hold for a Schottky diode, but with a larger value of ξ_o. Note that equation (5.19) has not been used to correct any of the experimentally determined values of ξ_o quoted in this thesis.

5.d Results - Comparison with Theory

Figure 5.12 shows the variation of the quantum efficiency with electric field for a typical diode plotted according to equation (5.14). It can be seen that this equation is obeyed except at the highest fields where the quantum efficiency per unit depletion region width reaches a maximum and then drops. This unexpected maximum has been seen in all the diodes so far studied and is discussed in section 5.e. The value of ξ_o in figure 5.12 is 6×10^5 V/cm. The analysis of section 5.c suggests that ξ_o is a constant which depends only on the semiconductor and hence is not expected to vary from diode to diode. To check this, measurements of the variation of the quantum efficiency with field were performed on a large number of diodes. The results are plotted in

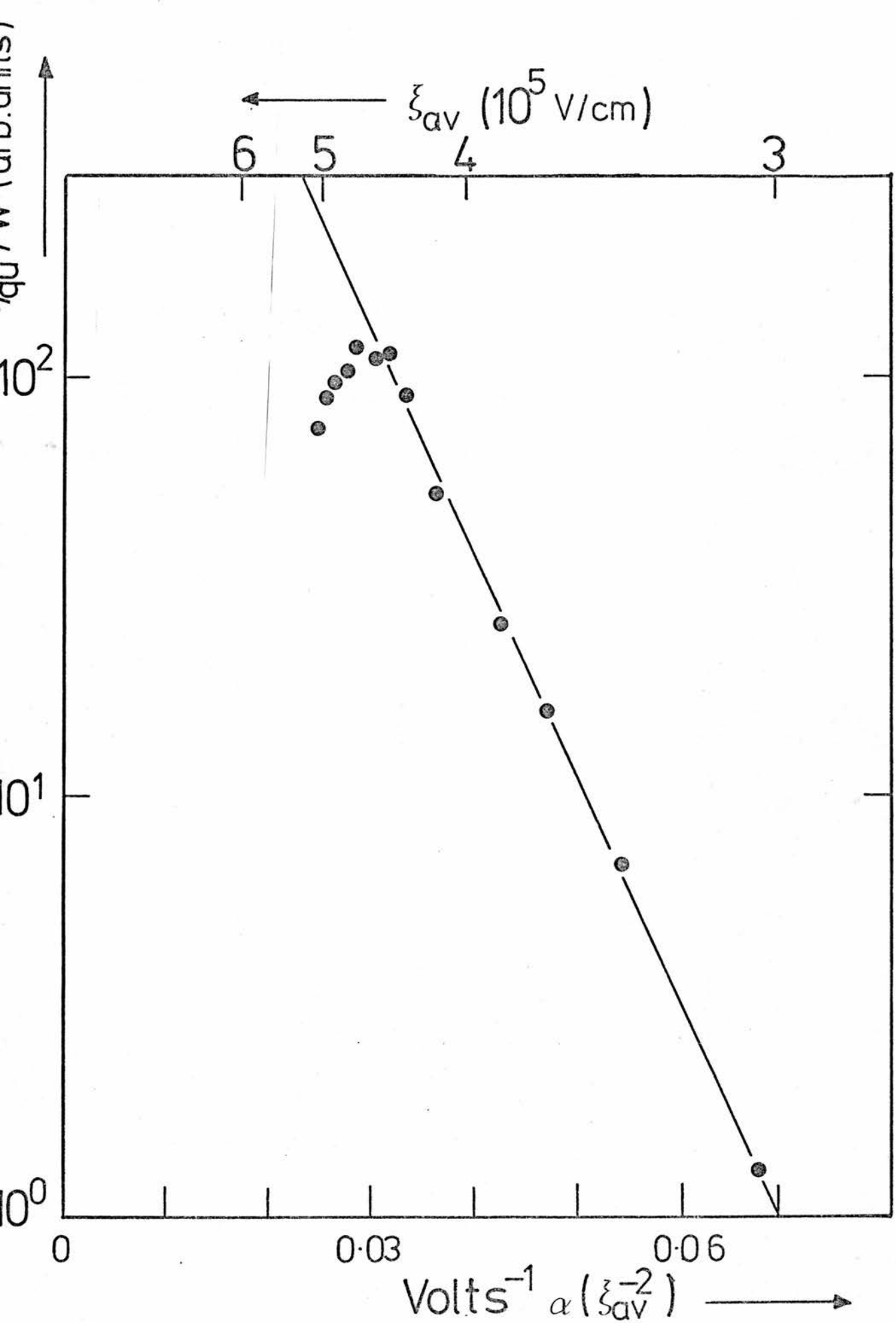

Figure 5.12 The variation of the quantum efficiency with field plotted according to equation (5.14).

figure 5.13. It can be seen from this figure that not only does $\mathcal{E}_o$ vary from diode to diode, but varies systematically with the donor density N_d. Note that figure 5.13 contains results for ZnSe:Mn as well as ZnS:Mn and that all of the results fall on a universal curve. The results for ZnSe:Mn were obtained at both 100 K and 300 K by S. M. H. Feiz of this laboratory.

The variation of $\mathcal{E}_o$ with N_d implies that the fundamental assumption of predominant optical phonon scattering in the theories of Wolff,[75] Schockley[76] and Baraff[73] for the variation of the electron distribution function with electric field is not applicable to ZnSe or ZnS. It is therefore not obvious how $\mathcal{E}_o$ is to be interpreted. If the cross section for the electrons which have an energy greater than the threshold for impact excitation is σ_o, then the mean cross section is given by

$$\sigma = \sigma_o f(\mathcal{E}) \qquad (5.20)$$

where $f(\mathcal{E})$ is the fraction of the electrons above the threshold energy. Thus, in the straight line region of figure 5.12

$$f(\mathcal{E}) \sim \exp - \left(\frac{\mathcal{E}_o}{\mathcal{E}}\right)^2 . \qquad (5.21)$$

Thus, for a given electric field, the fraction of the electrons which are above the threshold decreases as $\mathcal{E}_o$ increases. Figure 5.13 can now be interpreted as showing that for a given field, the fraction of the electrons which have energies greater than 2.23 eV decreases as N_d increases. If this interpretation is correct, then it can be concluded that ionised impurity scattering is important in determining the distribution function for electrons in ZnS at high fields. Ionised

Figure 5.13 The variation of the characteristic field with the donor density.

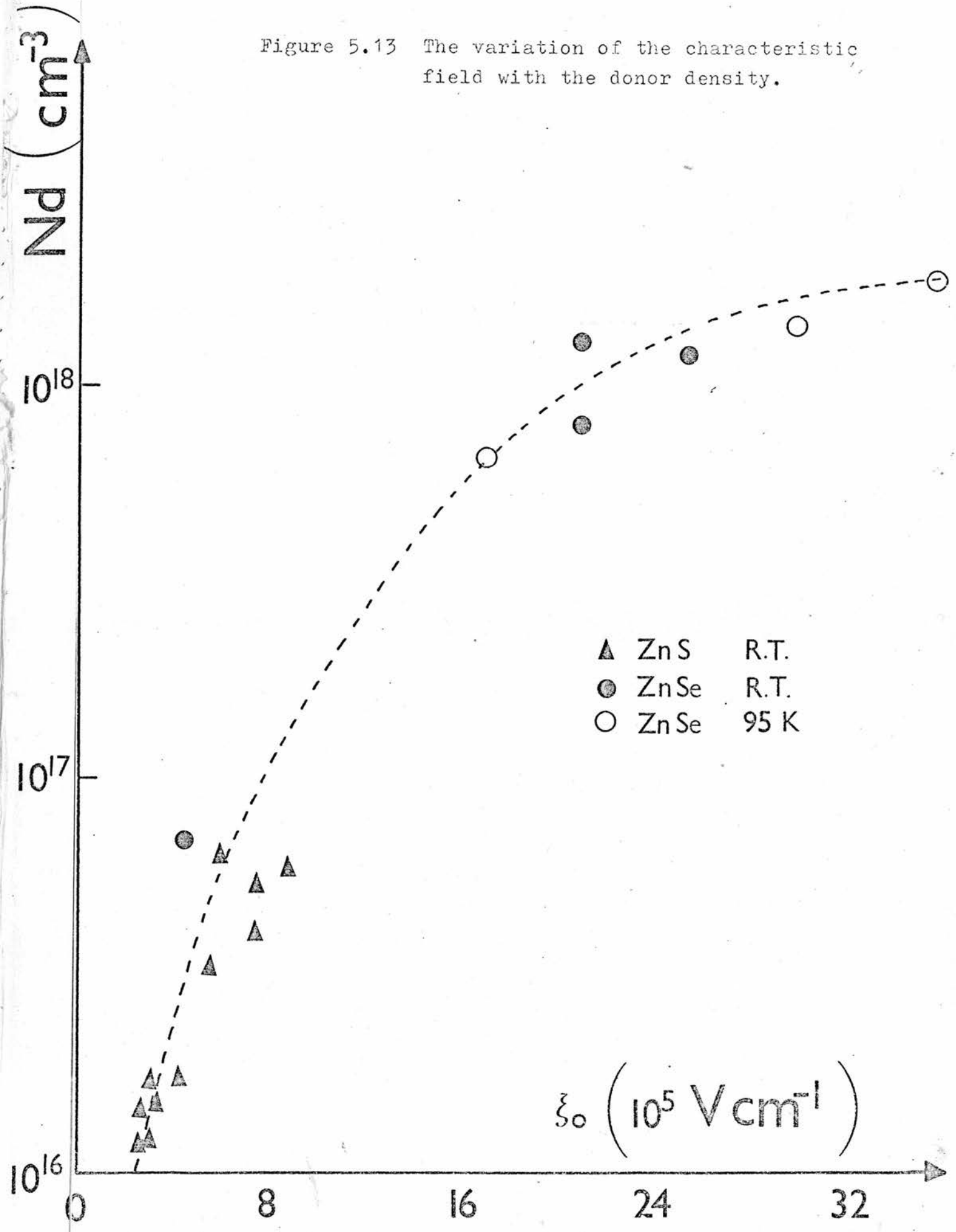

impurity scattering is normally considered to be insignificant for electrons with sufficient energy to emit an optical phonon[71] and the reasons for its importance in ZnS and ZnSe will be discussed in the next section.

5.e Discussion

5.e.i Actual Electron Distribution Function

The band structures of ZnS and ZnSe are reproduced from reference [68] in figures 5.14 and 5.15. The threshold energy for impact excitation is also indicated on these figures and it can be seen that the electrons responsible for the electroluminescence have to be in the X_3 minimum or higher. It should be noted from figures 5.14 and 5.15 that the band structures of ZnSe and ZnS are very similar, especially with regard to their conduction bands.

Under high electric fields, electrons tend to congregate in places where their group velocity is low and effective mass is large, i.e. near the conduction band minima. This is because scattering of the electrons is more efficient for slow incident particles. Hence, ionised impurity scattering is particularly effective near the conduction band minima at L_1, X_1 and X_3 because of the flatness of the bands. The importance of ionised impurity scattering is therefore a direct consequence of the non-parabolic nature of the band structure.

Some direct evidence that the electrons tend to congregate near the band minima has been obtained by Turvey and Allen.[77] It has already been noted that if the mean electron energy exceeds 2 eV, the effective electron temperature is about 1 500 K. These hot electrons

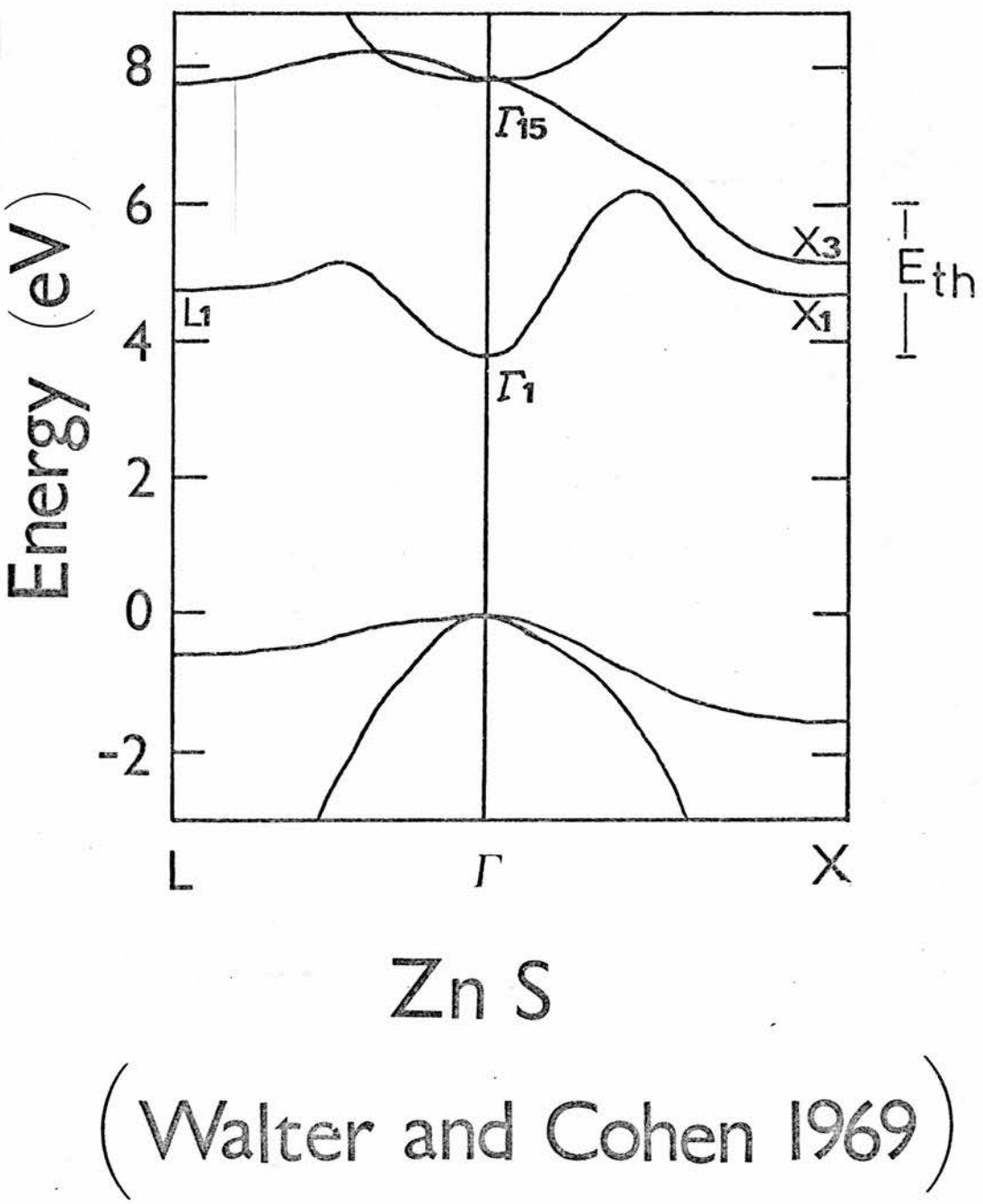

Figure 5.14 The band structure of ZnS.

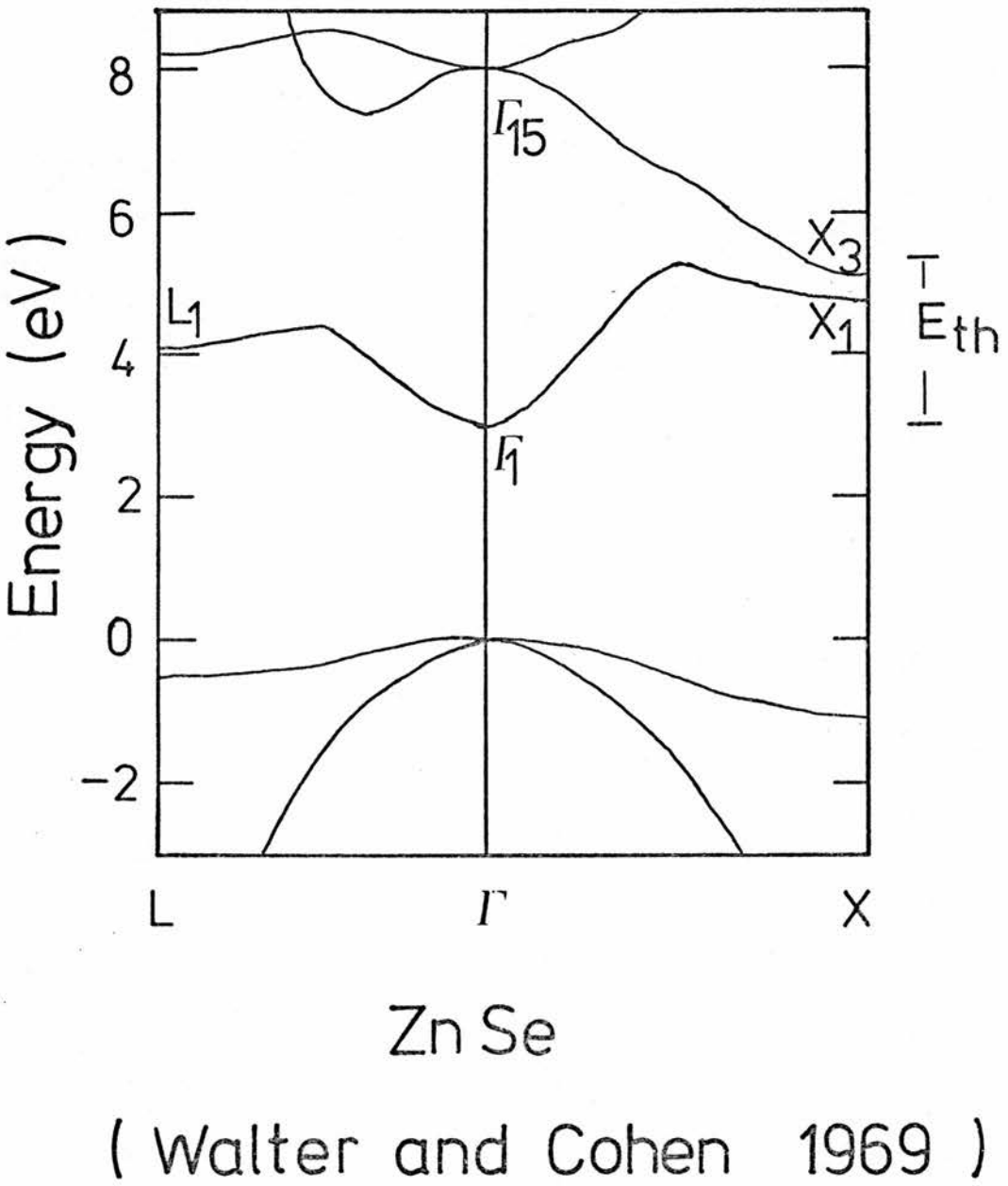

Figure 5.15 The band structure of ZnSe.

are expected to emit black body radiation. Turvey and Allen have observed a broad, structured peak extending from 0.4 to 2.65 eV in reverse biased Schottky diodes on ZnSe which does not contain any deliberately added impurities. They interpret the band as being due to hot electrons. However, they find that neither the spectrum nor the intensity of the emission can be explained unless it is assumed that the predominant transitions are between the conduction band minima. Hot electron emission has recently been observed in ZnS:Mn by Skolnick.[78]

5.e.ii Maximum in the Quantum Efficiency

Some insight into the high field quenching of the quantum efficiency can be obtained by plotting the electric field at the maximum quantum efficiency against the donor density. This is plotted in figure 5.16 for both ZnSe and ZnS and shows that a large donor density implies a large $\mathcal{F}_{max}$. The results for ZnSe:Mn were again obtained by S. M. H. Feiz and contain measurements at 100 K as well as room temperature. The similarity between the fields in the two systems suggests that the quenching in ZnSe:Mn and ZnS:Mn is due to the same process.

A number of possible explanations are listed in table 5.1 and are described in greater detail below.

1. At high drive voltages, the power dissipated in the depletion region causes its lattice temperature to increase. This increase in the lattice temperature reduces the radiative efficiency of the manganese $^4T_1 - {}^6A_1$ transition as is shown in figure 4.6. It can be seen from figure 5.16 that this is not the case as the $\mathcal{F}_{max}$ for diodes

Figure 5.16 The variation of the field at the maximum of the quantum efficiency curve with N_d.

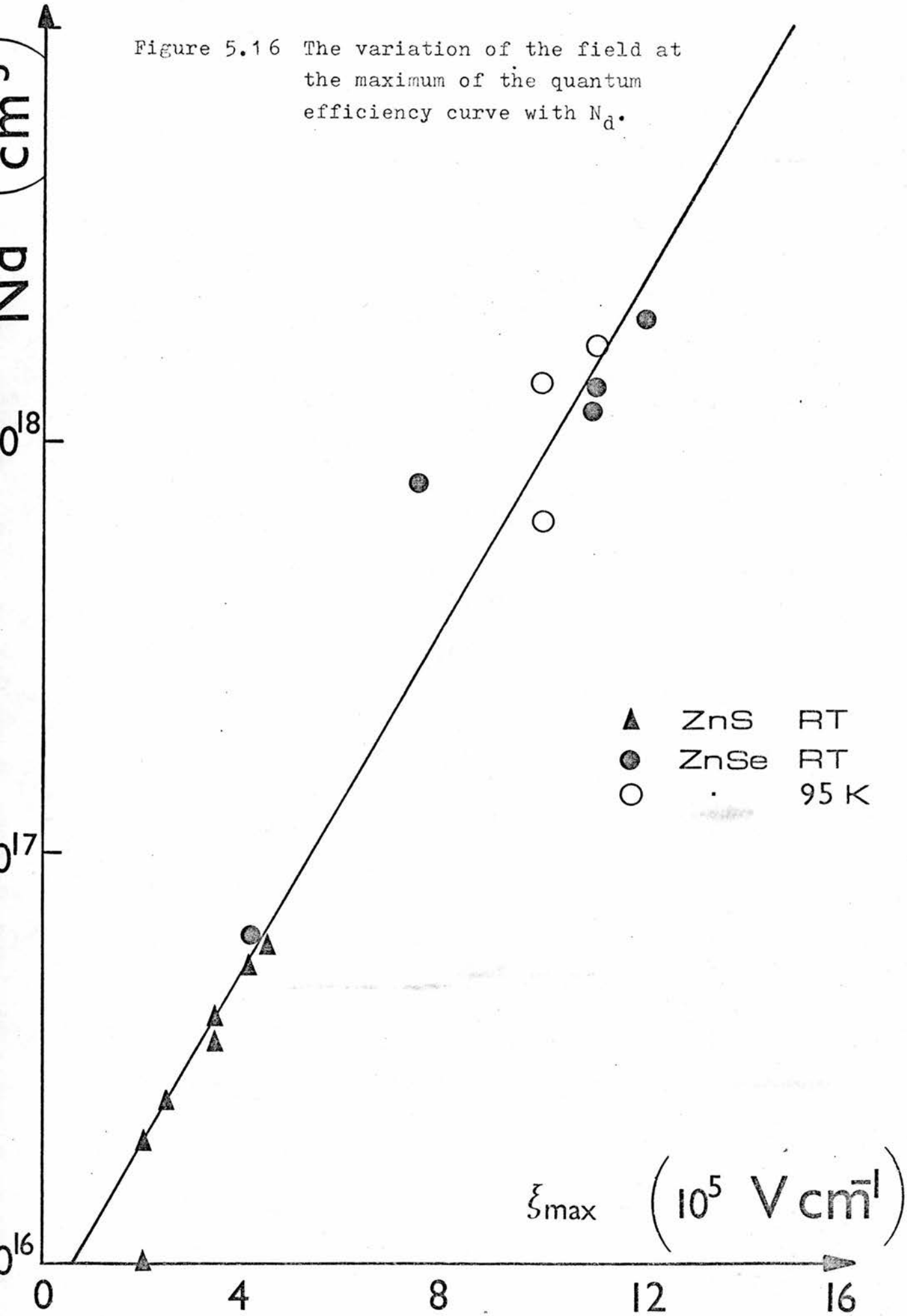

TABLE 5.1

Possible explanations for the drop in the quantum efficiency at high fields

Number	Mechanism	Comments
1	depletion region heating quenches the radiative efficiency	the quenching is not affected by temperature in ZnSe
2	the mean electron energy exceeds peak in cross section curve	possible - but cross section curve is not expected to be sharply peaked
3	electrons which diffuse to high energies can lose energy by:	possible - but depends on threshold energies in ZnS and ZnSe being roughly similar
	(a) impact ionisation of Mn	
	(b) impact ionisation of impurity centre, such as M centre [41]	different threshold energies for ZnS and ZnSe - also results would depend on the concentration of the centre
	(c) band to band ionisation	occurs at higher energy than (a) or (b) - large difference between ZnS and ZnSe
4	significant fraction of Mn impurities excited, leaving less available for excitation	expected to depend on current density rather than field
5	at high current densities, it is possible for an excited Mn centre to be impact ionised before it can decay radiatively	expected to depend on current density - Mn decay is ten times faster in ZnSe than ZnS
6	Auger quenching	ultimate limitation

which have been cooled to 100 K is equal, to within the spread of the experimental points, to that of the diodes at room temperature.

The fact that the maximum in the quantum efficiency appears to correspond to a certain electric field, suggests that it also corresponds to a particularly favourable electron distribution. Figure 5.16 shows a larger field is required in diodes which have a large donor concentration. This is, of course, consistent with ionised impurity scattering. Some information about the distribution of electrons at the fields necessary for light emission can be obtained from Gunn effect measurements.

The Gunn effect can be observed in semiconductors in which the first conduction band contains two minima, the higher energy minimum having the larger effective mass. In ZnSe and ZnS, the minimum at L_3 has a large effective mass and hence electrons close to this minimum are expected to have a low mobility. The variation of the drift velocity with electric field is therefore expected to have the form shown in figure 5.17, i.e. the drift velocity drops when electrons are transferred from the minimum at Γ_1 to L_3 and then increases again when the electric field is sufficiently large to force the electrons to higher energies. Shockley[79] and Ridley[80] have shown that a sample can not be biased stably in that part of figure 5.17 which has a negative gradient. In this case, two regions are formed in the sample, one with electric field $\mathcal{E}_L$ and a high field region, known as the domain with field $\mathcal{E}_V$. The domain travels across the sample with a velocity v_L and produces a current spike on arrival at the anode. For a sample with a thickness of about 100 μm, this domain translation produces oscillations in the microwave frequency range.

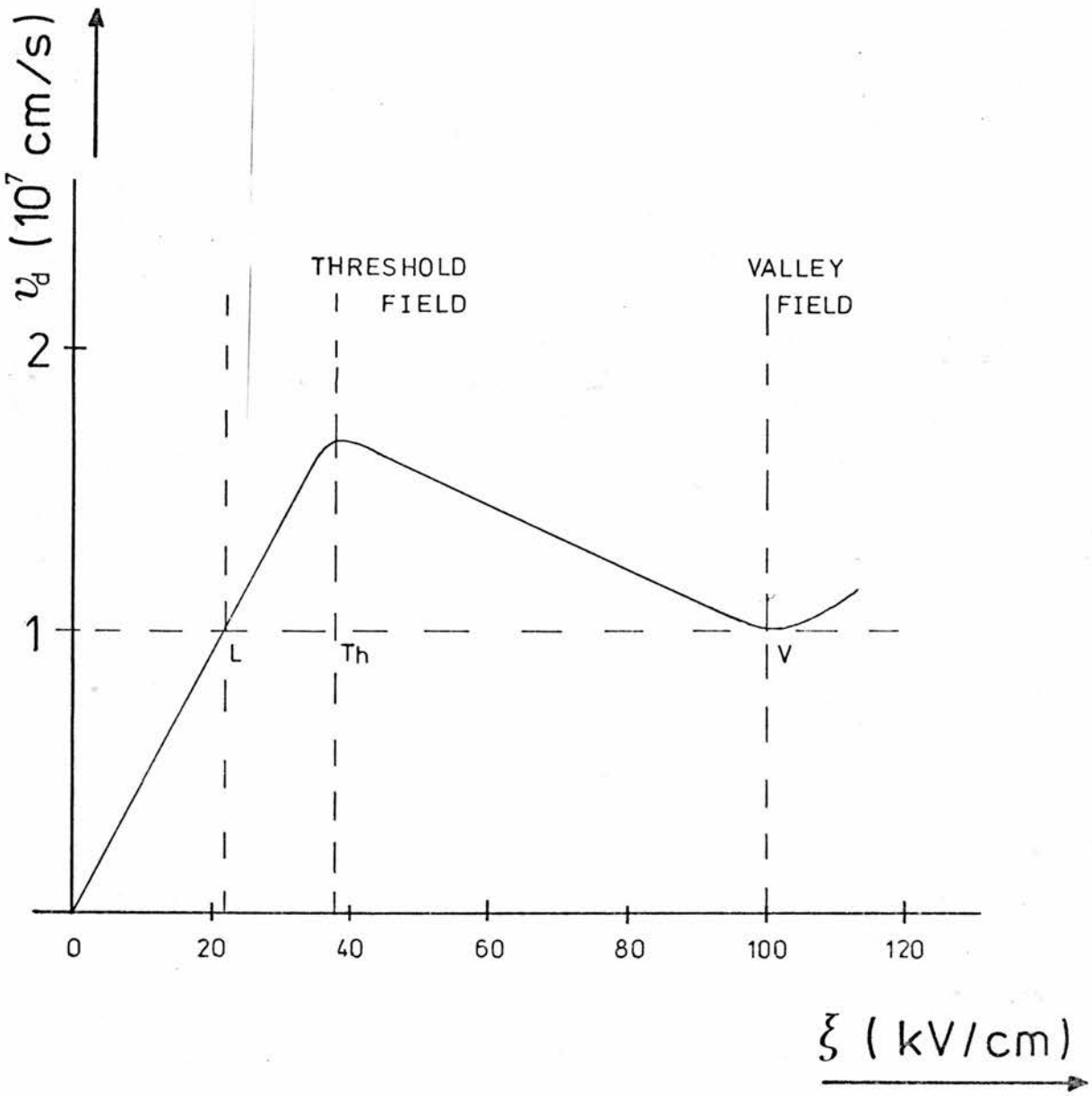

Figure 5.17 The approximate variation of the drift velocity with electric field deduced from Gunn effect measurements.

Ludwig and Aven[81] have analysed these oscillations and hence have been able to estimate $\mathcal{E}_L$, $\mathcal{E}_V$ and v_L as shown in figure 5.17. The electric field at V is estimated to be 10^5 V/cm at which field, a considerable fraction of the electrons have to be in L_3 or higher to account for the minimum in the drift velocity. For electroluminescence, the mean electric field at the quantum efficiency maximum varied between 1.0 and 12.0 x 10^5 V/cm as is shown in figure 5.16. It is therefore possible that the maximum in the quantum efficiency occurs when the mean electron energy is close to the threshold energy for impact excitation. From the discussion in section 5.d.ii, it follows that devices with a large N_d require a larger field to produce this energy distribution. It is not at all clear, however, why the quantum efficiency per unit depletion region width should drop when this field is exceeded.

In section 5.c, the cross section for impact excitation was assumed to be a Heaviside function. It turns out that the variation of the quantum efficiency with field is very insensitive to the actual shape of the cross section curve, except at very high fields. If a delta function had been assumed, the variation of the quantum efficiency with field would have been very similar at low fields. The shape of the cross section curve can, however, become important if the field becomes sufficiently large to make the mean electron energy greater than the threshold energy. Any further increase in the electric field will cause the quantum efficiency to drop if the cross section is a delta function, but not if it is a Heaviside function.

2. The second possible quenching mechanism is that the cross section for impact excitation is sharply peaked in energy and hence

the quantum efficiency drops when the mean electron energy exceeds the peak energy. Theoretically, there are two factors which will affect the width of the cross section curve. The first is due to the variation with energy of the matrix element which couples the initial electronic state to the final electronic state. The impact excitation of the manganese can be compared with the impact excitation of free atoms. In this case, the width of the cross section curve is typically half the threshold energy[82] for a spin forbidden system, although there is considerable variation from system to system.

The second broadening factor is due to the coupling between the manganese impurity and the phonons of the ZnS lattice. This is responsible for the broadening of spectral lines in optical absorption. In the absence of phonon coupling, the absorption spectrum of an electronic transition will be completely sharp. In practice, however, other transitions are possible in which the total energy is conserved by the emission or absorbtion of phonons. Thus

$$h\nu = \Delta E_{elect} + n\hbar\omega \qquad (5.22)$$

where

$h\nu$ is the photon energy

ΔE_{elect} is the change in the electronic energy

n is the number of phonons emitted

and $\hbar\omega$ is their energy.

If Ψ is the total wavefunction including both electronic and phonon parts, then the matrix element will take the form

$$M = \langle \Psi_f \mid \hat{o} \mid \Psi_i \rangle \qquad (5.23)$$

where $\hat{\sigma} \propto \underline{A} \cdot \underline{p}$ for an optical dipole transition.

In the Born Oppenheimer approximation, the total wavefunction factorises into an electronic part and a phonon part. As the operator $\hat{\sigma}$ only operates on the electronic part, the matrix element can be rewritten as

$$M = \langle \psi_f^{el} | \hat{\sigma} | \psi_i^{el} \rangle \langle \phi_f | \phi_i \rangle \quad (5.24)$$

where ψ_i^{el} is the initial electronic wavefunction and ϕ_i is the initial phonon wavefunction. The matrix element is therefore proportional to the overlap of the phonon wavefunctions. This varies with energy to produce the broadening which can be seen on the absorption spectrum in figure 4.2.

A similar argument could be given for the matrix element of the impact excitation process. In this case, however, $\hat{\sigma}$ would be given by the Coulomb interaction between the incident electron and the manganese d^5 electrons. As this does not affect the phonon part of the wavefunction, the matrix element can also be factorised as in equation (5.24). Thus, the widths of the absorption lines in figure 4.2 can be considered to be the minimum possible widths of the cross section curves. Note that the more energetic electrons can also impact excite the manganese to the $^4T_2$ state which will decay rapidly to the $^4T_1$ state responsible for the luminescence. Although this argument tends to suggest that the cross section is not strongly peaked, no definite statement can be made until quantitative calculations have been carried out.

3. Stratton[83] has analysed the behaviour of semiconductors under large applied fields assuming parabolic bands and phonon scattering. He finds that above a certain electric field, the mean electron energy has increased to above that at which phonon scattering is effective and hence the electrons can break away to higher and higher energies. The maximum electric field which can be applied before the electrons break away has been calculated by Ludwig and Aven[81] using Stratton's formula. This is about 2.8×10^4 V/cm for the Γ_1 minimum in ZnSe. Above this field, the electrons will transfer from Γ_1 to L_3, X_1 and X_3 where their progress to higher energies will be impeded by the more efficient scattering in these minima. (This is responsible for the Gunn effect described earlier.) It is possible that the maximum in the quantum efficiency is associated with dielectric breakdown in these minima. The energy of these electrons will then increase until they have sufficient energy to cause current multiplication either by impact ionisation of the manganese (figure 5.9(b)) or by direct band to band ionisation (figure 5.9(c)). If a significant fraction of the current is carried by the low energy electrons and holes produced by these processes, the fraction of hot electrons and hence the quantum efficiency will drop.

The first three mechanisms in table 5.1 have already been considered in detail. The fourth mechanism depends on a significant fraction of the manganese atoms being excited at one time. This will reduce the number available for excitation and hence the quantum efficiency of the device. In this case, however, the maximum in the quantum efficiency would be expected to depend on the current density rather than the electric field as in figure 5.16. A similar argument can be used against the fifth mechanism in which the excited manganese

atom is impact ionised before it can decay radiatively. In addition, the excited state lifetime is about ten times less in ZnSe than in ZnS and hence the required current density should be ten times greater.

The final possibility listed on table 5.1 is that at high current densities, the concentration of electrons injected into the depletion region is sufficient to Auger quench the luminescence (see chapter 4). The current density required is

$$j = n' e v_d$$

where $n' = 1/\gamma \tau_R$ is the electron density required to half the radiative efficiency of a phosphor (see equation (4.2)) and v_d is the drift velocity. The coefficient γ will be different from that calculated in chapter 4 because the electron distribution is different. If, however, γ is estimated to be 10^{-9} cm^3/s and v_d is taken to be 10^7 cm/s, the calculated current density is 1.6 A/cm^2. Although this is about ten times larger than what is observed in practice, the Auger process is a fundamental quenching mechanism which will ultimately limit the performance of these devices. The mechanism could, however, be more important in ZnS:Mn powder panels where current crowding is thought to occur between the powder particles.[78] This means that the current density is greater than would be expected in these regions.

None of these explanations is entirely satisfactory although mechanism 3. is thought to be the most likely. It would appear that more work is required to clarify the situation.

5.f Summary and Conclusions

Conducting ZnS:Mn crystals have been produced and their electroluminescent properties studied. It has been found that their behaviour is very similar to that of ZnSe:Mn crystals which were studied earlier.[70] The characteristic field for an electroluminescent device $\mathcal{E}_0$ has been found to vary systematically with the donor concentration and an explanation has been proposed which depends on efficient scattering of electrons in the upper conduction band minima by ionised donors. The quantum efficiency of all the devices so far studied reaches a maximum at an applied field which also depends on the donor density. This appears to be a fundamental effect and as such could be a fundamental limitation on the performance of electroluminescent ZnS:Mn displays. The first problem is that because insulating ZnS:Mn is used, a sufficiently large electric field has to be applied to the active region to produce avalanching before the electroluminescence can be excited. The large operating field means that the panels are operated in a region above the maximum in the quantum efficiency. Another problem becomes evident if the panels are to be used as part of a sequentially scanned array. Unless some memory is interfaced with each device, each element in an n-element display can only be pulsed for 1/n of the time. This means that the elements have to light up on the application of a large pulse of short duration. The drop in the quantum efficiency at large fields could make the pulsed operation of these devices very inefficient.

APPENDIX 5A

EQUATION FOR THE CROSS SECTION

Using the approximation of parabolic bands equation (5.8) for the cross section can be written as

$$\sigma(\mathcal{E}) = \frac{\int R(E)\, f(E,\mathcal{E})\, dE}{v_d \int f(E,\mathcal{E})\, dE} \quad (5A.1)$$

The drift velocity will be proportional to the electric field for low fields but will tend to a limit dictated by the band structure at high fields. As the fields required for electroluminescence are about ten times as large as the Gunn effect threshold, the drift velocity is expected to be a slowly varying function of the electric field. Thus, the variation of the averaged cross section with electric field is expected to be mainly due to f (E, $\mathcal{E}$). Compared with this, the drift velocity can be taken to be a constant.

Using equations (5.10) and (5.13), the electron distribution function (5.9) can be written as

$$f(E,\mathcal{E}) \propto E^{\frac{1}{2}} \exp - \frac{E}{E_{th}} \left(\frac{\mathcal{E}_0}{\mathcal{E}}\right)^2 \quad (5A.2)$$

The excitation rate has been assumed to have the form (5.11)

$$R(E) = R_0\, u(E - E_{th}) \quad (5A.3)$$

Substituting (5A.2) and (5A.3) into equation (5A.1) gives

$$\sigma\left(\frac{e}{\xi}\right) = \left(\frac{R_0}{v_d}\right)\left[\frac{\Gamma\left(\frac{3}{2}\right) - \Gamma_{\left(\frac{\xi_0}{\xi}\right)^2}\left(\frac{3}{2}\right)}{\Gamma\left(\frac{3}{2}\right)}\right] \qquad (5A.4)$$

where $\Gamma_a\left(\frac{3}{2}\right)$ is the incomplete gamma function defined by

$$\Gamma_a\left(\frac{3}{2}\right) = \int_0^a e^{-t}\, t^{\frac{1}{2}}\, dt \,. \qquad (5A.5)$$

This function is tabulated in, for example, reference [74] and equation (5A.4) is plotted in figure 5A.1. It can be seen that over the range of interest for electroluminescence, the cross section varies as

$$\sigma \sim \sigma_0 \exp - \left(\frac{\xi_0}{\xi}\right)^2 \qquad (5A.6)$$

to a good approximation.

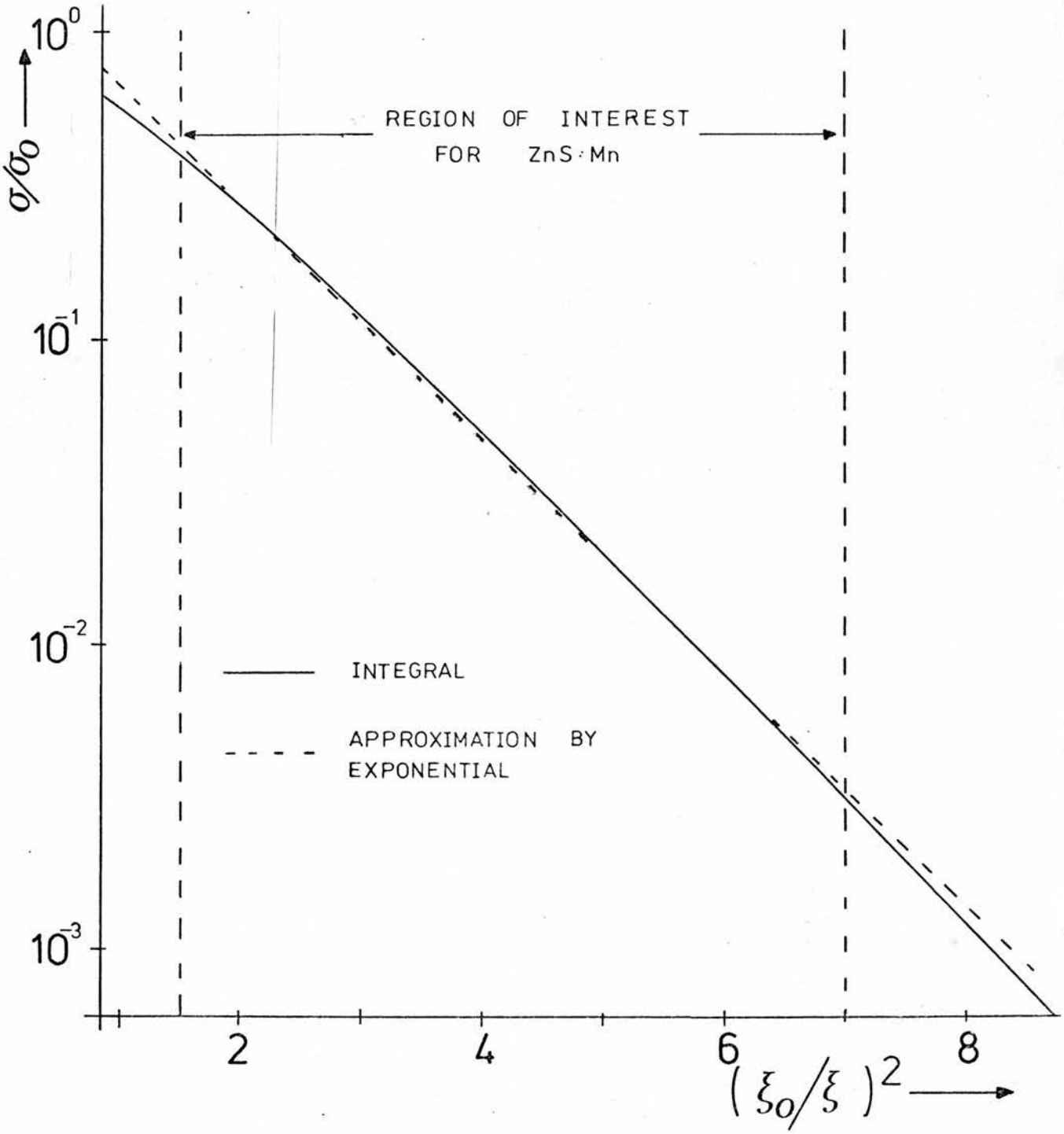

Figure 5A.1 Theoretical variation of the cross section with electric field.

APPENDIX 5B

CONNECTION BETWEEN γ AND σ

The two main experimental chapters of this thesis are concerned with the impact excitation of manganese which is characterised by a cross section σ and the Auger process of chapter 4 which is characterised by a coupling constant γ. As these two processes are the inverse of each other, it is of some interest to investigate the relationship between σ and γ.

Because of the large uncertainties in the densities of final states for both processes, and also because σ and γ are averages over slightly different initial and final states, a rigorous analysis is neither justified nor possible. However, the simple analysis given below illustrates the relationship between the two quantities in a semi-quantitative manner.

Consider a crystal of unit volume containing one electron. If the electron is above the X_3 upper conduction band minimum, it can impact excite a manganese centre. The excitation rate is given by Fermi's rule as

$$W_{IMPACT} = \frac{2\pi}{\hbar} |M|^2 \rho(E_1) \qquad (5B.1)$$

where M is the matrix element for the transition and $\rho(E_1)$ is the density of final states.

The definition of the cross section for impact excitation is given in equation (5A.1). This can be rewritten as,

$$\sigma = \langle W_{IMPACT} \rangle / v_d \qquad (5B.2)$$

where $\langle W_{IMPACT} \rangle$ is the excitation rate averaged over all the electrons. For an electron above the threshold energy, $\sigma = \sigma_o$ and hence

$$\sigma_o = \frac{2\pi}{\hbar} \frac{|M|^2 \rho(r_1)}{v_d} \qquad (5B.3)$$

If the electron is close to r_1, an excited manganese atom can undergo an Auger transition. The rate of these Auger transitions is given by

$$W_{AUGER} \equiv \gamma = \frac{2\pi}{\hbar} |M|^2 \rho(x_3) \qquad (5B.4)$$

Eliminating the matrix element from (5B.3) and (5B.4) gives

$$\sigma = \frac{\gamma}{v_d} \left(\frac{\rho(r_1)}{\rho(x_3)} \right) \qquad (5B.5)$$

The densities of the final states are not known. For both processes, this density of states has to be averaged over the initial electron energy distribution function. In addition, the final energy of the electron depends on the number of phonons participating in the manganese transition. Thus, the densities of states have also to be averaged over the phonon broadening. These averaged densities of

states should not be very different and hence to a first approximation

$$\sigma \sim \frac{\gamma}{v_d} . \qquad (5B.6)$$

CHAPTER 6

CONCLUSIONS

The properties of Schottky contacts on ZnSe were discussed in the first part of this thesis. It was noted that forward biased contacts could be used to obtain injection electroluminescence in semiconductors in which p-n junctions are impossible. The efficiency of these devices is small compared with p-n junctions although there are a number of applications for which this may not be too important. The main problems with this type of device are irreproducibility and ageing. This is associated with the presence of an oxide layer below the metal contact. In addition, the brightness is low. It may perhaps be possible to overcome some of these problems by exercising greater control over the oxide layer. This could involve the evaporation or growth of an oxide layer on to a clean semiconductor surface.

The second part of this thesis was concerned with the properties of conducting ZnS:Mn. This material is currently of some commercial interest as electroluminescent displays using ZnS:Mn are likely to be produced commercially in the near future. In chapter 4, a non-radiative Auger process which occurs in ZnS:Mn was investigated. It was shown that the non-radiative transition rate was proportional to the electron concentration. Besides the theoretical interest in this process, it is possible that it could be a useful contactless method for measuring the electron concentration in ZnS:Mn. There are still some problems in making good electrical contacts to ZnS and the technique could prove to be particularly useful in the current research into conducting thin films of ZnS:Mn.

Finally the mechanism of high field electroluminescence in ZnS:Mn has been investigated. It is thought that the manganese centres are impact excited by energetic electrons which are produced by the large electric field. The number of energetic electrons for a given field appears to be controlled by ionised impurity scattering rather than by optical phonon scattering which would be expected. This is thought to be related to the band structure of ZnS.

It was found that the efficiency of the electroluminescent process was quenched above a certain field which depended on the donor density. The quenching mechanism is not yet fully understood. It could, however, be extremely important in that it appears to be a fundamental property of ZnS:Mn and ZnSe:Mn. As such, it could prove to be a severe limitation on the usefulness of these materials for electroluminescent displays.

REFERENCES

1. Robinson, R. J. and Kun, Z. K., Appl. Phys. Letts. 27 (2), 74, (1975).

2. Ryall, M. D. and Allen, J. W., 'Investigation of Blue Light-Emitting Diodes', Report of work carried out under Agreement No. AT/2061/016 DCVD.

3. Destriau, G., J. de Chem. Phys. 33, 620, (1936).

4. Vecht, A., Werring, N. J., Ellis, R. and Smith, P. J. F., Proc. IEEE 61 (7), 902, (1973).

5. Mito, S., Susuki, C., Kanatani, Y. and Ise, M., SID Int. Symp. Digest, 86, (1974).

6. Nitsche, R., Bölsterli, H. U. and Lichtensteiger, M., J. Phys. Chem. Solids 21, 199 (1961).

7. Mott, N. F., Proc. Roy. Soc. A. 171, 27, (1939).

8. Schottky, W., Z. Phys. 118, 539, (1942).

9. Kar, S., Solid State Elect. 18, 169, (1975).

10. Bardeen, J., Phys. Rev. 71, 717, (1942).

11. Tanailaki, A. and Rasul, A., J. Phys. C. 9, 337, (1976).

12. Heine, V., Phys. Rev. 138, A1689, (1965).

13. Pelegrini, B., Solid State Elect. 17, 217, (1973).

14. Louie, S. G., Chelikowsky, J. R. and Cohen, M. L., Phys. Rev. B15, 2154, (1977).

15. Ludeke, R., Solid State Comm. 24, 725, (1977).

16. Spicer, W. E., Chye, P. W., Skeath, P. R., Su, C. Y. and Lindy, I., 'Insulating Films on Semiconductors 1979', edited by G. G. Roberts and J. Morant, 216, The Institute of Physics, Bristol and London, (1979).

17. Henish, H. K., 'Rectifying Semiconductor Contacts' (Oxford University Press, London, 1955), Chapter VII.

18. Goodman, A. M., J. Appl. Phys. 34, 329, (1963).

19. Atalla, M. M., Proc. Munich Symp. Microelectron, Oldenberg, Munich, 123, (1966).

20. Dewald, J. F., Bell System Tech. J. 39, 615, (1960).

21. Fowler, R. H., Phys. Rev. 37, 45, (1931).

22. Bethe, H. A., MIT Radiation Lab. Rept. 43, 12, (1942).

23. Sze, S. M., Crowell, C. R. and Kahng, D., J. Appl. Phys. 35, 2534, (1964).

24. Kahng, D., Solid State Electron. 6, 281, (1963).

25. Benzer, S., J. Appl. Phys. 20, 804, (1949).

26. Pankove, J. I. (editor), 'Topics in Applied Physics', 135-136, Springer-Verley, Berlin, Heidleberg, New York, (1977).

27. Goodman, A. M., J. Appl. Phys. 34, 329, (1963).

28. Cowley, A. M., J. Appl. Phys. 37, 3024, (1966).

29. Livingstone, A. W., Ph.D. Thesis, St. Andrews, (1973).

30. Tyagi, M. S. and Arora, S. N., Phys. Stat. Sol. (a) 32, 165, (1975).

31. Bjerkland H. and Holwech, I., Phys. Norv. 6, 139, (1972).

32. Mach, R., Treptow, H. and Ludwig, W., Phys. Stat. Sol. (a) 25, 567 (1974).

33. Wagner, C., Phys. Z. 32, 641, (1931).

34. Bethe, H. A., MIT Radiat. Lab. Rept. 43, 12, (1942).

35. Rhoderick, E. H., J. Phys. D. 5, 1920, (1972).

36. Padovani, F. A. and Stratton, R., Solid State Electron. 9, 695, (1966).

37. Livingstone, A. W., Turvey, K. and Allen, J. W., Solid State Electron. 16, 351, (1973).

38. Lawther, C. and Woods, J., Phys. Stat. Sol. (a) 44, 693, (1977).

39. Ryall, M. D. and Allen, J. W., J. Phys. Chem. Solids 34, 2137, (1973).

40. Grimmeiss, H. G., Ovrén, C. and Allen, J. W., J. Appl. Phys. 47, 1103, (1976).

41. Grimmeiss, H. G., Ovrén, C., Ludwig, W. and Mach, R., J. Appl. Phys. 48, 5122, (1977).

42. Rhoderick, E. H., 'Metal-Semiconductor Contacts', 31, Clarendon Press, Oxford, (1978).

43. Card, H. C. and Rhoderick, E. H., Solid State Electronics 16, 365, (1973).

44. Watanabe, H., Chikamura, T. and Wada, M., Japan J. Appl. Phys. 13, 357, (1974).

45. Kanter, H., Phys. Rev. B1, 522, (1976).

46. Allen, J. W., Ryall, M. D. and Wray, E. M., Phys. Stat. Sol. (a) 17, K101, (1973).

47. McClure, D. S., J. Chem. Phys. 39, 2850, (1963).

48. Nitsche, R., J. Phys. Chem. Solids 17, 163, (1960).

49. Oda, S. and Kukimoto, IEEE Trans. Elect. Devices ED-24, 956, (1977).

50. Vlasenko, S. A., Optics and Spectroscopy 8, 445, (1960).

51. Watts, 'Point Defects in Crystals', 86, John Wiley and Sons, (1977).

52. Busse, W., Gumlich, H.-E., Geoffrey A. and Parrot, R., Phys. Stat. Sol. (b) 93, 591, (1979).

53. Busse, W., Gumlich, H.-E., Meissner, B. and Theis, D., J. Lumin. 12/13, 693, (1976).

54. Manglesdorf, P. C., J. Appl. Phys. 30, 442, (1959).

55. Walentynowicz, E., Chimczac, E. and Gordon, W., J. Lumin. 17, 109, (1978).

56. Förster, Th., Ann. Physik 2, 55, (1948).

57. Dexter, D. L., J. Chem. Phys. 21, 836, (1953).

58. Van der Pauw, L. J., Philips Res. Repts. 13, 1, (1958).

59. Aven, M. and Mead, C. A., Appl. Phys. Letts. 7, 8, (1965).

60. Langer, J. M., Private Communication.

61. Alder, C. A., Cattell, A., Dexter, K. and Kirton, J., Electronic Letts. 16, 571, (1980).

62. Yamauchi, Y., Kishishita, H., Takeda, M., Ingouchi, T. and Mito, S., Digest 1974 Int. Elect. Dev. Mtg. (IEEE, New York, 1974), 352.

63. Tanaka, S., Kobayashi, H., Sarsakina, H. and Hamakana, Y., J. Appl. Phys. 47, 5391, (1976).

64. Marrello, V. and Onton, A., Appl. Phys. Letts. 34, 525, (1979).

65. Skolnick, M. S., J. Phys. D: Appl. Phys. 14, 301, (1981).

66. Ruhle, W., Marrello, V. and Onton, A., J. Lumin. 18/19, 729, (1979).

67. Eckett, P., Phys. Stat. Sol. (a) 23, 307, (1967).

68. Walter, J. P. and Cohen, M. E., Phys. Rev. 183, 763, (1969).

69. Allen, J. W., Livingstone, A. W. and Turvey, K., Solid State Electron. 15, 1363, (1972).

70. Allen, J. W., J. Lumin. 7, 228, (1973).

71. Livingstone, A. W. and Allen, J. W., J. Phys. C: Solid State Phys. 6, 3491, (1973).

72. Krupka, D. C., J. Appl. Phys. 43, 476, (1971).

73. Baraff, G. A., Phys. Rev. 128, 2057, (1962).

74. 'Tables of the Incomplete Γ -Function', edited by Karl Pearson, F.R.S., Cambridge University Press, (1957).

75. Wolff, P. A., Phys. Rev. 95, 1415, (1954).

76. Shockley, W., Czech. J. Phys. B11, 81, (1961) and Sold State Electron. 2, 35, (1961).

77. Turvey, K. and Allen, J. W., J. Phys. C: Solid State Phys. 6, 2887, (1973).

78. Skolnick, M. S., J. Phys. D: Appl. Phys. 14, 301, (1981).

79. Shockley, W., Bell Systems Tech. J. 33, 799, (1954).

80. Ridley, B. K., Proc. Phys. Soc. (London) 82, 954, (1963).

81. Ludwig, G. W. and Aven, M., J. Appl. Phys. 38, 5326, (1967).

82. Mott and Massey, 'The Theory of Atomic Collisions', 197, Oxford University Press, (1933).

83. Stratton, R., Proc. Roy. Soc. A246, 406, (1958).